Aberrant IL-20 Subfamily Signaling Disrupts Epithelial Barrier Function in Eosinophilic Esophagitis

Inauguraldissertation

zur

Erlangung der Würde eines Doktors der Philosophie

vorgelegt der

Philosophisch-Naturwissenschaftlichen Fakultät

der Universität Basel

von

Tanay Kaymak

2022

Originaldokument gespeichert auf dem Dokumentenserver der Universität Basel
edoc.unibas.ch

Genehmigt von der Philosophisch-Naturwissenschaftlichen Fakultät

Auf Antrag von

Prof. Dr. Jan Hendrik Niess
Prof. Dr. Gennaro De Libero
Prof. Dr. Dr. Hans-Uwe Simon

Basel, den 21.06.2022

Prof. Dr. Marcel Mayor
The Dean of the Faculty of Science

TABLE OF CONTENTS

ABBREVIATIONS

ACTB/Actb: Beta-actin

AGC: Automatic gain control

AJ: Adherens junctions

AJC: Apical junction complex

AKT: Protein kinase B

ALI: Air-liquid interface

APRIL: A proliferation-inducing ligand

BCA: Bicinchoninic acid

BMDM: Bone marrow-derived macrophage

BME: Basement membrane extract

BPE: Bovine pituitary extract

BSA: Bovine serum albumin

CAPN: Calpain

CCR: CC chemokine receptor

CLC: Charcot-Leyden crystal galectin

CLDN: Claudin

CPM: Counts per million mapped reads

Ctrl: Non-sensitized+non-challenged

CX3CR1: CX3C chemokine receptor 1

DAB: 3,3' Diaminobenzidine

DAPI: 4',6-diamidino-2-phenylindole

DC: Dendritic cell

DDA: Data dependent aquisition

DMSO: Dimethyl sulfoxide

DP: Desmoplakin

DSC: Desmocollin

DSG: Desmoglein

DSP: Desmoplakin

ECP: Eosinophil cationic protein

EDC: Epidermal differentiation complex

EDN: Eosinophil-derived neurotoxin

EDTA: Ethylenediaminetetraacetic acid

EGF: Epidermal growth factor

ELISA: Enzyme-linked immunosorbent assay

EoE: Eosinophilic Esophagitis

eos: Eosinophils

EPO: Eosinophil peroxidase

ERK-1/2: Extracellular-signal regulated kinases 1/2

eso: Esophagus

EtOH: Ethanol

EVPL: Envoplakin

FACS: Fluorescence-activated cell sorting

FAIMS: Field assymetric waveform ion mobility spectrometry

FBS: Fetal bovine serum

FCS: Fetal calf serum

FDR: False discovery rate

FITC: Fluorescein isothiocyanate

FLG: Filaggrin

FLG2: Filaggrin 2

fs: Forestomach

FSC: Forward scatter

GAPDH: Glyceraldehyde 3-phosphate dehydrogenase

GEO: Gene expression omnibus

GERD: Gastroesophageal reflux disease

GIT: Gastrointestinal tract

GM-CSF: Granulocyte-macrophage colony-stimulating factor

GO: Gene ontology

gs: Glandular stomach

GSEA: Gene set enrichment analysis

GWAS: Genome-wide association study

HCD: High-collision-dissociation

H&E: Hematoxylin and eosin

HPF/hpf: High-power field

HRP: Horseradish peroxidase

HTO: Hashtag oligos

IBD: Inflammatory bowel disease

IFNγ: Interferon gamma

Ig: Immunoglobulin

i.g.: intragastric

IHC: Immunohistochemistry

IL/Il: Interleukin

IL-4RA: Interleukin-4 receptor subunit alpha

IL-13RA1: Interleukin-13 receptor subunit alpha 1

IL-13RA2: Interleukin-13 receptor subunit alpha 2

IL-20R: Interleukin-20 receptor

IL-20RA: Interleukin-20 receptor subunit alpha

IL-20RB/IL-20R2: Interleukin-20 receptor subunit beta

IL-22RA1: Interleukin-22 receptor subunit alpha 1

IL-20s: IL-20 subfamily-stimulated

i.p.: intraperitoneal

JAK: Janus kinase

JAM: Junctional adhesion molecule

KGF/FGF7: Keratinocyte growth factor/Fibroblast growth factor 7

KLK: Kallikrein

KRT: Keratin

KSFM: Keratinocyte serum-free medium

LC-MS/MS: Liquid chromatography-tandem mass spectrometry

LPA: Lysophosphatidic acid

LPS: Lipopolysaccharide

MALT: Mucosa-associated lymphoid tissue

MAPK: Mitogen-activated protein kinase

MBP: Major basic protein

M-CSF: Macrophage colony-stimulating factor

MMP: Matrix metalloproteinase

NF-κB: Nuclear factor kappa-light-chain-enhancer of activated B cells

Non-chal: Sensitized+non-challenged

Non-sens: Non-sensitized+challenged

NS: Non-stimulated

OCLN: Occludin

OVA: Ovalbumin

PBS: Phosphate-buffered saline

PC: Principal component

PCA: Principal component analysis

PFA: Paraformaldehyde

PG: Plakoglobin

pIgR: Polymeric immunoglobulin receptor

PKP: Plakophilin

PMSF: Phenylmehtylsulfonyl fluoride

PPI: Proton-pump inhibitor

PPI-REE: PPI-responsive esophageal eosinophilia

PPL: Periplakin

PRIDE: Proteomics identification database

RCT: Randomized controlled trial

RIPA: Radioimmunoprecipitation assay

RNA-seq: RNA-sequencing

ROCK: Rho-associated protein kinase

RP-HLPC: Reversed-phase high-performance liquid chromatography

RPMI: Roswell Park Memorial Institute

RT: Room temperature

RT-qPCR: Reverse-transcription quantitative polymerase chain reaction

scRNA-seq: single-cell RNA-sequencing

SDS: Sodium dodecyl sulfate

Sens+chal: Sensitized+challenged

si: Small intestine

Siglec: Sialic acid-binding immunoglobulin-type lectin

SPF: Specific-pathogen-free

SPINK: Serine protease inhibitor kazal-type

SSC: Side scatter

STAT: Signal transducer and activator of transcription

TBS: Tris-buffered saline

TBS-T: Tris-buffered saline + Tween 20

TCEP: Tris(2-carboxyethyl)phosphine

tdT: tdTomato

TEAB: Triethyloammonium bicarbonate

TEER: Transepithelial electrical resistance

TFA: Trifluoroacetic acid

TGF-β1: Transforming growth factor beta 1

Th1: Type 1 helper T cell

Th2: Type 2 helper T cell

Th17: Type 17 helper T cell

TLR: Toll-like receptor

TMM: Trimmed mean of M values

TMT: Tandem mass tags

TMX: Tamoxifen

TNF: Tumor necrosis factor

2-ME: 2-Mercaptoethanol

UMI: Unique molecular identifier

WT: wild type

ZO: Zonula occludens

ABSTRACT

The esophageal epithelium is the first line of defense against harmful environmental antigens. Impairment of the epithelial barrier function is associated with esophageal disorders, including eosinophilic esophagitis (EoE). Members of the interleukin (IL)-20 subfamily are essential mediators between the immune system and epithelial cells. Nonetheless, the function of the IL-20 subfamily in the esophagus is unexplored.

In this Ph.D. thesis, we aim to describe the role of the IL-20 subfamily in regulating the esophageal epithelial barrier function during EoE. Analysis of esophageal biopsies and serum samples revealed elevated IL-19, IL-20, and IL-24 levels in active EoE. Combined transcriptome and proteome analysis of patient-derived esophageal organoids indicated that IL-20 subfamily cytokines downregulate the expression of filaggrins (FLG, FLG2) and other epithelial components resulting in a disturbed barrier function. Additionally, we observed that the genetic deletion of the IL-20 receptor subunit beta (IL-20RB/IL-20R2) attenuated experimental EoE and preserved esophageal FLG2 expression in an ovalbumin (OVA)-induced EoE mouse model. Furthermore, inhibition of the mitogen-activated protein kinase (MAPK) or signal transducer and activator of transcription 3 (STAT3) pathway revealed that IL-20 subfamily-mediated epithelial barrier dysfunction depends on the MAPK rather than the STAT3 pathway. Finally, MAPK inhibitor treatment reduces eosinophil and CD45^{+} immune cell infiltration in the EoE mouse model. Altogether, we have identified an IL-20 subfamily-mediated mechanism of esophageal barrier impairment in the pathophysiology of EoE.

1 INTRODUCTION

1.1   The esophageal epithelium

The esophagus is a dynamic fibromuscular tube that intertwines the oral cavity with the stomach. The esophagus' overt function is the transit of the food bolus. However, the esophageal epithelium represents a significant interface between the immune system and environmental factors (e.g., food antigens).

The primary function of the esophageal epithelium is to protect the underlying tissue from environmental substances and pathogens to prevent tissue damage and disease.
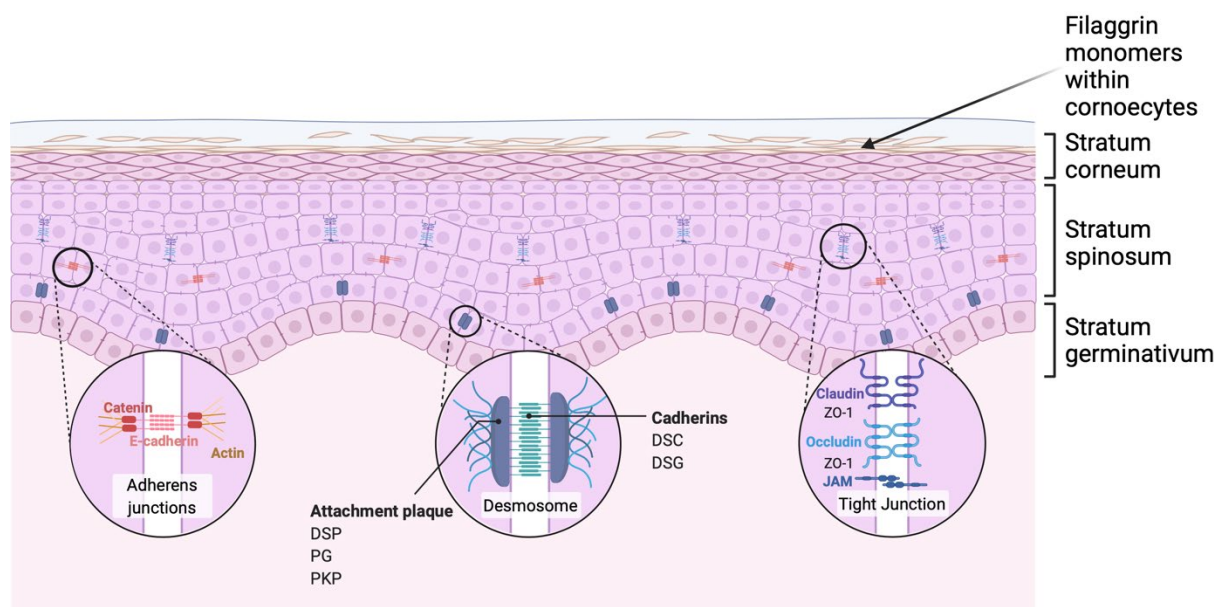
Figure 1.1   The esophageal epithelium

The esophagus is lined by a stratified squamous epithelium, subdivided into the basal stratum germinativum, the suprabasal stratum spinosum, and the superficial stratum corneum. A filaggrin-monomer cross-linked lipid-protein matrix and the apical junction complex consisting of tight junctions, adherens junctions, and desmosomes provide the epithelial barrier function. DSC: Desmocollin, DSG: Desmoglobin, DSP: Desmoplakin, JAM: Junctional adhesion molecule, PG: Plakoglobin, PKP: Plakophilin, ZO: Zonula occludens. Created with BioRender.com.

The human and rodent esophageal epithelium are subdivided into the stratum corneum (superficial layer), the stratum spinosum (suprabasal layer), and the stratum germinativum (basal layer) (Figure 1.1). However, unlike the rodent squamous epithelium in the esophagus, the human esophageal epithelium is not keratinized [1]. A first biochemical line of defense is provided by swallowed bicarbonate-containing saliva [2] and submucosal gland-derived watery mucus [3], which restores the esophageal pH decreased by acidic foods and beverages or refluxed gastric acid. However, the physical epithelial barrier has the most prominent protective function.

1.1.1 Stratum corneum

The stratum corneum is the superficial epithelial layer formed by a tight network of multilayered corneocytes cross-linked with an insoluble lipid-protein matrix [4]. A significant component of the stratum corneum is filaggrin (FLG), a structural protein forming the lipid-protein matrix from intermediate keratin filaments [4]. Together with the intercellular glycocalyx, the lipid-protein matrix protects from paracellular transit of luminal content.

1.1.1.1 The filaggrin family

The filaggrin family is part of the S100 fused-type protein family and consists of filaggrin (FLG) [5] and filaggrin 2 (FLG2) [6], which are encoded within the epidermal differentiation complex (EDC; chromosome 1q21) [7]. S100 fused-type proteins are a group of Ca^{2+}-binding multidomain proteins with two N-terminal EF-hand motifs connected to a large repetitive peptide [8]. Keratinocytes on the verge of becoming corneocytes express the FLG precursor protein profilaggrin [7, 9]. Posttranslational phosphorylation of profilaggrin prevents premature cleavage and aggregation with keratin filaments and thereby delays the collapse of the cytoplasm and flattening of

the corneocytes [5, 10, 11]. Furthermore, protease inhibitors, including SPINK5 and SPINK7, control the activity of proteases cleaving profilaggrin and other EDC proteins [12-16]. After dephosphorylation and cleavage, profilaggrin gives rise to 10-12 FLG monomers [17]. FLG-mediated keratin aggregation and alignment allow the formation of an insoluble keratin matrix that serves as a scaffold for the cornified envelope forming the impermeable barrier of the stratum corneum [18]. After that, caspase 14, calpain 1, and bleomycin hydrolase degrade FLG into the fundamental components of the natural moisturizing factor to ensure epithelial hydration [19-21].

The biological function of FLG2 is much less understood. However, the high similarity of the amino acid sequence, the co-localization in the epithelium, and the degradation of both family members by calpain-1 suggest that they possess similar functions [6, 19, 22]. It is also important to note that both FLG and FLG2 polymorphisms are associated with epithelial barrier impairment [23, 24].

1.1.2 Stratum spinosum

Like the FLG-sealed stratum corneum, the adjacent stratum spinosum plays a decisive role in regulating paracellular permeability. The apical junction complex (AJC) regulates the cell-cell adhesion in the stratum spinosum.

The AJC comprises three structures securing the intercellular network [25]:

The most apically located tight junctions are composed of claudins (CLDN), occludin (OCLN), zonula occludens, and junctional adhesion molecules (JAMs) controlling epithelial ion-permeability and macromolecular flux [26-28].

The subjacent adherens junctions (AJ) are equivalently involved in maintaining cell-cell adhesion by cadherin-cadherin interactions [29]. However, AJs also have a hand in regulating the intracellular cytoskeleton via the catenin family, which links E-cadherin to the actin filaments [30].

Desmosomes are the basalmost AJC structure. The interaction of desmogleins (DSG) and desmocollins (DSC) between adjacent cells supports cell-cell adhesion [31]. Indeed, dysfunction of merely one AJC component disrupts the epithelial barrier and predisposes to the development of esophageal diseases [32-35].

1.1.3   Stratum germinativum

The stratum germinativum represents the basal cell layer. It is composed of immature keratinocytes responsible for the constant renewal of the esophageal epithelium. Keratinocytes differentiate during a migratory process from the basal cell layer to the superficial stratum corneum. During migration, keratinocytes continuously flatten and expand laterally, forming a compact barrier [36]. In the meantime, the genetic signature of keratinocytes shifts from undifferentiated basal keratinocyte markers (e.g., keratin 5 (KRT5) and keratin 14 (KRT14)) to differentiated suprabasal keratinocyte markers (e.g., keratin 4 (KRT4) and keratin 13 (KRT13)) and structural proteins encoded within the EDC [37-39].

1.2   The esophageal immune system

The mucosal surfaces are the entry gates to our body for food-derived allergens and microorganisms and their microbial products. The epithelial barrier usually prevents noxious agents from entering the host system. However, when components of the luminal content overcome the physical and biochemical barriers, residing and infiltrating immune cells are vital in the clearance or tolerance of foreign antigens.

It is important to note that the esophageal immune system is fundamentally different from the rest of the mucosal immune system in the gastrointestinal tract (GIT). Although all immune cell populations are present, the number of tissue-resident immune cells in the esophagus is negligible compared to other parts of the GIT [40,

41]. In contrast to the lower intestine, the esophagus lacks mucosa-associated lymphoid tissues (MALTs), which allow luminal content sampling via microfold cells and immunoglobulin A (IgA) [42]. IgA, the predominant immunoglobulin of mucosal surfaces, prevents entry of luminal antigens into the circulation [43] and facilitates their transepithelial transport to MALTs [44]. Subsequent processing of antigens by the immune cells in the MALTs ensures a balance between immunogenic and immunotolerogenic reactions [45].
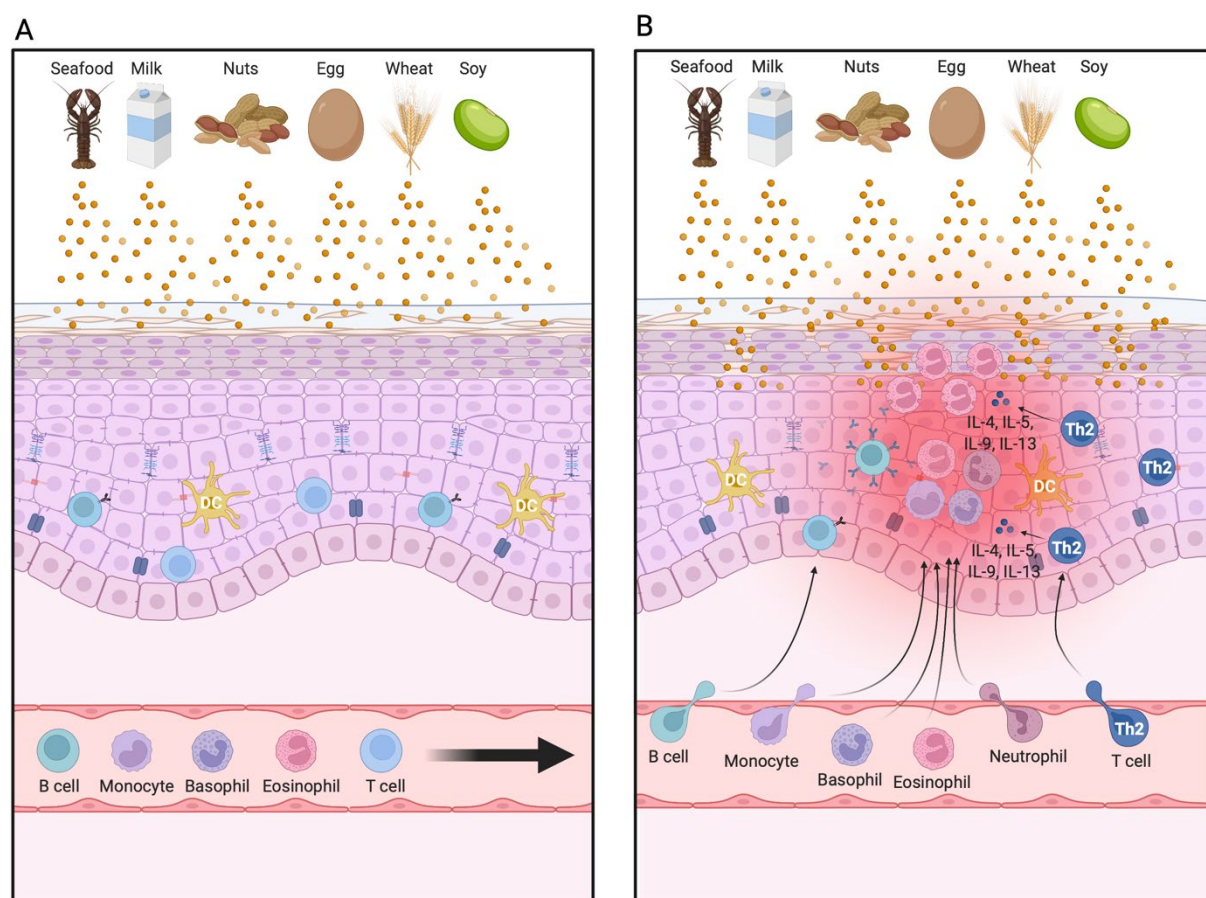
Figure 1.2   The esophageal immune system in health and inflammation

The esophageal immune system protects the organism from environmental antigens penetrating the epithelial barrier. (A) Tissue-resident immune cells sparsely inhabit the healthy esophagus.

(B) Detection of environmental antigens can induce an immune response with marked immune cell infiltration to clear foreign antigens and prevent tissue damage. DC: Dendritic cell, IL: Interleukin, Th2: Type 2 helper T cell. Created with BioRender.com.

In the lower intestine, the polymeric immunoglobulin receptor (pIgR) transports IgA from the basolateral to the luminal side by binding the J-chain of dimeric IgA in the lamina propria [46, 47]. In order to exert its functions following transcytosis, secretory IgA anchors to the thick viscous mucus layer via the proteolytically cleaved secretory component of the pIgR [48].

However, the esophagus does not express the pIgR and is lined by a thin and frequently flushed layer of watery mucus [3, 49, 50]. Therefore, the lack of MALTs and IgA suggest direct antigen sampling from the lumen by tissue-resident CD1$^+$ dendritic cells (DCs) in the esophagus [51].

1.2.1 Eosinophils

Eosinophils are myeloid lineage-derived polymorphonuclear granulocytes with pre-formed granules involved in antiparasitic and allergic immune reactions. The eosinophil granules consist of major basic protein (MBP), Charcot-Leyden crystals (CLC; galectin 10), eosinophil cationic protein (ECP), eosinophil peroxidase (EPO), and eosinophil-derived neurotoxin (EDN). They have cytotoxic properties and, together with mitochondrial DNA, form extracellular traps to clear infiltrating pathogens [52, 53]. However, excessive eosinophil degranulation can also cause tissue damage [52]. Furthermore, eosinophils play an essential role in tissue homeostasis and immunoregulation in the lamina propria and MALTs of the lower GIT. Toll-like receptor (TLR)-mediated activation of eosinophils increases their expression of APRIL, TGF-β1, and MMP9 to promote the T cell-independent generation and maintenance of IgA-secreting B cells and plasma cells [54].

In the steady-state, eosinophils are present in the thymus, mammary gland, uterus, and the lower GIT [55-57]. In contrast, the esophagus is devoid of eosinophils [40, 55]. However, esophageal inflammation often causes infiltration of eosinophils which is

orchestrated mainly by the eosinophil differentiation factor interleukin (IL)-5 and the eotaxin family (eotaxin-1 [58], eotaxin-2 [59] and eotaxin-3 [60]) [61]. IL-5 is responsible for eosinophil differentiation and mobilization from the bone marrow, as well as for their activation and survival [61-65]. The eotaxins are CC chemokines characterized by two adjacent cysteine residues near the amino terminus [58-60]. Eotaxins direct eosinophil trafficking from the circulation to the tissue via the CCR3 receptor [58-60, 66, 67]. Under homeostatic conditions, constitutive expression of eotaxin-1 recruits eosinophils into the thymus, mammary gland, uterus, and the lower GIT but not into the esophagus [55-57]. Under inflammatory conditions, esophageal epithelial cells secrete eotaxin-3 to attract eosinophils [68].

During inflammation, eosinophils produce an array of cytokines, including IL-4, IL-5, and IL-9, to promote type 2 helper T cell (Th2)-mediated inflammation [69] while suppressing type 1 helper T cell (Th1) and type 17 helper T cell (Th17)-mediated responses [70]. Furthermore, a bidirectional interplay with mast cells by direct cell-cell contact and TNF and GM-CSF-mediated paracrine signaling can increase the number, activity, and survival of infiltrating eosinophils to promote Th2-mediated chronic inflammatory diseases like eosinophilic esophagitis [71, 72].

1.3   Eosinophilic Esophagitis (EoE)

Eosinophilic Esophagitis (EoE) is a food allergen-driven chronic inflammatory disease of the esophagus [73]. The inflammatory process in EoE is Th2-mediated and predominated by esophageal eosinophil infiltration [73, 74]. Adult patients mostly experience dysphagia, food impaction, and chest pain [73]. In children, the clinical symptoms are age-dependent and include failure to thrive, food refusal, vomiting, and abdominal pain [75].

EoE was first described as a distinct disorder in the 1990s by Attwood et al. [76] and Straumann et al. [77]. Before, EoE was perceived as a subtype of gastroesophageal reflux disease (GERD) [78-80]. GERD and EoE are the two most frequent causes of chronic esophagitis [81]. Initial guidelines recommended performing a proton-pump inhibitor (PPI) trial and pH monitoring to distinguish these two entities with overlapping clinical and histologic features [80]. EoE was initially defined as PPI-resistant with normal pH monitoring [80]. However, the PPI trial revealed a new phenotype of PPI-responsive esophageal eosinophilia (PPI-REE) [82, 83]. PPI-REE was first considered a distinct entity with EoE-like symptoms [84]. Nevertheless, studies showed that PPI-REE could neither be distinguished clinically, endoscopically nor histologically from EoE [85, 86]. Furthermore, RNA-sequencing (RNA-seq) presented a largely overlapping transcriptomic signature between EoE and PPI-REE, substantiating a common underlying Th2-mediated pathogenesis [87, 88]. Subsequently, PPI resistance was removed from the diagnostic criteria of EoE [73, 81].

1.3.1   Epidemiology

Continuously increasing incidence (4.4-7.4/100'000) and prevalence (43-56.7/100'000) of EoE in Switzerland and the western hemisphere [89, 90] poses a growing economic burden on the health care system [91]. Interestingly, men are more commonly affected by EoE than women (ratio of 3:1) [89, 92]. Risk factors associated with EoE are of environmental and genetic origin, including early-life exposure to antibiotics and PPI treatment, cesarean section, preterm labor, maternal fever, pre-existing atopic diseases, and genetic risk variants primarily found in the esophageal epithelium [93-95].

1.3.2 Diagnosis

Diagnosis requires an endoscopic evaluation for signs of EoE (concentric mucosal rings, longitudinal furrows, white exudates, edema, esophageal strictures) and biopsy sampling from at least two different locations in patients with EoE symptoms [73, 96]. Eosinophil infiltration per high-power field (eos/hpf) is quantified and an eosinophil count of >15 eos/hpf qualifies for an EoE diagnosis [73]. Other frequently described histopathological features are basal zone hyperplasia, dilated intercellular spaces, eosinophil abscesses, and thickened lamina propria fibers [97].

Finally, to confirm the diagnosis, other reasons for symptoms of esophageal dysfunction and esophageal eosinophilia (>15 eos/hpf) including GERD, eosinophilic gastrointestinal disorders, motility disorders, hypereosinophilic syndrome, Crohn's disease, and infections need to be excluded [73].

1.3.3 Therapy

First-line therapy options for EoE include diets, PPIs, and swallowed topical corticosteroids [81]. Current therapies successfully control esophageal symptoms in a proportion of patients [81]. Nevertheless, they do not modify the natural disease course of EoE [98]. However, the growing understanding of EoE pathophysiology leads to the emergence of biological therapy agents interfering with the underlying mechanisms of EoE.

1.3.3.1 Diets

Dietary therapy approaches include elemental diets based on an amino acid, allergen-free formula [99], or empirical elimination of the four to six most common food allergens milk, nuts, egg, wheat, soy, and seafood [100, 101]. Dietary therapy effectively induces and maintains remission in 72-90% of EoE patients [99-102]. However, long-term

therapy adherence is low due to severe restrictions on food choices and quality of life [103-105].

1.3.3.2 Proton-Pump Inhibitors (PPIs)

PPIs were initially used to distinguish EoE from GERD [80]. Recently, they became a first-line therapy option [81] due to newly appreciated anti-inflammatory effects in EoE and PPI-REE [85-88, 106]. PPIs prevent the binding of STAT6 to the eotaxin-3 promoter in epithelial cells from the proximal and distal esophagus, reducing eotaxin-3 expression [107-109]. In PPI-REE, PPI treatment reverses the transcriptomic Th2 signature and reduces IL-5, IL-13, and eotaxin-3 [87, 88, 106]. Furthermore, PPIs restored the esophageal barrier integrity in PPI-REE but not in EoE patients [110]. PPI treatment induces histological remission in 50.5% and improves symptoms in 60.8% of patients [111].

1.3.3.3 Topical corticosteroids

Topical corticosteroids are used for treatment since the identification of EoE as a distinct disease entity. Recently developed, new orodispersible tablet formulations induce (85%) [112, 113] and maintain (75%) [114] disease remission successfully without severe side effects in children and adults (e.g., esophageal candidiasis, adrenal insufficiency, or growth impairment) [114, 115].

1.3.3.4 Biologicals

Lack of natural disease course modification and sustained remission after discontinuation of current treatments [98] generated the need to develop biological drugs interfering with the Th2-driven [74] and epithelium-centered [116, 117] pathophysiology of EoE.

1.3.3.4.1 Anti-IL-5 antibodies

The first tested biological agents for EoE treatment were antibodies against soluble IL-5 due to its fundamental role in eosinophil proliferation, maturation, and activation [62, 63, 118, 119]. Although anti-IL-5 treatments could reduce esophageal and blood eosinophilia, neither histological remission nor symptomatic relief was achieved [120-122]. Despite targeting soluble IL-5 did not appear to be an effective approach, a promising antibody against the IL-5 receptor α-chain, approved for eosinophilic asthma [123], is currently under investigation for the treatment of EoE in a placebo-controlled randomized controlled trial (RCT; NCT03473977).

1.3.3.4.2 Anti-IL-4RA antibody

The human anti-IL-4RA monoclonal antibody dupilumab targets the shared heterodimeric receptor complex (IL-4RA and IL-13RA1) of IL-4 and IL-13. Dupilumab induced and maintained reduction of eosinophil counts, improvement of histological and endoscopic activity, esophageal distensibility, and, most importantly, significant improvement of patient symptoms in a clinical phase 2 RCT [124]. Preliminary results from a phase 3 RCT [125] confirmed these findings.

1.3.3.4.3 Janus kinase (JAK) inhibitors

A third biological treatment option is Janus kinase (JAK) inhibitors due to their implementation in the treatment of inflammatory bowel disease (IBD) [126, 127]. Although clinical trials for JAK inhibitor treatment of EoE are lacking, the JAK1/JAK3 inhibitor tofacitinib induced clinical and endoscopic remission in a case report study of a therapy-resistant EoE patient [128]. Thus, JAK inhibitors may be considered in the future EoE treatment regimen.

1.3.4 Complications

Despite all advances in developing biological treatment options, EoE is a chronic inflammatory disease with a progressive fibrostenotic disease course [129] requiring long-term treatment. Treatment discontinuation is associated with a high risk of relapse [98]. Advanced fibrosis causes strictures and fosters food impaction, often requiring bolus removal in an emergency endoscopy [130, 131]. Esophageal dilation can temporarily treat strictures [132]. However, the increased prevalence of food impaction and irreversible fibrostenotic remodeling with increased risk of perforation or rupture in untreated EoE urge the importance of prompt diagnosis and management of EoE [130, 133, 134].

1.3.5 Esophageal Epithelial Barrier Impairment

Emerging evidence indicates that primary defects of the esophageal epithelial barrier triggered by predisposing genetic polymorphisms play a critical role in the pathophysiology of EoE (Figure 1.3). Genome-wide association studies (GWAS) and candidate-gene analyses identified most EoE risk genes to be expressed by the esophageal epithelium [95, 135, 136]. The EoE transcriptome [137] assessed by RNA sequencing of endoscopic specimens from healthy donors and EoE patients revealed the downregulation of several genes in the EDC, including *FLG* [138]. Hyperproliferation of the undifferentiated basal layers and loss of the differentiated suprabasal layers characterize the esophageal epithelium in EoE [35, 139]. Consequently, downregulated epithelium-specific genes of the EoE transcriptome are associated with keratinization, epidermal development, and differentiation [139]. Furthermore, the concurring reduction of proteins encoded by EDC genes results in functional impairment of the esophageal epithelial barrier in EoE [32, 35, 140]. Experimental approaches indicate that aberrant cytokine signaling can further

deteriorate the perturbed epithelial barrier function. Exemplary, in the biopsies of EoE patients, highly expressed IL-13 [141] not only reproduces congruent transcriptional changes similar to the EoE transcriptome [138, 139, 142] but also disturbs the barrier function in reconstituted esophageal epithelium [35, 143-145].
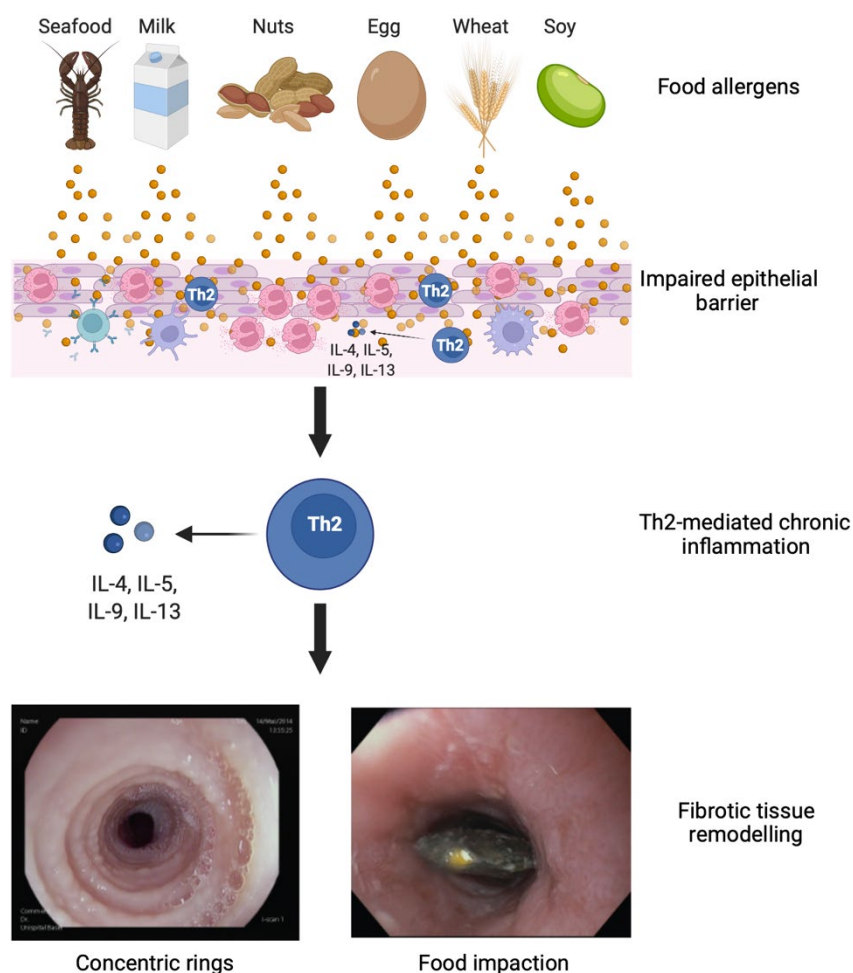
Figure 1.3   Epithelium-centered EoE pathogenesis

Food allergens infiltrate the esophageal epithelium and trigger EoE due to an impaired barrier function. The chronic Th2-mediated immune response in EoE leads to fibrotic tissue remodeling and causes symptoms of esophageal dysfunction (e.g., dysphagia and food impaction). IL: Interleukin, Th2: Type 2 helper T cell. Created with BioRender.com.

Moreover, proteases in a homeostatic interplay with protease-inhibitors inherit a vital role in regulating the epithelial barrier. Protease activity is unleashed due to another protease removing a pro-peptide, while protease-inhibitors bind activated proteases

to regulate their proteolytic activity [146]. An unpoised protease-protease inhibitor interplay disrupts the epithelial barrier by degrading structural proteins and releasing proinflammatory cytokines [12, 14, 147]. Protease-protease inhibitor homeostasis can be disturbed by an increase in proteases or a reduction in protease inhibitors. An example of the former is the IL-13-regulated esophagus-specific protease Calpain-14 (CAPN14), which belongs to the classical calcium-activated calpain family and is an EoE risk gene [135, 136, 145, 148]. IL-13-mediated increase of CAPN14 in the esophageal epithelium impairs the integrity of the esophageal epithelial barrier by degradation of desmosomal proteins in EoE [145, 149]. On the other hand, reduction of the serine protease inhibitor kazal-type (SPINK) family members SPINK5 and SPINK7 in EoE increases the proteolytic activity of kallikrein 5 (KLK5) and other proteases impairing the esophageal epithelial barrier [12, 14]. In contrast to CAPN14, SPINKs are not regulated by IL-13 [14]. Expression of SPINKs increases with differentiation of the epithelium [14].

1.4   The IL-20 subfamily

The IL-20 subfamily is part of the IL-10 family and includes IL-19 [150], IL-20 [151], and IL-24 [152]. The IL-20 subfamily cytokines were identified as IL-10 homologs based on the similarity of their amino acid sequence and co-localization on chromosome 1q32 [151].

1.4.1   IL-20 receptor (IL-20R) complexes

IL-10 family cytokines bind and signal through heterodimeric type 2 cytokine family receptors. The IL-20 subfamily cytokines can signal through two heterodimeric receptor complexes assembled by combining the interleukin-20 receptor subunit beta (IL-20RB/IL-20R2) with the interleukin-20 receptor subunit alpha (IL-20RA) or

interleukin-22 receptor subunit alpha 1 (IL-22RA1) (Figure 1.4) [151, 153]. IL-19, IL-20, and IL-24 are recognized by the type 1 IL-20 receptor (IL-20RA+IL-20RB). IL-20 and IL-24 but not IL-19, also signal through the type 2 IL-20 receptor (IL-22RA1+IL-20RB) [153, 154]. Expression of the IL-20R complexes in the epithelium of tissues like the intestine, skin, and lung defines the intrinsic biological function of the IL-20 cytokine subfamily as a mediator between the immune system and the epithelium [151, 154, 155].

Conversely, immune cells widely express the IL-20RB subunit but lack the expression of an α-subunit and hence do not express a functional IL-20R complex [151, 155]. Consistently, multiple studies report activation of the STAT3 pathway upon signaling of IL-19, IL-20, and IL-24 through the type 1 and type 2 IL-20R complex in epithelial cells but not in immune cells [151, 153-155].
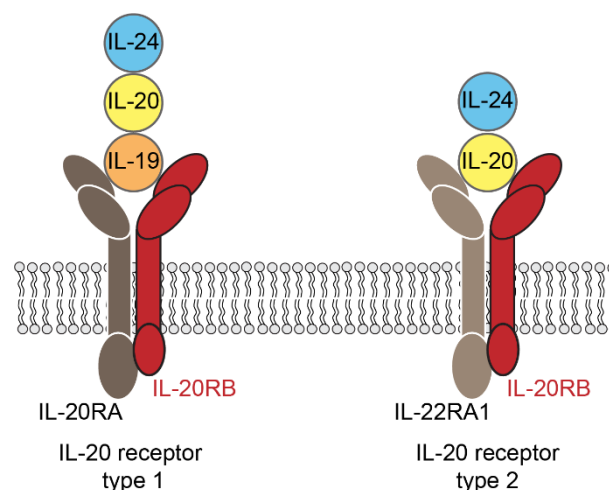
Figure 1.4   **The IL-20 receptors**

The two heterodimeric IL-20R complexes have a common β-subunit but dimerize with distinct α-subunits. The IL-20R type 1 can bind IL-19, IL-20, and IL-24. In contrast, the IL-20R type 2 can only propagate signaling by IL-20 and IL-24. IL: Interleukin, IL-20RA: Interleukin-20 receptor subunit alpha, IL-20RB: Interleukin-20 receptor subunit beta, IL-22RA1: Interleukin-22 receptor subunit alpha 1.

1.4.2 Cellular sources

Even though immune cells are not the target of IL-20 cytokines, they represent a main source [156]. Of all immune cell populations, myeloid cells are the primary producers of IL-20 subfamily cytokines [150, 156]. Monocytes and macrophages constitutively produce IL-20 cytokines [150, 156]. However, sensing microbial products (e.g., LPS) via TLRs can boost their production substantially [150, 156]. Besides TLR-ligands, GM-CSF, TNF, and IL-4 represent other factors that increase the expression of IL-19 and IL-20 by monocytes [150, 157].

Other immune cell populations also produce IL-20 subfamily members. B cells and DCs produce IL-19 and IL-20, respectively [156, 157]. Th2 cells produce low levels of IL-24 [156, 158], while none of the T cell subsets produce IL-19 and IL-20 [156]. Furthermore, it was initially thought that epithelial cells are only responders to the IL-20 subfamily cytokines, but *in vitro* experiments showed that keratinocytes produce all three IL-20 subfamily cytokines comparable to myeloid cells [155]. IL-20 and IL-24 are constitutively expressed by primary keratinocytes, whereas IL-19 expression is only detectable after IL-1β stimulation or to a lower extent after IL-4 stimulation [155].

1.4.3 Signaling

Given that the IL-20 subfamily cytokines bind two different receptor complexes, which share receptor subunits with other IL-10 family receptor complexes, it raises the question of redundancy for IL-20 subfamily members and the type 1+2 IL-20R complexes. One possibility to achieve cytokine-specific effector functions would be activating different intracellular signaling pathways. STAT3 appears to be the primary IL-20 subfamily-activated pathway through both IL-20R complexes [151, 153, 154]. However, the activation of STAT5, AKT, and ERK1/2 by IL-20 subfamily cytokines has also been reported [159, 160], indicating divergent effects of IL-20 subfamily members

by activating different signal transduction pathways. Another way to dissect signal specificity is tissue-specific expression patterns of the IL-20R subunits. A broader expression of the IL-20RA and IL-20RB subunits across tissue types suggests preferential signaling through the type 1 IL-20R complex [151, 154]. Signal transduction through the type 1 IL-20R complex can be induced equally by all three IL-20 subfamily members [153]. However, in tissues that express all three IL-20R subunits, it is unclear which IL-20R complex IL-20 and IL-24 preferentially bind. Enhanced cell proliferation at lower ligand concentrations by the type 2 IL-20R compared to the type 1 IL-20R complex indicates predominant signal transduction of IL-20 and IL-24 through the former [154].

1.4.4 Biological functions

When discovered, IL-20 was associated with hyperproliferation and aberrant differentiation of the epithelium [151]. While IL-19 was attributed an anti-inflammatory effect similar to IL-10 [150] and IL-24 was found to be proapoptotic and inhibiting tumor growth [161]. However, all IL-20 subfamily members are now linked to epithelial abnormalities [151, 162-164].

The IL-20 subfamily plays a role in Th2-mediated allergic skin and airway inflammation [164-168]. IL-19 and IL-24 facilitate epidermal hyperplasia in a murine skin inflammation model induced by IL-23 injection [162]. Furthermore, overexpression of IL-20 and IL-24 in transgenic mice resulted in neonatal lethality due to epithelial barrier impairment caused by aberrant epidermal proliferation and differentiation [151, 163]. Additionally, epithelial barrier impairment in atopic dermatitis is partly the result of IL-20 and IL-24 mediated downregulation of FLG [165, 169]. Comparable to hyperplastic and hyperproliferative effects in the skin, IL-19 and IL-20 mediate airway hyperplasia and remodeling in allergic asthma and chronic rhinosinusitis [167, 170, 171]. However,

the biological functions of the IL-20 subfamily in the esophagus have not been investigated.

1.5   Aims of the study

The IL-20 subfamily is a mediator between the immune system and the epithelial compartment modulating the epithelial differentiation and barrier function in Th2-mediated chronic inflammatory diseases [164-168]. However, whether the IL-20 subfamily has a crucial role in the differentiation and barrier function of the esophageal epithelium in EoE is yet to be examined.

To address the role of the IL-20 subfamily in EoE, in this Ph.D. thesis, we aim:

i.   To characterize the expression pattern of the IL-20 subfamily cytokines in EoE and to identify the cells that express the IL-20 subfamily cytokines and IL-20R complexes in the esophagus.

ii.   To explore the role of the IL-20 subfamily in the development of EoE.

iii.   To elucidate whether the IL-20 subfamily signaling pathway regulates the esophageal barrier function in EoE.

2 MATERIAL AND METHODS

2.1   Esophageal biopsies from human subjects

Patients referred to the Clarunis – University Center for Gastrointestinal and Liver Diseases for diagnostic esophagogastroduodenoscopy (upper endoscopy) were examined for EoE or suitability as control. Biopsies were obtained from the proximal and distal esophagus and evaluated by an independent pathologist. When endoscopic and histologic signs of esophagitis and motility disorders were absent, no eosinophil infiltration was reported in distal biopsies, and history of EoE was excluded, subjects were considered control individuals. Patients with EoE had a confirmed EoE diagnosis, presented with ≥ 15 eos/hpf in proximal biopsies and symptoms of esophageal dysfunction (e.g., dysphagia and food impaction), and no endoscopic and histologic signs of GERD. All patients signed a written informed consent before upper endoscopy. Detailed patient characteristics are listed in Table 2.1. The study protocol (ethics protocol EKBB 2019-00273) was authorized by the Ethics Committee for Northwest and Central Switzerland (EKNZ) before the commencement of the study.

Table 2.1 Patient characteristics

	Controls (n=30)	Active EoE (n=22)	EoE steroids/ remission (n=12)
Age, mean ± SD	37.74 ± 11.09	38.77 ± 8.55	37.33 ± 11.52
Male sex n (%)	21 (67.74)	16 (72.73)	9 (75)
Body weight, kg, mean ± SD (n)	76.7 ± 17.8 (31)	80.97 ± 18.11 (18)	68.57 ± 9.45 (12)
Time since first EoE symptoms, y. mean ± SD	-	8.09 ± 4.92	7.67 ± 8.02
Time since first EoE diagnosis, y. mean ± SD	-	3.14 ± 3.82	3.25 ± 2.64
History of esophageal dilatations, n (%)	0 (0)	0 (0)	2 (16.67)
History of atopic diseases, n (%)	7 (22.58)	16 (72.73)	9 (75)
Having experienced, n (%)			
− Nausea/Vomiting	11 (36.67)	0 (0)	1 (8.33)
− Heartburn	11 (36.67)	3 (13.64)	4 (33.33)
− Epigastric pain	9 (30)	1 (4.55)	1 (8.33)
− Regurgitation	13 (43.33)	3 (13.64)	3 (25)
− Bloating	2 (6.67)	0 (0)	0 (0)
− Dysphagia	4 (13.33)	22 (100)	12 (100)
− Odynophagia	0 (0)	3 (13.64)	3 (25)
− Food impaction	0 (0)	21 (95.45)	9 (75)
PPI treatment, n (%)	12 (38.71)	7 (31.82)	4 (33.33)
Steroids treatment, n (%)	0 (0)	0 (0)	9 (75)
Peak eos/hpf, mean ± SD	-	83.05 ± 34.96	35.17 ± 59.06
− ≥15 eos/hpf n (%)	-	22 (100)	5 (41.67)
Endoscopist assessment, n (%)			
No signs of EoE	28 (90.32)	1 (4.55)	1 (8.33)
Moderate to severe signs of EoE	3 (9.68)	21 (95.45)	11 (91.67)
− edema	1 (4.76)	10 (45.45)	5 (41.67)
− exsudates	0 (0)	14 (63.64)	6 (50)
− furrows	3 (9.68)	19 (86.36)	7 (58.34)
− rings	0 (0)	14 (63.64)	6 (50)
− stricture	0 (0)	3 (13.64)	2 (16.67)

2.2 Animals

2.2.1 Mouse lines

C57BL/6 (WT), *Il19-TdTomato (Il19^{tdT})* were previously generated in our research group [172], *Il20R2$^{-/-}$* mice were kindly provided by Franz Oswald, Internal Medicine I, University Hospital Ulm, Ulm, Germany [173], *Stat3$^{flox/flox}$* mice were kindly provided by Radek Skoda, Department of Biomedicine, University of Basel, Basel, Switzerland [174], *Cx3cr1^{CreER}* (B6.129P2(Cg)-Cx3cr1$^{tm2.1(cre/ERT2)Litt}$/WganJ) and *Krt5-CreERT2* (B6N.129S6(Cg)-Krt5$^{tm1.1(cre/ERT2)Blh}$/J) were all bred and kept under specific pathogen-free (SPF) conditions in the animal facility of the Department of Biomedicine at the University of Basel in Switzerland. *Stat3$^{flox/flox}$* mice have been crossed with *Krt5-CreERT2 mice* to obtain *Stat3$^{\Delta Krt5}$* mice. The tamoxifen-inducible, Cre-mediated recombination will lead to the excision of *Stat3* in Keratin-5$^+$ squamous epithelial cells. *Il19$^{flox/flox}$* mice have been generated as described below and bred with *Cx3cr1^{CreER}* mice to generate *Il19$^{\Delta CX3CR1}$* mice. The tamoxifen-inducible, Cre-mediated recombination will excise *Il19* in CX3CR1$^+$ cells. Animals (age 6-12 weeks) were randomly assigned to the different experimental groups. At least three mice per group were used for *in vitro* and *in vivo* experiments. Animal experiments have been conducted following the Swiss Federal and Cantonal regulations (animal protocol number 2938 (canton Basel Stadt)).

2.2.2 Generation of *Il19-flox* mouse

The *Il19-flox* mice were generated by Biocytogen Pharmaceuticals (Wakefield, USA). Briefly, homology regions comprising 4.5 kb upstream of the *Il19* exon 4 and 4.0 kb downstream of 3'UTR were subcloned from a BAC clone (RP23-190F9; Invitrogen) from a *C57BL/6J* mouse genomic BAC library. Downstream of 3'UTR, an FRT-flanked Neo resistance positive selection cassette was introduced, and upstream of exon 4

and downstream of 3xStop, two loxP sites were inserted, respectively. *C57BL/6* embryonic stem (ES) cells were transfected after linearization with the targeting vector by electroporation. Southern blotting with 5'probe, 3'probe, and Neo probe (3') was

A

B

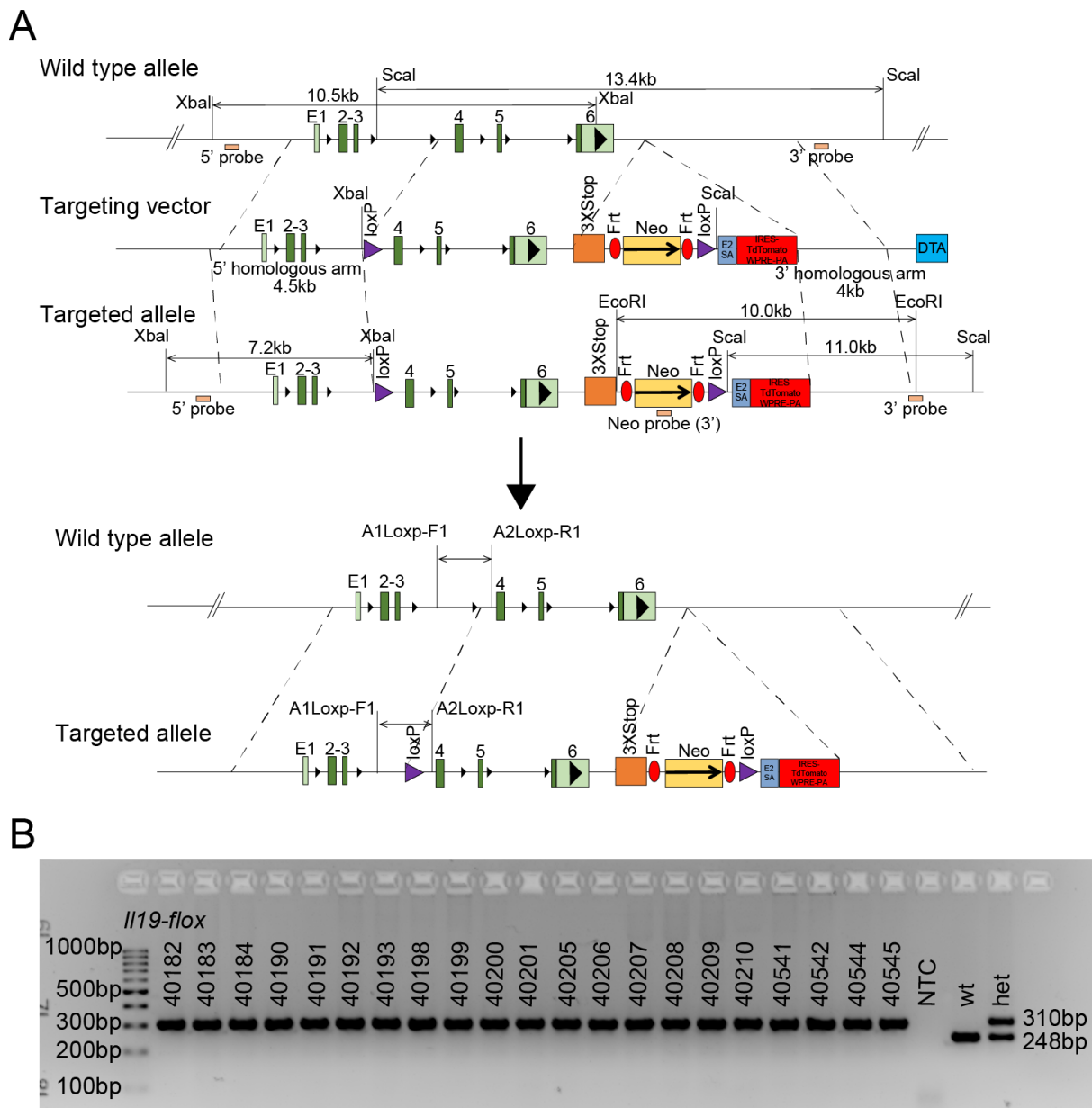**Figure 2.1   Construct of *Il19-flox* and PCR of the genotyping**

(A) Construct scheme for *Il19-flox*. E (exon), Frt: Flippase recognition target, IRES: Internal ribosome entry sites, WPRE: Woodchuck hepatitis virus posttranscriptional regulatory element. (B) PCR products from the genotyping of the *Il19-flox* mice. Product sizes: 248 bp (wt), 310 bp (mutant); wt: wildtype, het: heterozygous, NTC: non-template control.

used to identify seven positive clones, followed by injection of three positive clones into *Balb/c* blastocysts and implantation into pseudopregnant females. Flp mice were crossed with chimeric mice to obtain F1 mice bearing the recombined allele containing the floxed *Il19* and E2 SA IRES-TdTomato-WPRE-pA allele (Figure 2.1). *Il19-flox* mice were genotyped by PCR using the following denaturation protocol at 95^0C for 3 min, 40 amplification cycles at 95^0C 30 sec, 62^0C 30 sec, 72^0C 25 sec, and elongation at 72^0C for 10 min. The respective genotyping primers are listed in Table 5.1.

2.3   Patient-derived 3D Cell Culture

2.3.1   Patient-derived esophageal organoids

Patient-derived esophageal organoids have been generated from esophageal biopsies obtained by upper endoscopy from control and EoE subjects according to an adapted protocol reported by Kasagi et al. [175]. In brief, biopsies were obtained during upper endoscopy, stored on ice in keratinocyte serum-free medium (KSFM; Keratinocyte-SFM (Gibco)), and were processed within a few hours. KSFM was supplemented with 100 U/ml Penicillin, 100 µg/ml Streptomycin (Gibco), 50 µg/ml bovine pituitary extract (BPE; Gibco), 1 ng/ml epidermal growth factor (EGF; Gibco). For processing, the KSFM medium was replaced with 10 U/ml Dispase I (Corning), followed by incubation for 10 min at room temperature (RT). The biopsies were washed with PBS to remove the Dispase I and digested using 0.05% Trypsin-EDTA (Sigma-Aldrich) for 10 min in a ThermoMixer C (Eppendorf) at 37°C and 800rpm. Biopsies were further dissociated using the plunger of a tuberculin syringe when filtered through a 70 µm cell strainer and further filtered through a 35 µm cell strainer (BD Bioscience) into a round bottom polystyrene tube using 250 µg/ml soybean trypsin inhibitor (Sigma-Aldrich). The single-cell suspension was then transferred into a 15 ml falcon tube and centrifuged at 300xg and 4°C for 5 min. The pelleted cells were

resuspended in 100 µl KSFM and counted with an EVE automated cell counter (NanoEntek). The single-cell suspension was pelleted again (300xg, 4°C for 5mins) and resuspended in Cultrex Basement Membrane Extract (BME), Type 2, Pathclear (R&D Systems) to be seeded at a density of 25'000-30'000 cells in a 40 µl droplet in a suspension plate. BME droplets were incubated for 25 min at 37°C for polymerization before adding KSFM-C (The Ca^{2+} concentration was titrated to 0.6 mM using $CaCl_2$; Sigma-Aldrich) supplemented with 10 µM Y27632 small molecule ROCK inhibitor (Tocris). The medium was replaced every two days with new medium not containing the Y27632 small molecule ROCK inhibitor. Patient-derived esophageal organoids were cultured for 5-11 days, and culture conditions were maintained at 37^0C, 5% CO_2.

2.3.2 Patient-derived esophageal air-liquid interface culture (ALI)

Esophageal biopsies from control subjects collected during upper endoscopy were stored in KSFM medium (Keratinocyte-SFM medium containing 50 µg/ml BPE, 100 U/ml Penicillin, 100 µg/ml Streptomycin and 1ng/ml EGF). After isolation of a single-cell solution from biopsies by pre-digestion with 10 U/mL Dispase I (Corning) followed by tissue digestion in 0.05% Trypsin/EDTA (Sigma-Aldrich), biopsies were filtered through 70 µm and 35 µm cell strainers. The single-cell solution of primary keratinocytes was expanded in KSFM (Ca^{2+} 0.09mM) medium in T25 Primaria culture flasks (Corning) and passaged using TrypLE Express Enzyme (Gibco). The expanded primary keratinocytes (≥P2) were seeded on 0.4 µm polyester membrane inserts of 12-well or 24-well transwell plates (Corning) at a density of 200'000 keratinocytes per 0.6 cm^2 (12-well plates) or 155'000 keratinocytes per 0.5 cm^2 (24-well plates). For the first two days, ALI cultures were cultivated with KSFM medium (Ca^{2+} 0.09 mM) until forming a confluent monolayer. KSFM medium was replaced with a Calcium-rich KSFM medium (Ca^{2+} 1.8mM) on day 2 and replenished every other day until day 7.

The medium in the upper compartment was removed on day 7 to induce cornification by air exposure. Additionally, from day 7 on, the calcium-rich KSFM was supplemented with 10ng/ml KGF/FGF7 (R&D Systems) and 75ug/ml L-Ascorbic acid (Sigma-Aldrich). ALI cultures were cultivated for 14 days, and culture conditions were maintained at 37^0C, with 5% CO_2. Where indicated, ALI cultures were treated with100 ng /ml IL-19, IL-20, IL-24, and 50 µM ERK1/2 inhibitor PD98059 (Cell Signaling Technology) or 1 µM cucurtabicin 1 (Tocris) between day 7 and day 14.

2.4   Cell lines

The esophagus squamous cell carcinoma cell line KYSE-180 (ACC 379) was purchased from the Leibniz Institute DSMZ-German Collection of Microorganisms and Cell Cultures. KYSE-180 cells were cultured in 90% Roswell Park Memorial Institute (RPMI) 1640 / 10% FBS supplemented with 100 U/ml Penicillin, 100 µg/ml Streptomycin. The cells were sub-passaged with 0.25% Trypsin-EDTA (SAFC Biosciences) upon 60-80% confluency. Culture conditions were maintained at 37^0C, 5% CO_2, and the medium was replenished every 2-3 days.

2.5   In vivo assays

2.5.1   Ovalbumin (OVA)-induced EoE mouse model

The experimental EoE mouse model protocol has been adapted according to a protocol reported by Noti et al. [176]. Concisely, both ears of the mice were treated with 1 nmol MC903 (calcipotriol; Tocris) in 20 µl absolute ethanol followed by 10 µl of 5 mg/mL ovalbumin (OVA) Grade 5 (Sigma-Aldrich) dissolved in PBS for sensitization. The same volume of ethanol and OVA without MC903 was used as vehicle control. The sensitization phase spans 14 days, and treatment is performed daily. Sensitization is followed by the challenge phase from day 14 to day 18, where the drinking water is

replaced with autoclaved water containing 1.5 g OVA / L. Additionally, mice are challenged with 50 mg OVA dissolved in 100 µl water on days 15 and 17. On day 18, the experiment is terminated, and the mice are sacrificed for organ collection (Figure 2.2). 100uL (75 mg/kg body weight) tamoxifen (MedChemExpress) dissolved in corn oil (Sigma-Aldrich) is injected into *Stat3$^{\Delta Krt5}$* and *Il19$^{\Delta CX3CR1}$* mice, and their respective *Stat3$^{flox/flox}$* and *Il19$^{flox/flox}$* littermates via intraperitoneal injection (i.p.) daily from day 10 until day 18. Animals are categorized in 4 experimental groups: ctrl: non-sensitized+non-challenged, non-sens: non-sensitized+challenged, non-chal: sensitized+non-challenged, sens+chal: sensitized+challenged.
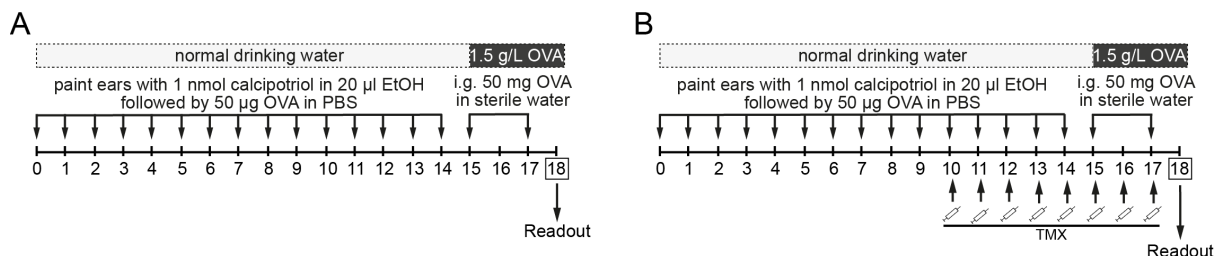
Figure 2.2   OVA-induced experimental EoE mouse model

(A) Schematic illustration of the OVA-induced EoE model characterized by a 14-day sensitization period towards OVA and a subsequent 4-day challenge period with OVA via the drinking water and oral gavage (intragastric; i.g.). (B) Schematic illustration of the OVA-induced EoE model in mouse strains with tamoxifen-inducible genetic modifications. EtOH: Ethanol, OVA: Ovalbumin, PBS: Phosphate-buffered saline, TMX: Tamoxifen.

2.5.2   Treatment of mice with PD98059 (ERK-inhibitor)

Where indicated, *WT* mice were treated with PD98059 (10 mg/kg; MedChemExpress) diluted in 90% saline and 10% dimethyl sulfoxide (DMSO) v/v i.p. daily from day 14 until day 18. (Figure 2.3).
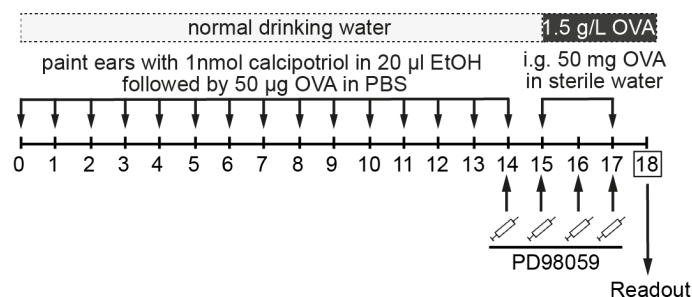
Figure 2.3   ERK-inhibitor (PD98059) treatment in experimental EoE model

Schematic illustration of intraperitoneal (i.p.) ERK-inhibitor treatment with PD98059 in mice during the challenge period of the experimental OVA-induced EoE model. EtOH: Ethanol, OVA: Ovalbumin, PBS: Phosphate-buffered saline.

2.6   In vitro assays

2.6.1   Cytokine stimulation

Patient-derived esophageal organoids, ALI cultures, and KYSE-180 cells were treated with 100 ng/ml IL-19 (R&D Systems), IL-20 (R&D Systems), and IL-24 (R&D Systems) for 6-24 hours (KYSE-180), 24 hours (patient-derived esophageal organoids) or 8 days (ALI cultures). Where indicated, pretreatment with the STAT3 inhibitor cucurtabicin 1 (Tocris) or ERK1/2 inhibitor PD98059 (Cell Signaling Technology) at a final concentration of 1-10 µM or 50 µM was performed 2 h or 1 h prior to cytokine stimulation.

2.6.2   Measurement of transepithelial electrical resistance (TEER) and fluorescein isothiocyanate (FITC)-dextran flux

The integrity of the epithelium in ALI cultures was assessed by transepithelial electrical resistance (TEER) measurements using an EVOM 3 (World Precision Instruments) on days 0, 2, 4, 7, 9, 11, 12, 13, and 14. Permeability of the epithelium in ALI cultures was measured by a paracellular flux assay with FITC-dextran 3-5 kDa (Sigma-Aldrich)

on the last day of culture in intervals of 15 to 30 min for a total of 3 hours and quantified with a fluorescence plate reader (BioTek).

2.6.3 Bone marrow cell isolation and mouse bone marrow-derived macrophages

Murine femurs and tibias were prepared by removing remnant connective tissue and muscles. After that, the bones were cut at the epiphysis and flushed with RPMI 1640 medium (Sigma-Aldrich) to extract the bone marrow. The bone marrow is then filtered through a 70 µm cell strainer. Filtered bone marrow cells were then put in culture and differentiated into macrophages. Shortly, macrophages were generated by culture in RPMI 1640 medium supplemented with 10% FCS, 0.05 mM 2-ME, 100 U/ml penicillin, 100 µg/ml streptomycin, and 20 ng/ml M-CSF (BioLegend). The medium was replaced every other day. After 7 days of culture, macrophages were stimulated with either 100 ng/ml Lipopolysaccharide (LPS) from *Escherichia coli* O111:B4 (Sigma-Aldrich) and 10 ng/ml recombinant mouse IFN-γ (rmIFN-γ; BioLegend) (M1 phenotype) or with 10 ng/ml recombinant mouse IL-4 (rmIL-4; BioLegend) and 10 ng/ml recombinant mouse IL-13 (rmIL-13; BioLegend) (M2 phenotype) for 6 hours.

2.7 Cell isolation from the mouse esophagus

The esophagus is first separated from the trachea and liberated by cutting the proximal and distal ends. The esophagus is then pulled out from the mediastinum and washed in PBS. Before mincing the esophagus for tissue digestion, the remnant connective tissue is removed, cut open longitudinally, and repeatedly washed in PBS. Tissue digestion for 30 min in a shaking water bath (200 rpm) at 37°C is performed in a digestion medium composed of RPMI 1640 (Sigma-Aldrich) with 0.5 mg/ml collagenase IV (Sigma-Aldrich) and 10 U/ml DNase I (Roche). Samples are vortexed

every 10 min preventing the clumping of tissue pieces. Tissue digest is filtered through a 70 µM cell strainer (Sarstedt), obtaining a single-cell solution, which is centrifuged for 5 min at 600xg (4°C), allowing transfer into conical 96-well plates (Sarstedt) for flow cytometry analysis.

2.8   Flow cytometry, cell staining, and antibodies

The esophageal single-cell suspension was stained for 30 min at 4°C with fixable viability dye eFluor455UV (Invitrogen) and anti-CD16/CD32 (Fc receptor) clone 93 (BioLegend) for live/dead cell discrimination and to avoid non-specific binding. Viability staining and Fc-block were followed by centrifugation for 2 min at 500 rpm to pellet the cells and discard the supernatant. Cells were then resuspended in FACS buffer (PBS containing 2% Fetal Bovine Serum (FBS), 0.1% sodium azide, and 10 mM EDTA) and stained for 20 min at 4°C for surface antigen markers. After cell surface marker staining, centrifugation for 2 min at 500rpm is repeated, and the supernatant is discarded. Before stained cells could be acquired on a Fortessa flow cytometer (BD Biosciences), cells stained with biotin-conjugated antibodies had to be stained for 20 min at 4°C with streptavidin for lineage exclusion. All cells were fixated for 20 min with 4% paraformaldehyde (PFA) at RT in the dark. Data analysis was performed using FlowJo software version 10.4.0 (TreeStar). In all analyses, doublets were excluded by doublet discrimination on forward scatter (FSC-H) versus FSC-A plot. Cells were stained using the following antibodies:

Superbright 645-conjugated anti-mouse CD45 clone 30-F11 (Invitrogen), APC-conjugated anti-mouse CD49b (Integrin α2) clone DX5 (Invitrogen), APC/Fire 750-conjugated anti-mouse CD117 (c-kit) clone 2B8 (BioLegend), BV711-conjugated anti-mouse Siglec-F clone E50-2440 (BD Biosciences), FITC-conjugated anti-mouse IgE clone 23G3 (Invitrogen), PE/Cy7-conjugated anti-mouse CD64 (FcγR1) clone X54-

5/7.1 (BioLegend) and FITC-conjugated anti-mouse CD11b clone M1/70 (BioLegend). Biotin-conjugated anti-mouse CD11c clone N418 (BioLegend), anti-mouse CD3e clone 145-2C11 (BioLegend), Biotin-conjugated anti-mouse CD19 clone 6D5 (BioLegend), Biotin-conjugated anti-mouse NK1.1 clone PK136 (BioLegend) and Biotin-conjugated anti-mouse TER-119/Erythroid cells clone TER-119 (BioLegend) followed by either eFluor450/Pacific Blue-conjugated Streptavidin (Invitrogen) or PE-Cy5-conjugated Streptavidin (BioLegend) for lineage exclusion. Eosinophils were identified by discrimination of living, lin⁻, CD45⁺, Siglec-F⁺ cells (Figure 2.4). IL-19 producing macrophages were discriminated as live, lin⁻, CD45⁺, CD11b⁺, CD64⁺, tdTomato⁺ cells.
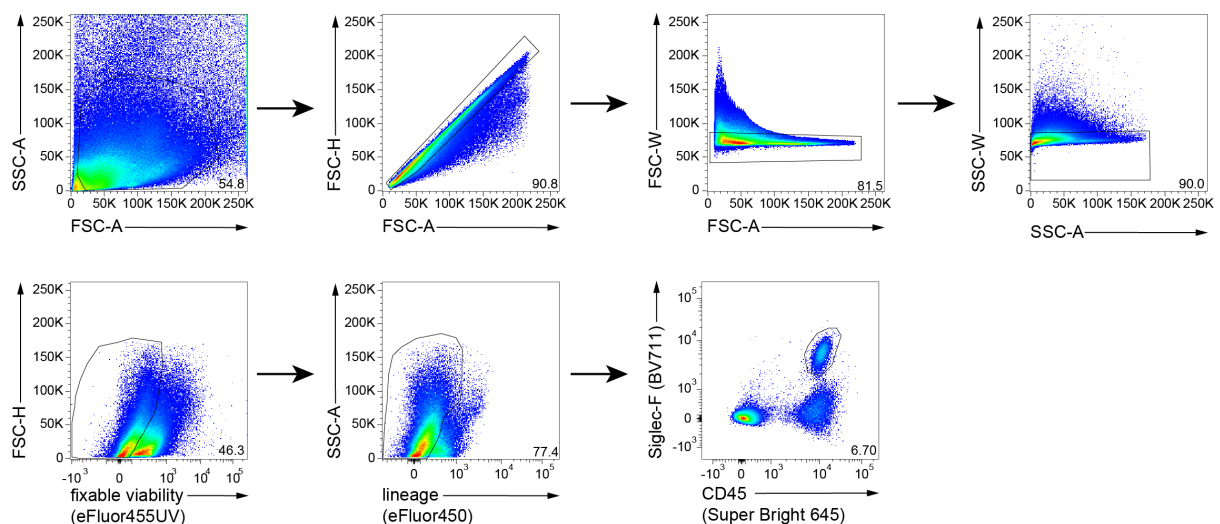
Figure 2.4   Eosinophil gating strategy

Representative flow cytometry dot plots depicting the gating strategy to discriminate live, lin⁻, CD45⁺, Siglec-F⁺ eosinophils in the single-cell suspension isolated from the murine esophagus. FSC: Forward scatter, SSC: Side scatter.

2.9   Histology and Imaging

2.9.1   Histogel embedding

Organoids were separated from BME with 1.5 U/mL Dispase II (Sigma-Aldrich), washed with PBS/1% BSA, and fixated with 1 ml 4% PFA for 30-60 min at RT.

Organoids are centrifuged with 300xg for 5 min at 4°C and washed again with PBS/1% BSA to remove PFA. Centrifugation (300xg for 5mins at 4°C) is repeated, and organoids are resuspended in 70 µl Histogel (Epredia). Histogel is polymerized for 60 min. Afterward, organoids are transferred and stored in 50% EtOH. Paraffin embedding is performed using the TPC 15 Tissue Processor (Medite Medizintechnik) and the TES Valida embedding station (Medite Medizintechnik).

2.9.2   Hematoxylin-Eosin (H&E) staining

Human and mouse esophageal tissues, patient-derived organoids, and ALI cultures are fixed in 4 % PFA and embedded in paraffin blocks. 4 µm sections are stained with H&E, and images are acquired using a Nikon Eclipse Ti2 microscope with a Nikon DS-Ri2 (RGB CMOS) camera. Eosinophil numbers are quantified using Fiji (ImageJ, Version 2.0.0-rc-68/1.52h) [177].

2.9.3   Immunohistochemistry (IHC)

Human and mouse esophageal and patient-derived organoid sections were deparaffinized in xylene and rehydrated in graded EtOH. Antigens were retrieved by incubation in citrate buffer solution (pH=6) for 20 min at 95°C in a microwave tissue processor (KOS). Sections were incubated in 3% hydrogen peroxide (Roth) for 10 min at RT to block endogenous peroxidases. A 1-hour incubation at RT in PBS containing 0.1% Tween20 and 5-10% goat serum (all Sigma-Aldrich) blocked unspecific binding before incubation with the respective primary antibody; a rabbit anti-human IL-20RA monoclonal antibody (Sino Biological Inc.), a rabbit anti-human IL-20RB polyclonal antibody (Abcam), a rabbit anti-Ki67 monoclonal antibody SP6 (Abcam; kindly provided by Rishika Agarwal, Skin biology group, Department of Biomedicine, University of Basel, Basel, Switzerland) or a rabbit anti-human FLG2 polyclonal

(Novus; 1:200) overnight at 4°C. The next day, thoroughly PBS washed sections were incubated for 2 hours at RT with the anti-rabbit IgG horseradish peroxidase-conjugated secondary antibody (Jackson ImmunoResearch; 1:500). Staining was revealed using the chromogenic substrate 3,3' Diaminobenzidine (DAB; BD Pharmingen). Sections were counterstained with hematoxylin, dehydrated with graded EtOH and xylene, and mounted with a xylene-based mounting medium. Images were acquired with a Nikon Eclipse Ti2 microscope using the Nikon DS-Ri2 (RGB CMOS) camera and analyzed with Fiji (ImageJ, Version 2.0.0-rc-68/1.52h) [177] or QuPath [178] software.

2.9.3.1 Ventana Discovery Ultra automated stainer

Ventana Discovery Ultra (Roche Diagnostics Suisse SA) automated stainer was used for FLG staining in human paraffin sections. Briefly, tissue sections were deparaffinized and rehydrated. Cell Conditioning buffer 1 (CC1, Ventana) was used for antigen retrieval at 95°C for 40 min. Sections were incubated with the manually applied primary rabbit anti-human FLG polyclonal (Abcam, 1:100) for 1 hour at 37°C. Sections were similarly incubated with an HRP-Polymer secondary antibody for 1 hour at 37°C after the primary antibody was washed away. To further amplify the FLG signal prior to detection, an amplification kit (Ventana) was used. The Ventana DISCOVERY ChromoMap DAB (Ventana) detection kit was used for FLG signal detection. Hematoxylin II and the bluing reagent (Ventana) were used to counterstain the tissue, followed by dehydration, clearance, and mounting with a permanent mounting medium and coverslips. Images were acquired with a Nikon Eclipse Ti2 microscope using the Nikon DS-Ri2 (RGB CMOS) camera and analyzed with Fiji (ImageJ, Version 2.0.0-rc-68/1.52h) [177] or QuPath [178] software.

2.9.4 Immunofluorescence staining

Murine esophageal tissues were fixed with 4% PFA and embedded in paraffin. All tissues were cut at 4 µm. Sections were blocked and permeabilized with PBS containing 0.1% Tween20 and 5-10% Goat serum (all Sigma-Aldrich). Murine esophageal sections were stained with chicken anti-Keratin 5 polyclonal clone Poly9059 (BioLegend) and Alexa Fluor 488 AffiniPure goat anti-chicken IgY (IgG) (H+L) secondary antibody (Jackson ImmunoResearch) together with rabbit anti-Stat3 monoclonal clone D3Z2G (Cell Signaling Technology) and Alexa Fluor 647 goat anti-rabbit IgG secondary antibody (Invitrogen). Nuclear staining was performed using Nuc Blue™ Live Cell Stain (Invitrogen) in all samples, and images were acquired using a Nikon A1R confocal microscope. The NIS software maintained the brightness and contrast settings between all images.

2.10 RNA extraction and reverse-transcription quantitative PCR (RT-qPCR)

2.10.1 Esophageal organoid RNA isolation

Patient-derived organoids were retrieved from BME by digestion with 1.5 U/mL Dispase II (Sigma-Aldrich) for 20-25 min at 37°C. After BME digestion, the patient-derived organoids were washed with PBS/1% BSA and centrifuged at 300xg for 5mins at 4°C. PBS was discarded, and 1 ml RNA lysis buffer (Qiagen) was added. The patient-derived organoids were vortexed and resuspended with a pipette until all organoids were dissolved and transferred to 1.5 ml Eppendorf Tube (Sarstedt) for storage at -80°C until further usage. RNA was isolated with the RNeasy Plus Mini Kit (Qiagen) according to the manufacturers' instructions.

2.10.2   RNA isolation and RT-qPCR

RNA was obtained from human esophageal biopsies, mouse esophagus, bone marrow-derived macrophages, and the KYSE-180 cell line with TRI Reagent (Sigma-Aldrich) or Direct-zol RNA MiniPrep (Zymo Research) according to the manufacturers' instructions. DNA contaminants were removed using the DNase Max Kit (Qiagen). The High-Capacity cDNA Reverse Transcription (Applied Biosystems) kit was used according to the manufacturers' instructions for reverse transcription of the RNA. Quantitative PCRs were run on an ABI ViiA 7 cycler using the SYBR Green PCR (Qiagen) or TakyonLow Rox SYBR MasterMix blue (Eurogentec) kits. Relative expression of genes was calculated using the $2^{\wedge}(-\Delta Ct)$ formula after normalization of Ct values to *GAPDH* or *ACTB* for human samples and *Actb* for mouse samples used as housekeeping genes. Primers are listed in Table 5.2.

2.11   RNA-sequencing (RNA-seq)

2.11.1   Bulk RNA-sequencing

On day 11 of culture, patient-derived organoids derived from five healthy donors underwent a 24-hour cytokine treatment with 100ng/ml IL19, IL20, and IL24. At the same time, unstimulated esophageal organoids from the same donors were kept in culture. RNeasy Plus Mini Kit (Qiagen) was used according to the manufacturers' instructions to isolate total RNA, which was quality-checked on a Bioanalyzer instrument (Agilent Technologies, Santa Clara, CA, USA) with the RNA 6000 Nano Chip (Agilent Technologies, Santa Clara, CA, USA) and quantified by Spectrophotometry with the NanoDrop ND-1000 Instrument (NanoDrop Technologies, Wilmington, DE, USA). RNA-sequencing (RNA-seq) libraries were prepared at the Genomics Facility Basel of the ETH Zurich, Basel. 220ng total RNA of each sample was processed for library preparation with the TruSeq Stranded mRNA LT Sample

Prep Kit (Illumina, San Diego, CA, USA). RNA-seq library quality was checked on the Fragment Analyzer (Advanced Analytical, Ames, IA, USA) with the Standard Sensitivity NGS Fragment Analysis Kit (Advanced Analytical) (average concentration was 126±13 nmol/L and average library size was 345±7 base pairs), and samples were pooled to equal molarity. Each pool was quantified by PicoGreen Fluorometric measurement to be adjusted to 1.5 pM and used for clustering on the NextSeq 500 instrument (Illumina). Paired-end 38nt reads were assembled using the NextSeq 500 High Output Kit 75-cycles (Illumina). Raw fastq files were produced using the Illumina RTA version 2.4.11 and bcl2fastq-2.18.0.12.

Data analysis was conducted by the Bioinformatics Core Facility, Department of Biomedicine, University of Basel. Read quality was determined with the FastQC tool (version 0.11.5). Reads were mapped to the human genome hg38 "analysis set" with STAR (version 2.7.0c) [179] with default parameters, except filtering out multi mapping reads with more than 10 alignment locations (*outFilterMultimapNmax=10*) and filtering reads without evidence in the spliced junction table (*outFilterType= "BySJout"*). All subsequent analyses were done with the R software (version 4.0.3) and Bioconductor 3.12 packages. The *featureCounts* function from the Bioconductor Rsubread package (version 2.0.1) [180] was used to count the number of reads (5' ends) overlapping with the exons of each gene (Ensembl release 96), estimating an exon union model [181, 182].

Differential gene expression analysis was done with the Bioconductor package edgeR (version 3.30.3) [183]. Normalization between samples was performed using the TMM method [184]. Genes with CPM values above 1 in at least four samples were used for the differential expression analysis. A model accounting for the condition and donor effects was fitted to the read counts using a quasi-likelihood testing framework (edgeR

functions *glmQLFit* and *glmQLFTest*) [185] to test for differences between the stimulated and unstimulated organoids. P-values were adjusted by controlling the false discovery rate (FDR; Benjamini-Hochberg method), and genes with an FDR lower than 1% were considered significant. Gene set enrichment analysis (GSEA) was performed with the function camera [186] from the edgeR package (using the default parameter value of 0.01 for the correlations of genes within gene sets) using gene sets from the c5 collection (Gene Ontology categories) of the MSigDB Molecular Signature Database (version 7.0) [187]. Gene sets containing less than ten genes were excluded, and gene sets with an FDR lower than 5% were considered significant. The processed read count table of the RNA-seq dataset is available on GEO under accession GSE181261 (https://www.ncbi.nlm.nih.gov/geo/query/acc.cgi?acc=GSE181261).

2.11.2 Reanalysis of public RNA-seq datasets

Raw data for the accessions GSE58640 [137], GSE65335 [142], and GSE103356 [14] were recovered from the GEO database and analyzed as previously described to identify genes and gene sets differentially regulated between (i) esophageal tissues from patients with eosinophilic esophagitis vs. control donors, (ii) IL-13 stimulated vs. unstimulated differentiated EPC2 immortalized esophageal epithelial cells and (iii) SPINK7-silenced vs. control differentiated EPC2 cells, respectively.

For unidentifiable reasons, in GSE58640, all samples but one included paired-end reads. Therefore, the sample GSM1415921 sequenced with single-end reads was excluded, resulting in 15 samples (6 healthy donors and 9 EoE patients). Donors of different sex were present in both groups, a factor associated with the second component of principal component analysis. We, thus, included sex as a covariate in the model for differential expression analysis.

2.11.3 Single-cell RNA-sequencing (scRNA-seq)

Esophageal tissue samples from *WT* and *Il20R2^-/-* mice with experimental EoE were processed as previously described, and TotalSeq-B antibodies (BioLegend) were applied to barcode the individual single-cell suspensions. Hash-tagging antibodies TotalSeq-B0301 to B0305 (BioLegend) were applied to samples from *WT* mice and TotalSeq-B0306 to B0310 to samples from *Il20R2^-/-* mice. The pooled and hash-tagged single-cell suspension was sorted for viable CD45.2$^+$ (BioLegend) cells by fluorescence-activated cell sorting (FACS). Volumes aiming at a targeted recovery of 10,000 cells were loaded onto two wells of a 10x Genomics Chromium Single Cell Controller to generate 3'end libraries using v3 chemistry. Single-cell libraries were sequenced on an SP flow-cell of an Illumina NovaSeq 6000 sequencer at the Genomics Facility Basel of the ETH Zurich (with 90nt-long R2 reads).

Cellranger (version 6.0.1) was used for library and cell barcode demultiplexing, read alignment to the mouse transcriptome (Ensembl release 98) [188], and generation of the table of UMI counts. Further processing of the UMI counts table was done by using R 4.0.5 and Bioconductor 3.12 packages, notably DropletUtils (version 1.10.3) [189, 190], scran (version 1.18.7) [191], and scater (version 1.18.6) [192], mainly following the steps reported in the Bioconductor OSCA book (https://bioconductor.org/books/release/OSCA/) [181, 191]. All Cells were demultiplexed into their sample of origin using the function *hashedDrops* from the DropletUtils package (with default parameters except *min.prop=0.01* and providing as input the relative abundances of HTOs in the ambient solution). Based on the detected distributions, cells with 0% or more than 10% of UMI counts were attributed to the mitochondrial genes [193]. Cells with less than 1,000 UMI counts or less than 500 detected genes were excluded. Doublets determined by the *hashedDrops* function or

the scDblFinder package (version 1.4.0) were excluded. 2,633 KO cells (ranging from 500 to 897 cells per sample) and 3,421 WT cells (ranging from 271 to 877 cells per sample) were used for the subsequent analysis steps. UMI counts were normalized with size factors estimated from pools of cells created with the scran package *quickCluster* function [191, 194]. To differentiate between natural biological variability and technical noise, we modeled the variance of the log-expression across genes using a Poisson-based mean-variance trend. The scran package *denoisePCA* function was taken advantage of to denoise log-expression data by removing principal components corresponding to technical noise (20 PCs retained). The single-cell RNA-sequencing (scRNA-seq) dataset is available on GEO under accession GSE190482 (https://www.ncbi.nlm.nih.gov/geo/query/acc.cgi?acc=GSE190482).

2.12   Proteomics

Patient-derived organoids were lysed using 100 µl protein lysis buffer (5% SDS, 10 mM TCEP, 100 mM Triethyloammonium bicarbonate (TEAB), pH = 8.5) after BME was digested by 1.5 U/ml Dispase II (Sigma-Aldrich). Complete lysis of patient-derived organoids was confirmed after one cycle in the tissue lyser (Qiagen) at 4°C and 25/s, followed by three freeze-thaw cycles with dry ice. After complete lysis, the samples were centrifuged at maximum speed for 20min (4°C), and the protein lysate was transferred without debris into a new 1.5 ml Eppendorf tube. Protein concentration was assessed by BCA assay (Thermo Fisher Scientific). Sample aliquots containing 50 µg of total protein were reduced for 10 min at 95°C and alkylated at 15 mM iodoacetamide for 30 min at 25°C in the dark. According to the manufacturer's instructions, proteins were purified and digested using S-traps microcolumns (Protifi, NY, US). Samples were dried under vacuum and stored at -80 °C until further use.

Sample aliquots comprising 5 µg of peptides were labeled with isobaric tandem mass tags (TMT 10-plex, Thermo Fisher Scientific) as previously described [195] using a Freedom Evo 100 liquid handling platform (Tecan Group Ltd., Männedorf, Switzerland). Briefly, peptides were resuspended in a 10 µl labeling buffer (2 M urea, 0.2 M HEPES, pH 8.3), and 2.5 µl of each TMT reagent was added to the individual peptide samples, followed by a 1-hour incubation at 25°C, shaking at 500 rpm. The addition of 0.75 µl aqueous 1.5 M hydroxylamine solution followed by incubation for 10 min at 25°C stopped the labeling reaction. After pooling, adding 1M phosphate buffer (pH 12) increased the pH to 11.9 to remove TMT labels linked to peptide hydroxyl groups after incubation for 20 min at 25°C. Subsequently, the reaction was quenched by decreasing the pH to < 2 with 2 M hydrochloric acid. Finally, the peptide sample was further acidified using 5 % TFA, desalted using Sep-Pak Vac 1cc (50 mg) C18 cartridges (Waters) according to the manufacturer's instructions, and dried under vacuum.

Fractionation of TMT-labeled peptides was achieved by high-pH reversed-phase separation using an XBridge Peptide BEH C18 column (3,5 µm, 130 Å, 1 mm x 150 mm, Waters) on an Agilent 1260 Infinity HPLC system. Peptides were loaded on a column in buffer A (20 mM ammonium formate in water, pH 10) and eluted using a two-step linear gradient from 2% to 10% in 5 min and then to 50% buffer B (20 mM ammonium formate in 90% acetonitrile, pH 10) over 55 min at a flow rate of 42 µl/min. The elution of peptides was monitored with a UV detector (215 nm, 254 nm). Thirty-six fractions were collected and pooled into 12 fractions using a post-concatenation strategy described previously [196] and vacuum-dried.

0.1% aqueous formic acid was used to resuspend dried peptides subjected to LC-MS/MS analysis using an Exploris 480 Mass Spectrometer fitted with an Ultimate 3000

nano-LC (both Thermo Fisher Scientific) and a custom-made column heater adjusted to 60°C. Peptides were resolved using an RP-HPLC column (75μm × 30cm) packed in-house with C18 resin (ReproSil-Pur C18–AQ, 1.9 µm resin; Dr. Maisch GmbH) at a flow rate of 0.3 µLmin-1. Peptide separation was achieved using the following gradient: from 2% B to 10% B over 5 min to 30% B over 70 min to 50 % B over 15 min to 95% B over 2 min, followed by 18 min at 95% B. Buffer A was 0.1% formic acid in water, and buffer B was 80% acetonitrile and 0.1% formic acid in water.

The mass spectrometer was run in DDA mode with a FAIMS device attached. FAIMS was operated in standard resolution mode with two alternating CV voltages of -45 and -60V. Total cycle time of approximately 3 s (1.5s per CV voltage). Each MS1 scan was followed by high-collision-dissociation (HCD) of the most abundant precursor ions with dynamic exclusion set to 30 seconds. For MS1, the AGC target was set to 300% with a fill time of 25 ms using a resolution of 120,000 FWHM (at 200 m/z). MS2 scans were acquired at a target setting of 200%, a maximum accumulation time of 100 ms, and a resolution of 30,000 FWHM (at 200 m/z) with the enabled TurboTMT option. Singly charged ions and ions with unassigned charge states were excluded from triggering MS2 events. The normalized collision energy was 38%, the mass isolation window was set to 0.7 m/z, and one Microscan was acquired for each spectrum. The precursor fit threshold was set to 70 % at a fit mass window size of 0.7 m/z.

The acquired raw files were compared against a protein database containing sequences of the predicted SwissProt entries of *homo sapiens* (www.ebi.ac.uk, release date 2020/04/17) and commonly observed contaminants (in total 20,742 sequences) using the SpectroMine software (Biognosys, version 1.0.20235.13.16424). Standard Pulsar search settings for TMT ("TMT_Quantification") were applied. The global minimum value substituted missing

intensities, and in a given sample, the intensities of all peptides belonging to the same protein were summed up.

The discrepancies in protein levels between the stimulated and unstimulated organoids were tested using the package limma (version 3.44.3) [197] by fitting a linear model accounting for the condition and donor effects to the TMM-normalized logCPM (counts per million) values with the *eBayes* function options *trend=TRUE* and *robust=TRUE*. Given the low number of differentially expressed proteins, we used an FDR cutoff of 20% for significance. The GSEA was performed similarly to the RNA-seq dataset. The mass spectrometry proteomics data were deposited to the ProteomeXchange Consortium via the PRIDE [198] partner repository with the dataset identifier PXD031509 and 10.6019/PXD031509.

2.13   Enzyme-linked immunosorbent assay (ELISA)

The serum concentration of IL-19, IL-20, and IL-24 in controls and active and inactive EoE subjects were assessed using the human IL-19 Quantikine ELISA Kit (R&D Systems), the human IL-20 Quantikine ELISA Kit (R&D Systems), and the human IL-24 DuoSet ELISA (R&D Systems) kit.

Total IgE and OVA-specific IgE titers were determined with the ELISA MAX™ Deluxe Set Mouse IgE kit (BioLegend) and the LEGEND MAX™ Mouse OVA-specific IgE ELISA kit (BioLegend) in the serum of *WT*, *Il19^{tdT}*, and *Il20R2^{-/-}* mice. Absorbance was measured at 450 nm and 570 nm on a microplate-ELISA reader (BioTek). The absorbance at 570 nm was subtracted from absorbance at 450 nm.

2.14   Immunoblotting

Ice-cold RIPA buffer containing sodium orthovanadate, PMSF, and protease inhibitor cocktail (Santa Cruz) was used to lyse KYSE-180 cells after stimulation with IL-19, IL-

20, and IL-24 for the indicated period. Protein concentrations were assessed by Bicinchoninic Acid (BCA) assay. After that, electrophoretic separation was used for transferring 10-20 µg protein of each sample onto a nitrocellulose membrane. The membrane was blocked with 5% dry milk in Tris Buffered Saline + 0.1% Tween20 (TBS-T) buffer for 1 hour and incubated with one of the following primary antibodies overnight at 4°C: phospho- NF-κB (p65), NF-κB, phospho- ERK1/2, ERK1/2, phospho-STAT3, STAT3 (all from Cell Signaling Technology) and β-actin (BD Biosciences) at 1:1000 or 1:2000 dilution, respectively. After washing thrice in TBS-T for 5 min, the membrane was incubated with horseradish peroxidase-conjugated secondary antibodies anti-rabbit IgG (H+L) and anti-mouse IgG (H+L) (both Jackson ImmunoResearch) at 1:30000 dilution for 1 hour at RT. After washing another three times in TBS-T for 5 min, the blots were developed using SuperSignal™ West Femto Maximum Sensitivity Substrate or SuperSignal™ West Pico PLUS Chemiluminescent Substrate (both Thermo Scientific).

2.15   Statistical analysis

Data are presented as dot plots and represent individual values with medians. Generation of graphs and statistical analysis was performed with GraphPad Prism software. Based on the experimental set-up, p-values were calculated by either Mann-Whitney U, Wilcoxon, Kruskal-Wallis, or two-way ANOVA tests. The Grubbs test identified outliers. P values were defined as following: *$p \leq 0.05$, **$p \leq 0.01$, ***$p \leq 0.001$, ****$p \leq 0.0001$.

3 RESULTS

3.1 Increased IL-20 subfamily expression in EoE

3.1.1 Elevated IL-20 subfamily expression in esophageal biopsies and serum of patients with active EoE

A substantial role in Th2-mediated allergic diseases of the skin [165] and the airways [166, 167] sparked our interest in investigating the IL-20 subfamily in the esophagus and EoE. Treatment-naïve EoE patients with active disease have significantly increased expression of *IL19* and *IL20* and tendentially increased expression of *IL24* in esophageal biopsies compared to control individuals (Figure 3.1A). On the other hand, topical corticosteroid-treated inactive EoE patients have lower expression of *IL19, IL20,* and *IL24* (Figure 3.1A+B). Besides increased esophageal expression, serum concentrations of IL-19, IL-20, and IL-24 are significantly increased in patients with active EoE (Figure 3.1C). Like tissue expressions, IL-20 subfamily serum concentrations were reduced in topical corticosteroid-treated inactive EoE patients (Figure 3.1C).
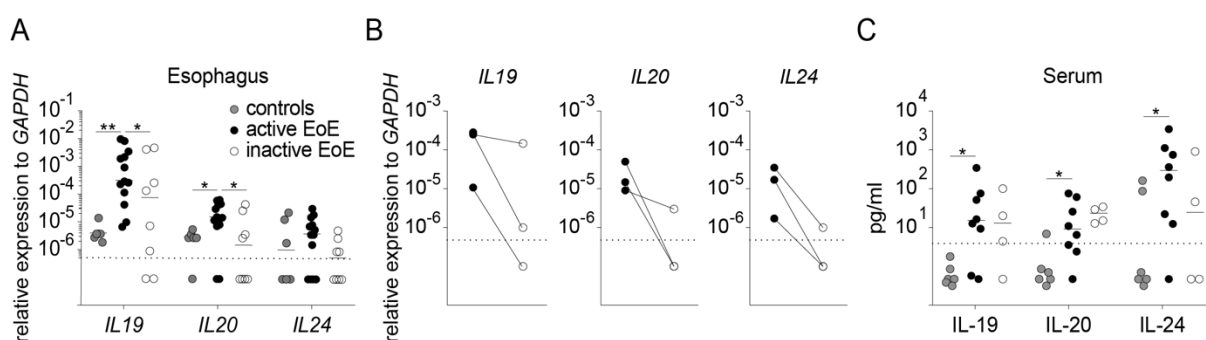

Figure 3.1   Increased IL-20 subfamily cytokines in active EoE

(A) Esophageal mRNA expression of IL19, IL20, and IL24 in control individuals *and patients with* active and inactive EoE *assessed* by RT-qPCR. (B) mRNA expression of IL19, IL20, and IL24 in paired esophageal biopsies of patients with active and inactive EoE after treatment with topical corticosteroids *assessed* by RT-qPCR. (C) IL-19, IL-20, and IL-24 serum concentrations of control

individuals *and patients with* active and inactive EoE measured by ELISA. Data are presented as individual values with medians, and each dot or line represents one biological replicate; *p ≤ 0.05, **p ≤ 0.01 by Mann-Whitney U test. *GAPDH:* Glyceraldehyde 3-phosphate dehydrogenase, IL: Interleukin

3.1.2 Increased expression of IL-20 subfamily cytokines in the experimental EoE mouse model

To investigate the IL-20 subfamily *in vivo*, we established an experimental EoE mouse model (Figure 2.2). Based on sensitization to food particles via a damaged epithelial barrier in EoE patients [199-201], we adopted an experimental mouse model induced by epicutaneous sensitization towards ovalbumin (OVA) [176]. Epicutaneous sensitization of *WT* mice and subsequent challenge with OVA by oral gavage and supplementation of the drinking water (chal+sens) resulted in esophageal eosinophil infiltration as the hallmark attribute of experimental EoE (Figure 3.2A-D). Control groups of untreated (ctrl), non-sensitized but challenged (non-sens), and sensitized but not challenged (non-chal) mice did not acquire features of an experimental EoE (Figure 3.2A-D).
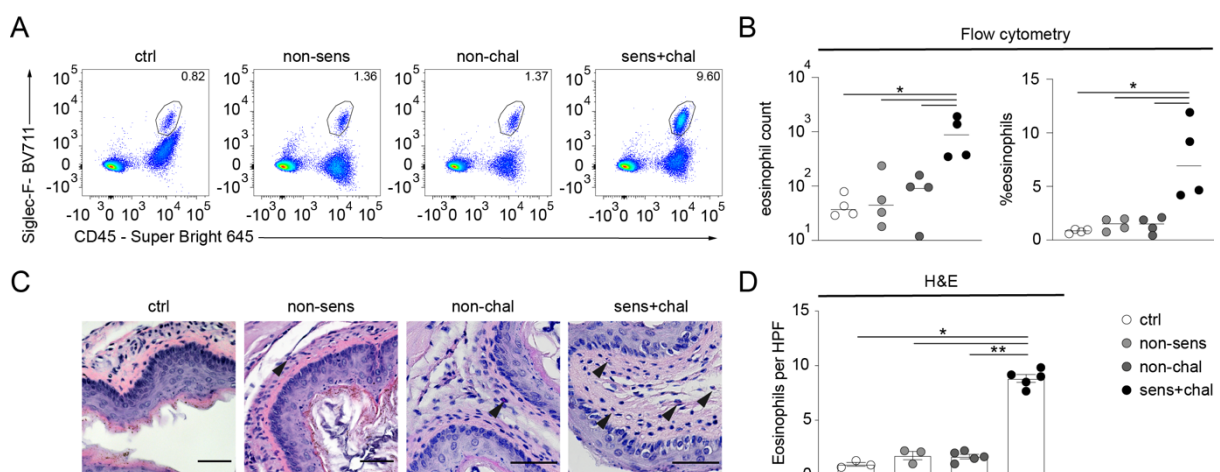

Figure 3.2   Esophageal eosinophilia characterizes experimental EoE

(A) Representative flow cytometry dot plots showing infiltrating eosinophils in the esophagus of *WT* mice on day 18 of the OVA-induced experimental EoE mouse model. (B) Absolute number and percentage of esophagus infiltrating eosinophils as assessed by flow cytometry. (C) Representative

H&E staining of esophagus sections from *WT* mice on day 18 of the OVA-induced experimental EoE mouse model. Arrows mark eosinophils. Scale bars, 50 µM. (D) Quantified esophageal eosinophils from (C); ctrl: non-sensitized+non-challenged, non-sens: non-sensitized+challenged, non-chal: sensitized+non-challenged, sens+chal: sensitized+challenged. Data are presented as individual values with medians, and each dot represents one biological replicate. *p<0.05, **p<0.01, by Mann-Whitney U test. HPF: High-power field.

Coherent with patient data, the development of experimental EoE in mice induces increased expression of *Il19*, *Il20*, and *Il24* compared to animals in the ctrl and non-chal experimental groups (Figure 3.3).
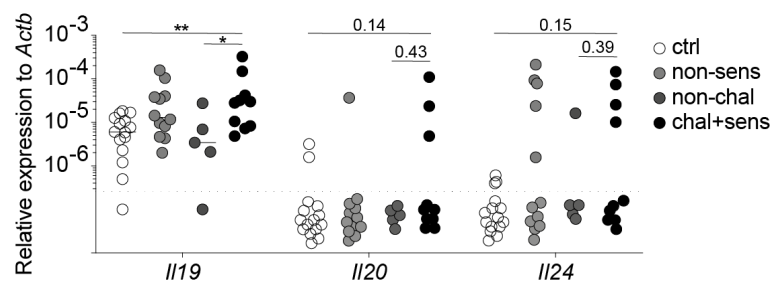

Figure 3.3   Esophageal IL-20 subfamily expression increases in the experimental EoE mouse model

Il19, *Il20,* and *Il24* mRNA levels in the esophagus of *WT* mice on day 18 of the OVA-induced experimental EoE mouse model assessed by RT-qPCR; ctrl: non-sensitized+non-challenged, non-sens: non-sensitized+challenged, non-chal: sensitized+non-challenged, sens+chal: sensitized+challenged. Data are presented as individual values with medians, and each dot represents one biological replicate. *p<0.05, **p<0.01, by Mann-Whitney U test. Actb: Beta-actin, Il: Interleukin.

3.1.3   Macrophages in the esophagus can produce IL-20 subfamily cytokines

Elevated IL-20 subfamily cytokines in EoE patients and the experimental EoE mouse model prompted us to explore the cellular source of IL-20 subfamily cytokines in the esophagus. To identify cells that produce IL-19, we took advantage of an *Il19^{tdT}* reporter mouse line previously generated by our research group [172]. Flow cytometry analysis portends esophageal macrophages to be the source of IL-19 in experimental

EoE (Figure 3.4A+B). Expression of *Il19*, *Il20,* and *Il24* by M1 polarized murine bone marrow-derived macrophages (BMDMs) and *Il19* expression by M2 polarized BMDMs (Figure 3.4C) substantiates the indication that macrophages are a source of IL-20 subfamily cytokines in the esophagus.
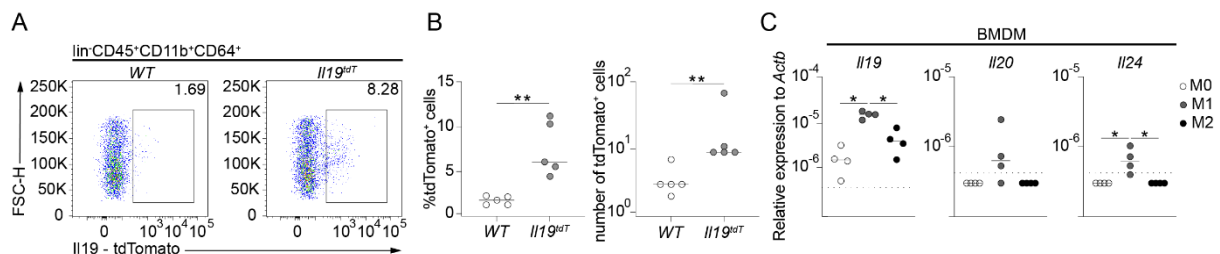

Figure 3.4   Esophageal macrophages produce IL-20 subfamily cytokines

(A) Representative flow cytometry dot plots indicate infiltration of IL-19-producing macrophages (CD45+CD11b+CD64+tdTomato+) into the esophagus of *Il19^{tdT}* mice with experimental EoE.

(B) Absolute cell number and percentage of IL-19-producing macrophages (CD45+CD11b+CD64+tdTomato+) infiltrating the esophagus as assessed by flow cytometry.

(C) mRNA levels of *Il19*, *Il20,* and *Il24* in M0, M1, and M2 polarized BMDMs assessed by RT-qPCR. Data are presented as individual values with medians, and each dot represents one biological replicate. *p<0.05, **p<0.01, by Mann-Whitney U test. Actb: Beta-actin, BMDMs: Bone marrow-derived macrophages, FSC: forward scatter, Il: Interleukin, WT: wild type.

3.2   IL-20 receptor (IL-20R) complex expression in the esophagus

3.2.1   Epithelial cells in patient biopsies express the IL-20R type 1

Examining the existence of a functional IL-20R in the esophagus, we analyzed the expression of the IL-20R subunits, *IL20RA*, *IL20RB*, and *IL22RA1*, in esophageal biopsies. RT-qPCR analysis indicated the expression of all three receptor subunits in the esophagus (Figure 3.5A). In addition, the expression of *IL20RA* and *IL20RB* were lower in the biopsies of patients with active and inactive EoE than in control individuals (Figure 3.5A).

IL-20Rs are generally expressed by epithelial cells [151, 154, 155]. To assess IL-20 subfamily sensory cells in the esophagus, we conducted immunohistochemistry (IHC) staining for IL-20RA and IL-20RB, identifying prevailing expression by esophageal epithelial cells (Figure 3.5B).
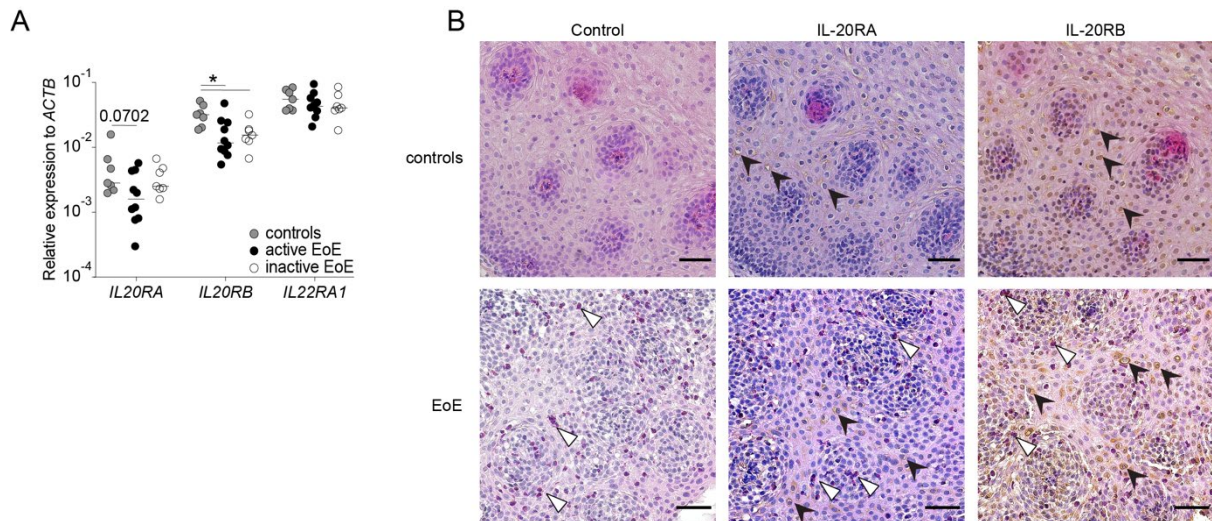

Figure 3.5   The esophageal epithelium expresses the IL-20R complexes

(A) mRNA levels of *IL20RA*, *IL20RB*, and *IL22RA1* in esophageal biopsies from control individuals and patients with active and inactive EoE assessed by RT-qPCR. (B) Representative control staining and staining for IL-20RA and IL-20RB in histological sections from the proximal esophagus of control individuals and patients with active EoE. White arrowheads mark eosinophils; black arrowheads mark IL-20RA and IL-20RB staining. Scale bars, 50 µm. Data are presented as individual values with medians, and each dot represents one biological replicate. *$p \leq 0.05$ by Mann-Whitney U test. ACTB: Beta-actin, IL: Interleukin.

3.2.2   Pronounced expression of type 1 IL-20R by squamous epithelium in the murine gastrointestinal tract

Because we detected increased IL-20 subfamily expression in the experimental EoE model, we aimed to characterize the expression of the type 1 IL-20R in the murine gastrointestinal tract. RT-qPCR results revealed enriched expression of the *Il20ra* and

Il20rb subunit in the upper gastrointestinal tract lined by squamous epithelium compared to the columnar epithelium lined organs of the lower intestine (Figure 3.6).
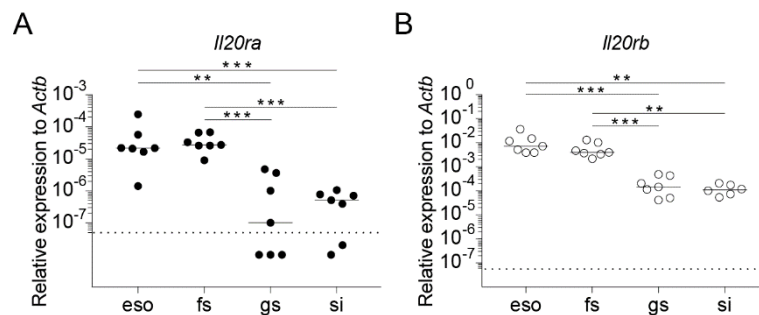

Figure 3.6   Accentuated expression of Il20r subunits in squamous epithelium-lined organs in the murine gastrointestinal tract

(A) *Il20ra* and (B) *Il20rb* mRNA levels in the esophagus (eso), forestomach (fs), glandular stomach (gs), and small intestine (si) of *WT* mice assessed by RT-qPCR. Data are presented as individual values with medians, and each dot represents one biological replicate. **$p < 0.01$, ***$p < 0.001$, by Mann-Whitney U test. Actb: Beta-actin.

3.2.3   Lack of a functional IL-20R in murine immune cells

Production of IL-19 by macrophages in the murine esophagus raised the question of an autocrine or paracrine effect on nearby immune cells. We, therefore, analyzed the expression of *Il20r* subunits by BMDMs. Indeed, BMDMs express the *Il20rb* subunit, with an enriched pattern in M2 polarized BMDMs. However, BMDMs did express neither of the α-subunits *Il20ra* and *Il22ra1* (Figure 3.7A). Single-cell RNA-sequencing (scRNA-seq) of FACS-sorted CD45+ immune cells from the murine esophagus substantiates the lack of an α-subunit (Figure 3.7B), indicating that immune cells do not express a functional IL-20R.
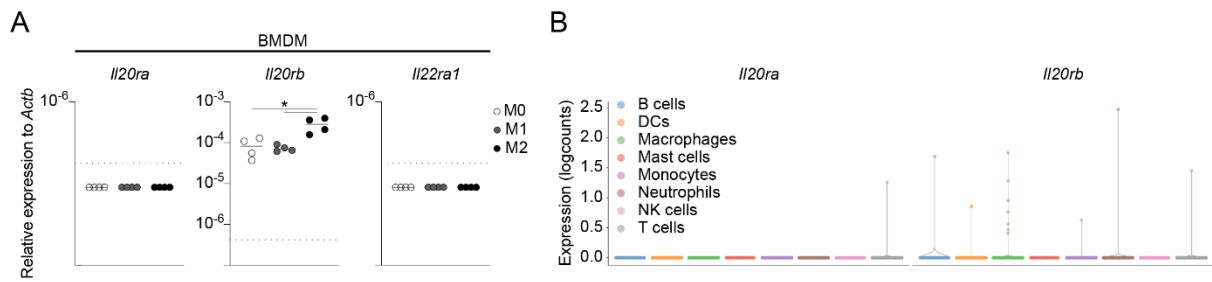
Figure 3.7   Murine immune cells do not express the α-subunit of type 1 and type 2 IL-20R

(A) *Il20ra*, *Il20rb*, and *Il22ra1* mRNA levels in murine M0, M1, and M2 polarized BMDMs assessed by RT-qPCR. (B) Normalized *Il20ra* and *Il20rb* expression levels by annotated cell types from the scRNA-seq dataset of CD45$^+$ immune cells from the murine esophagus. Data are presented as individual values with medians, and each dot represents one biological replicate. *p<0.05, by Mann-Whitney U test. Actb: Beta-actin, BMDMs: Bone marrow-derived macrophages, Il: Interleukin.

3.3   Effects of IL-20 subfamily cytokines on the esophageal epithelium

3.3.1   Characterization of patient-derived esophageal organoids

Identification of epithelial cells as the main target of IL-20 subfamily cytokines in the esophagus incited us to generate patient-derived esophageal organoids from biopsies collected by upper endoscopy. Organoids generated according to a protocol from Kasagi et al. [175] form in a self-organizing manner when cultured in a droplet of a 3D-collagen matrix. Initially, they form small cell aggregates (day 0-7) and grow over time (Figure 3.8A+B). At a later stage of development (day 9-11), they form distinct onion ring-like epithelial layers resembling the multilayered squamous epithelium of the esophagus (Figure 3.8A+B). Increasing differentiation and keratinization of the esophageal organoids are reflected by an expanding keratinized core in the center and the persistence of undifferentiated, proliferating cells in the outer layers (day >11; Figure 3.8A+B). Patient-derived esophageal organoids from EoE patients developed similarly and without a morphological difference from control individual-derived organoids over 11 days (Figure 3.8A+B).
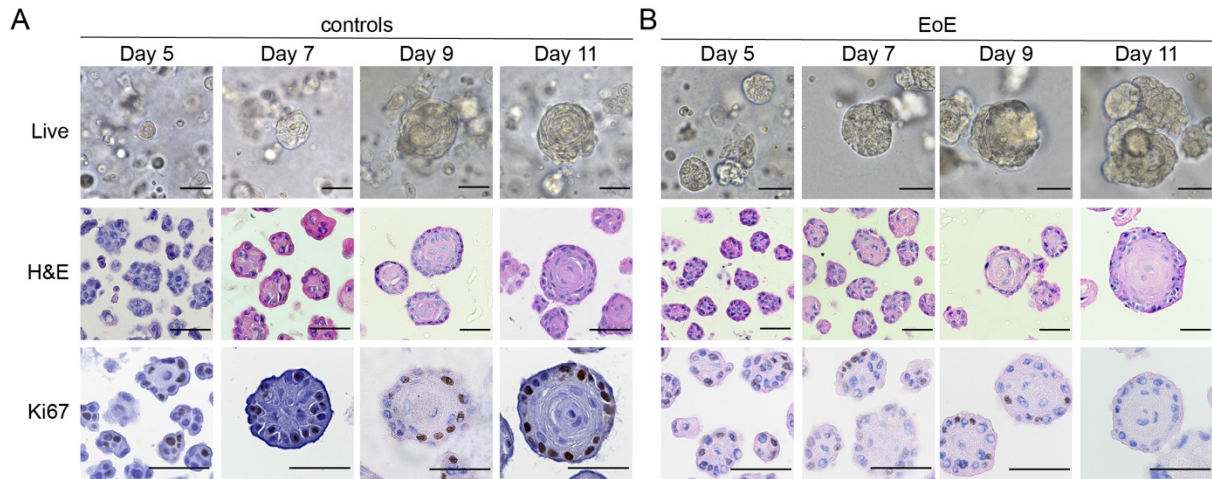
Figure 3.8 Differentiation and proliferation of patient-derived esophageal organoids

Representative in culture bright-field images (Live) and H&E and Ki67 staining of differentiating primary esophageal organoids from (A) control individuals and (B) EoE patients. Scale bars, 50 µM.

To confirm epithelial features in patient-derived esophageal organoids, we performed IHC for the IL-20R subunits. While IL-20RB was constantly expressed from day 5 on (Figure 3.9A+B), IL-20RA expression was marginal during the first days and gradually increased until day 11 in organoids from control individuals and EoE patients (Figure 3.9A+B).
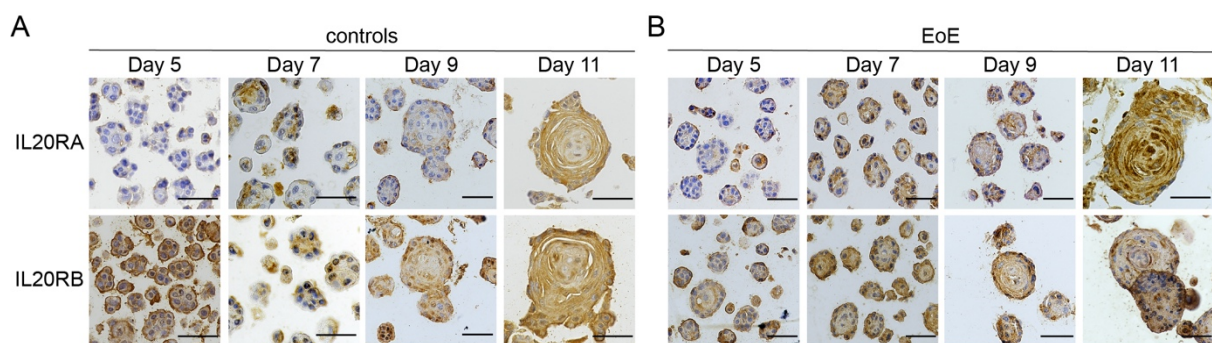

Figure 3.9 Differentiated patient-derived esophageal organoids express the type 1 IL-20R

Representative IL-20RA and IL-20RB staining of primary esophageal organoids from (A) control individuals and (B) EoE patients. Scale bars, 50 µM.

3.3.2 The IL-20 subfamily regulates the expression of epithelial barrier components in patient-derived esophageal organoids

After confirming the expression of the type 1 IL-20R by differentiated patient-derived organoids, we aimed to investigate the effect of the IL-20 subfamily on the esophageal epithelium. Therefore, we analyzed the transcriptome and proteome of patient-derived esophageal organoids from control individuals stimulated with IL-19, IL-20, and IL-24. Principal component analysis (PCA) revealed that the RNA-sequencing (RNA-seq) of paired non-stimulated and IL-20 subfamily cytokine-stimulated organoids was prevailed by inter-individual discrepancies (Figure 3.10A). However, deeper principal components unveiled segregation of the samples based on stimulation status (Figure 3.10B).
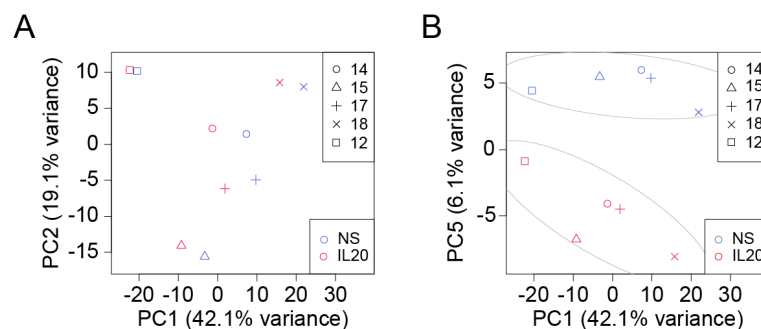

Figure 3.10   IL-20 subfamily cytokine-stimulated esophageal organoids cluster separate from unstimulated esophageal organoids in RNA-seq

Segregation of paired non-stimulated and IL-20 subfamily stimulated (IL-20) esophageal organoids from control individuals (12, 14, 15, 17, and 18) according to (A) interindividual differences and (B) IL-20 subfamily stimulation status by PCA based on the normalized expression levels in the RNA-seq samples. NS: non-stimulated, PC: Principal component, PCA: Principal component analysis.

To obtain information about IL-20 subfamily-induced molecular changes in the esophageal epithelium, we analyzed the differential expression of genes and performed a gene set enrichment analysis (GSEA). Differentially expressed genes included esophageal epithelial barrier components indispensable for maintaining

barrier function. More particularly, keratins (i.e., *KRT4*, *KRT13*, *KRT24*), elements of desmosomes (i.e., *DSG1* and *DSG4, DSC1,* and *DSC2* and *DSP*), constituents of the tight junction complex (i.e., *OCLN* and *CLDN17*), S100 fused type protein family members, such as *FLG* and *FLG2* and serine protease inhibitor kazal-type (SPINK) family associates like *SPINK7* (Figure 3.11A+B).
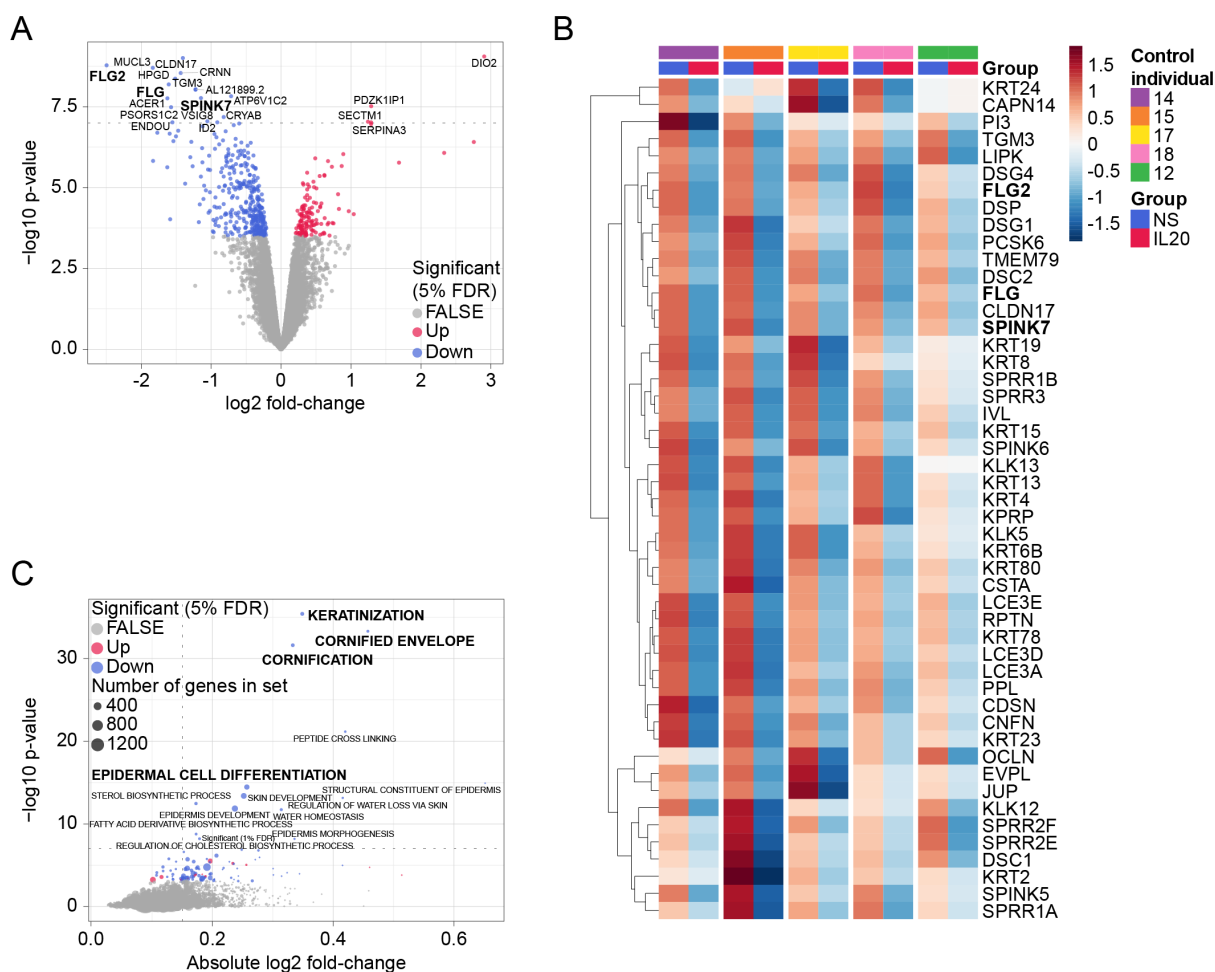

Figure 3.11   IL-20 subfamily stimulation reduces the expression of genes involved in epithelial differentiation and barrier function in patient-derived esophageal organoids

(A) Volcano plot of the differentially expressed genes between non-stimulated (NS) and IL-20 subfamily stimulated (IL-20) primary esophageal organoids. Annotated genes have a p-value lower than 10^{-7}, and genes of specific interest for the study are labeled in bold. (B) Heatmap shows the centered and scaled expression of a selected subset of epithelium-associated genes, significantly differentially expressed in esophageal organoids from control individuals (12, 14, 15, 17, and 18) upon stimulation with the IL-20 subfamily cytokines. Genes of specific interest for the study are highlighted in bold. (C) GSEA based

on differential expression analysis from the RNA-seq dataset. The x-axis shows the average absolute log-fold change across genes of each category. Labeled categories have a p-value lower than 10^{-7} and an absolute average log-fold change of > 0.15. GSEA: Gene set enrichment analysis, NS: non-stimulated

Most differentially expressed genes in the esophageal epithelium were downregulated upon stimulation with IL-20 subfamily cytokines. The downregulated genes were related to keratinization, cornification, cornified envelope, and epidermal differentiation (Figure 3.11C). However, the IL-13 receptor subunits *IL4R*, *IL13RA1,* and *IL13RA2* were increased (Figure 3.12).
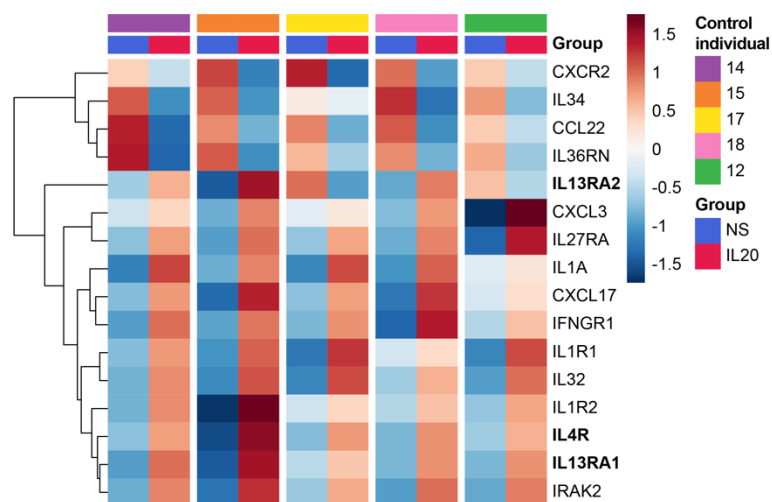

Figure 3.12   IL-20 subfamily stimulation increases expression of IL-13 receptor subunits in patient-derived esophageal organoids

Heatmap depicts the centered and scaled expression levels of selected cytokines and cytokine receptors in the RNA-seq dataset of paired non-stimulated (NS) and IL-20 subfamily-stimulated (IL-20) primary esophageal organoids from control individuals (12, 14, 15, 17, and 18). Genes of specific interest for the study are highlighted in bold.

3.3.3   Specific and overlapping effects of the IL-20 subfamily, IL-13, and SPINK7-deficiency on the esophageal epithelium

We compared the transcriptome of our IL-20 subfamily-stimulated patient-derived esophageal organoids to previously described transcriptomic changes of the

esophageal epithelial barrier by IL-13 stimulation (GSE65335) [142] and SPINK7-deficiency (GSE103356) [14] and epithelial changes reported in the EoE transcriptome (GSE58640) [137]. A common feature of the four data sets was the downregulation of the four gene ontology (GO) categories "CORNIFICATION", "CORNIFIED_ENVELOPE", "EPIDERMAL_CELL_DIFFERENTIATION", and "KERATINIZATION" (Figure 3.13A+B).
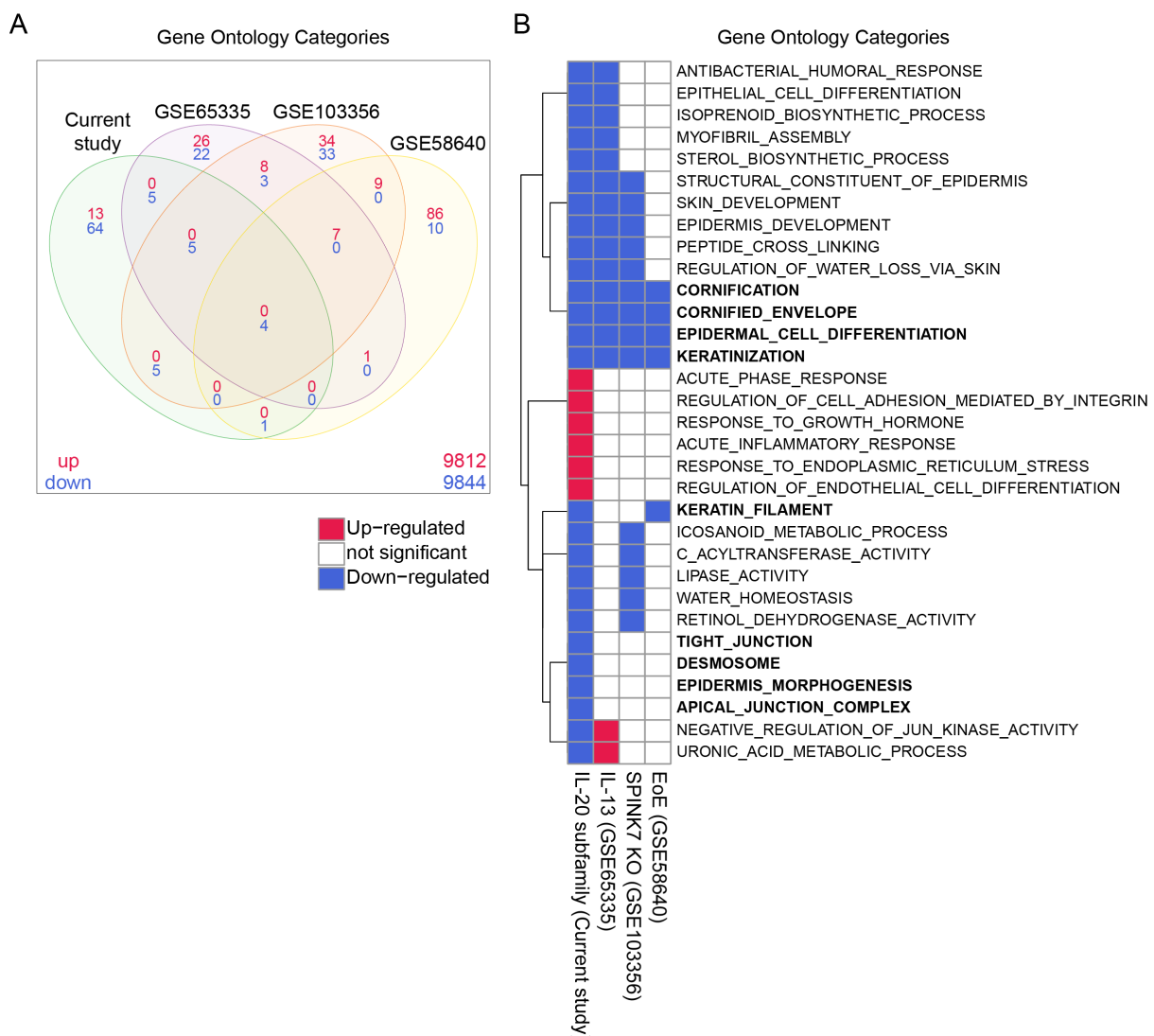

Figure 3.13   Comparison of significantly regulated GO categories between the IL-20 subfamily-stimulated esophageal organoid transcriptome and public RNA-seq transcriptomes

(A) Venn diagram of differentially expressed GO categories in the GSEA analysis of the IL-20 subfamily-stimulated esophageal organoids dataset and reanalyzed public datasets: esophageal keratinocytes

stimulated with IL-13 (GSE65335), SPINK7-deficient esophageal keratinocytes (GSE103356), and the EoE transcriptome (GSE58640). (B) Heatmap showing a selected subset of GO categories significantly differentially expressed in our dataset and their differential expression in the public datasets. GO categories of specific interest for the study are highlighted in bold. EoE: Eosinophilic esophagitis, GO: Gene ontology, GSEA: Gene set enrichment analysis, IL: Interleukin, SPINK: Serine protease inhibitor kazal-type.

One aspect of our data set only shared with the EoE transcriptome was the downregulation of the GO category "KERATIN_FILAMENT" (Figure 3.13A+B). Further characteristic changes in the epithelium induced by the IL-20 subfamily are reflected by the downregulation of the GO categories "TIGHT_JUNCTION", "DESMOSOME", "EPIDERMIS_MORPHOGENESIS", and "APICAL_JUNCTION_COMPLEX" (Figure 3.13B).

Analyzing differentially expressed genes summarized in the ancestral GO category "EPIDERMIS_DEVELOPMENT" revealed that the expression of *FLG* and *DSG1* was downregulated in all four data sets (Figure 3.14A+B). Despite the substantial overlap with IL-13 stimulation and SPINK7-deficiency, the IL-20 subfamily specifically downregulated several components of the intercellular junctional network, including *DSP*, *DSC2*, *DSG4*, *PPL*, and *EVPL* (Figure 3.14B). Furthermore, IL-20 subfamily stimulation reduced the expression of the serine protease inhibitors *SPINK5*, *SPINK6*, and *SPINK7* (Figure 3.14B).

A

GO_EPIDERMIS_DEVELOPMENT

B

GO_EPIDERMIS_DEVELOPMENT
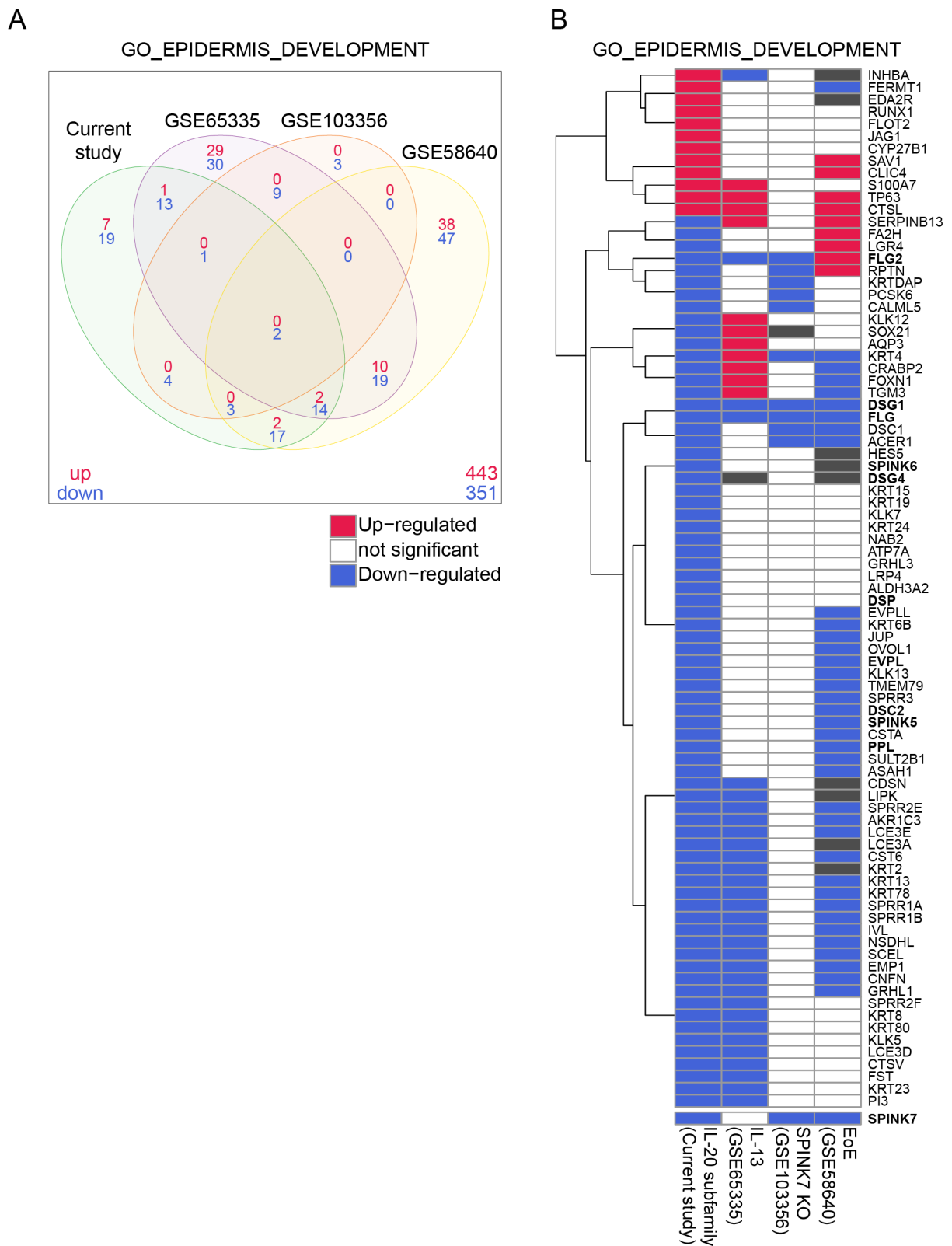

Figure 3.14 **Comparison of differently expressed genes in the GO category "EPIDERMIS_DEVELOPMENT" between the IL-20 subfamily-stimulated esophageal organoid transcriptome and public RNA-seq transcriptomes**

(A) Venn diagram of significant differentially expressed genes from the GO category "EPIDERMIS_DEVELOPMENT" in the IL-20 subfamily-stimulated esophageal organoids dataset and

reanalyzed public datasets: esophageal keratinocytes stimulated with IL-13 (GSE65335), SPINK7-deficient esophageal keratinocytes (GSE103356), and the EoE transcriptome (GSE58640).

(B) Heatmap showing a selected subset of significant differentially expressed genes from the GO category "EPIDERMIS_DEVELOPMENT" in our dataset and their differential expression in the public datasets. Genes of specific interest for the study are highlighted in bold. EoE: Eosinophilic esophagitis, GO: Gene ontology, IL: Interleukin, SPINK: Serine protease inhibitor kazal-type.

3.3.4 Proteome analysis confirms IL-20 subfamily-mediated reduction of epithelial barrier components in patient-derived esophageal organoids

In order to elaborate on whether the IL-20 subfamily-induced transcriptomic differences translate to the protein level, we performed a proteomics analysis of IL-20 subfamily-stimulated esophageal organoids. For proteomics, we used organoids from different control individuals to generalize the significance of our findings. Coherent with the transcriptomic data, the PCA was dominated by high inter-individual differences (Figure 3.15A).
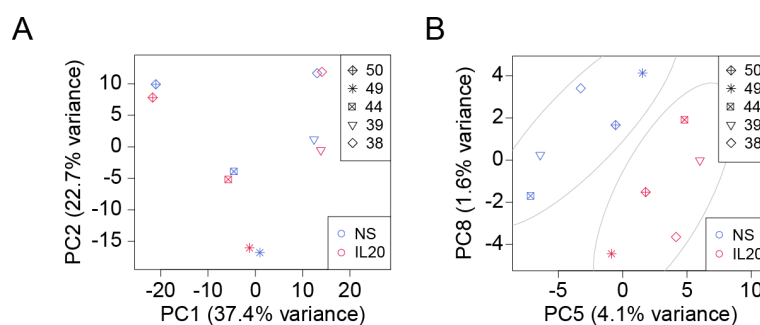
Figure 3.15   IL-20 subfamily cytokine-stimulated esophageal organoids cluster separate from unstimulated esophageal organoids in proteomics

Segregation of paired non-stimulated (NS) and IL-20 subfamily stimulated (IL-20) esophageal organoids from control individuals (38, 39, 44, 49, and 50) according to (A) interindividual differences and (B) IL-20 subfamily stimulation status by PCA based on the normalized protein levels in the proteomics samples. NS: non-stimulated, PC: Principal component, PCA: Principal component analysis.

Correspondingly, the segregation of non-stimulated and IL-20 subfamily-stimulated esophageal organoids was identifiable in deeper principal components (Figure 3.15B). Although the magnitude of differential expression was lower than at the transcriptomic level, proteins related to epithelial cornification and differentiation were downregulated in IL-20 subfamily-stimulated esophageal organoids (Figure 3.16A-C).
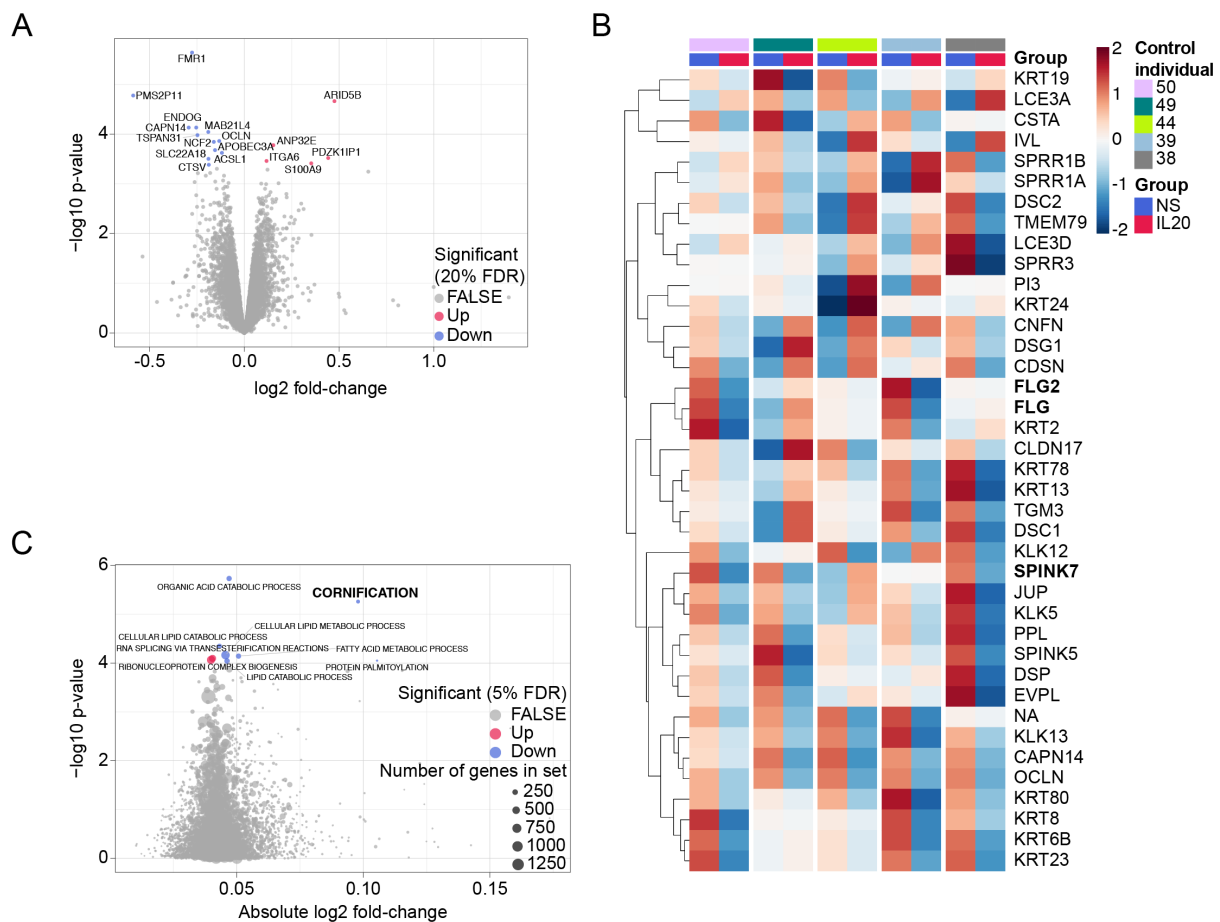

Figure 3.16   IL-20 subfamily stimulation reduces proteins involved in epithelial differentiation and barrier function in patient-derived esophageal organoids

(A) Volcano plot of the differentially expressed proteins between non-stimulated (NS) and IL-20 subfamily stimulated (IL-20) primary esophageal organoids. All significant differentially expressed proteins are labeled. (B) Heatmap showing the centered and scaled expression levels of a selected subset of epithelium-associated proteins from the significant differentially expressed genes in Figure 3.11A+B in esophageal organoids from control individuals (38, 39, 44, 49, and 50). Proteins of specific interest for the study are highlighted in bold. (C) GSEA based on differential expression analysis from

the proteomics dataset of paired non-stimulated (NS) and IL-20 subfamily-stimulated (IL-20) primary esophageal organoids. GSEA: Gene set enrichment analysis, NS: non-stimulated.

Despite noticeably altered expression of epithelial barrier components, IL-20 subfamily-stimulated esophageal organoids only exhibited minor indications for basal hyperproliferation but did not manifest morphological alterations or changes in IL-20R expression (Figure 3.17A+B). Nonetheless, RT-qPCR and IHC confirmed the regulatory effect of the IL-20 subfamily on *FLG*, *FLG2,* and *SPINK7* expression in control individual- and EoE patient-derived esophageal organoids (Figure 3.17C+D).
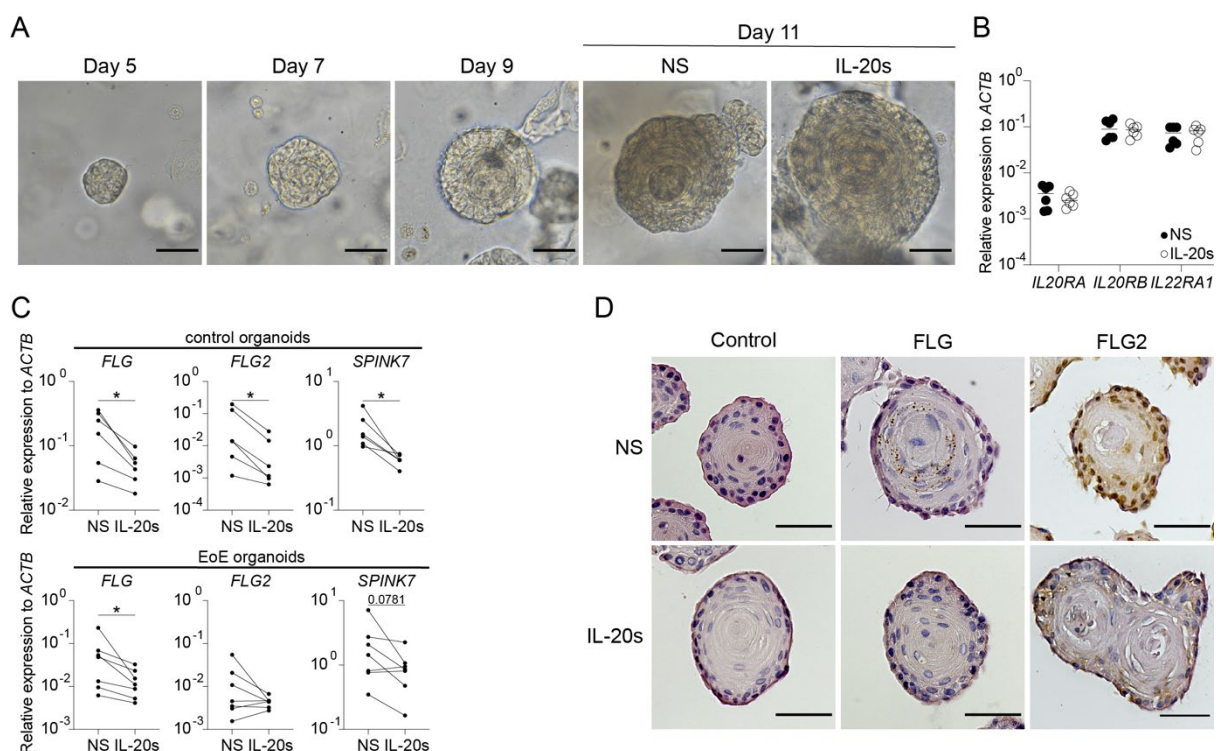

Figure 3.17   IL-20 subfamily stimulation does not alter the morphology and IL-20R expression but reduces FLG, FLG2, and SPINK7 in patient-derived esophageal organoids

(A) Representative bright-field imaging of control individual-derived esophageal organoids from day 5 to day 11 of culture. On day 11, esophageal organoids were stimulated with IL-19, IL-20, and IL-24 (IL-20s). Scale bars, 50 µM. (B) *IL20RA*, *IL-20RB*, and *IL22RA1* mRNA levels of non-stimulated (NS) and IL-20 subfamily-stimulated (IL-20s) esophageal organoids assessed by RT-qPCR. (C) *FLG*, *FLG2*, and *SPINK7* mRNA levels of paired NS and IL-20s esophageal organoids from control individuals and EoE patients assessed by RT-qPCR. (D) Representative control and IHC staining for FLG and FLG2 of NS

and IL-20s esophageal organoids from control individuals. Scale bars, 50 μM. Data are presented as individual values with medians, and each dot or line represents one biological replicate; *p ≤ 0.05 by Mann-Whitney U or Wilcoxon test. ACTB: Beta-actin, EoE: Eosinophilic esophagitis, FLG: Filaggrin, FLG2: Filaggrin 2, IL: Interleukin, SPINK: Serine protease inhibitor kazal-type.

3.3.5 The esophageal barrier of EoE patients displays lower FLG, FLG2, and SPINK7 expression.

Based on the observation of increased IL-20 subfamily expression in active EoE, we assessed the expression of *FLG*, *FLG2,* and *SPINK7* in patient biopsies. RT-qPCR analysis revealed reduced *FLG*, *FLG2,* and *SPINK7* expression in the esophagus of patients with active EoE compared to control individuals and topical corticosteroid-treated inactive EoE patients (Figure 3.18A). Moreover, IHC verified reduced FLG and FLG2 in esophageal sections of active EoE patients and partially restored FLG and FLG2 in inactive EoE patients (Figure 3.18B+C). Our data delineate that IL-20 subfamily cytokines modulate the expression pattern of genes and proteins responsible for epithelial barrier function, including the filaggrin family and the esophagus-specific serine protease inhibitor SPINK7.
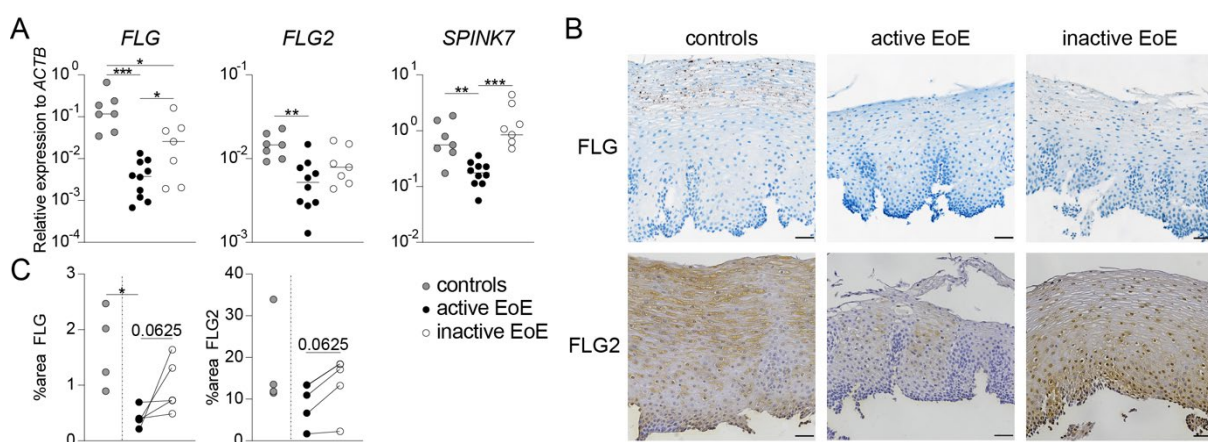

Figure 3.18   Lower expression of FLG, FLG2, and SPINK7 in the esophageal epithelium of patients with active EoE

(A) Expression levels of *FLG*, *FLG2*, and *SPINK7* in the esophagus of control individuals and patients with active and inactive EoE assessed by RT-qPCR. (B) Immunohistochemistry staining for FLG and

FLG2 in sections from the proximal esophagus of control individuals and patients with active and inactive EoE. Scale bars, 50 µM. (C) Quantified percentage of area stained for FLG and FLG2 in (B) using QuPath software. Data are presented as individual values with medians, and each dot or line represents one biological replicate; *p ≤ 0.05, **p ≤ 0.01, ***p ≤ 0.001 by Mann-Whitney U or Wilcoxon test. ACTB: Beta-actin, FLG: Filaggrin, FLG2: Filaggrin 2, SPINK: Serine protease inhibitor kazal-type.

3.4 Experimental EoE depends on IL-20 subfamily signaling

3.4.1 IL-20R2-deficiency is protective in the EoE mouse model

IL-20 subfamily-mediated regulation of epithelial barrier constituents prompted us to investigate the consequences of impaired IL-20 subfamily signaling on the development of EoE. Therefore, we induced the experimental EoE mouse model in *WT*, IL-19-deficient (*Il19^{tdT}*), and *Il20R2$^{-/-}$* mice with a complete abrogation of IL-20 subfamily signaling. In virtue of the epithelial expression pattern of IL-20R complexes, we measured total immunoglobulin E (IgE) and OVA-specific IgE titers in *WT*, *Il19^{tdT}*, and *Il20R2$^{-/-}$* mice. Animals in the experimental groups non-chal and sens+chal from all three genotypes developed increased total and OVA-specific IgE titers upon sensitization (Figure 3.19A+B).
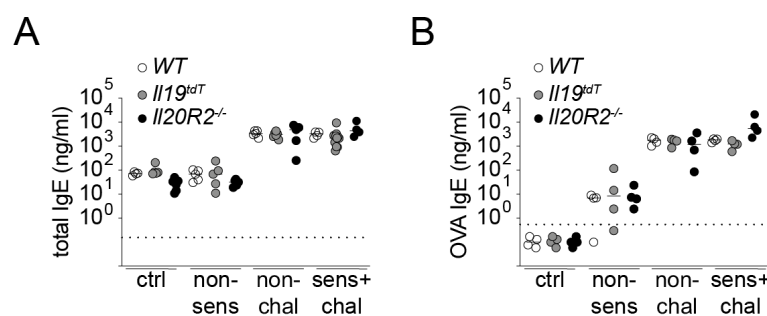
Figure 3.19   Increased total and OVA-specific IgE titers in OVA-sensitized *WT*, *Il19^{tdT}*, and *Il20R2$^{-/-}$* animals

(A) Total and (B) OVA-specific IgE titers in *WT*, *Il19^{tdT},* and *Il20R2$^{-/-}$* mice. Data are presented as individual values with medians, and each dot or line represents one biological replicate. ctrl: non-sensitized+non-challenged, non-sens: non-sensitized+challenged, non-chal: sensitized+non-challenged, sens+chal: sensitized+challenged. IgE: Immunoglobulin E, OVA: Ovalbumin.

Figure 3.20   IL-20R2-deficiency attenuates experimental EoE

(A) Representative H&E staining of esophageal sections from *WT*, *Il19*^{tdT}, and *Il20R2*^{-/-} mice with experimental EoE. Black arrowheads mark eosinophils. Scale bars, 50 µm. (B) Quantification of 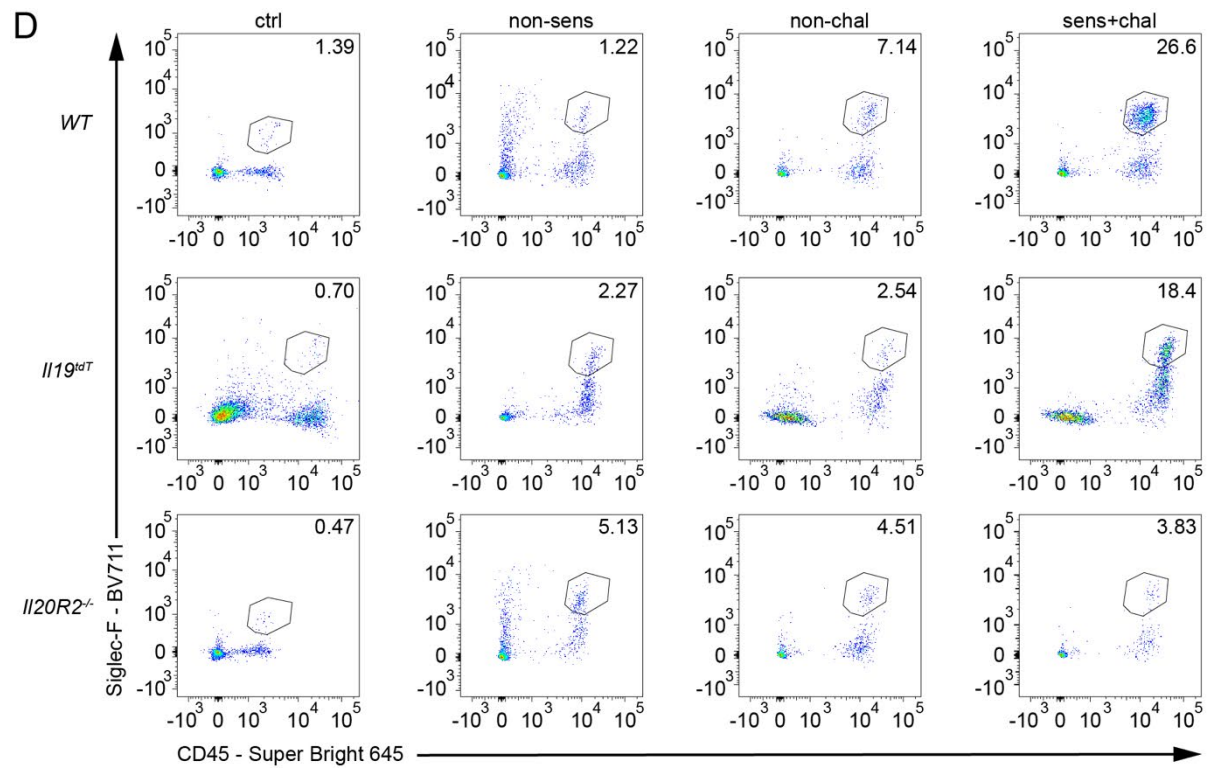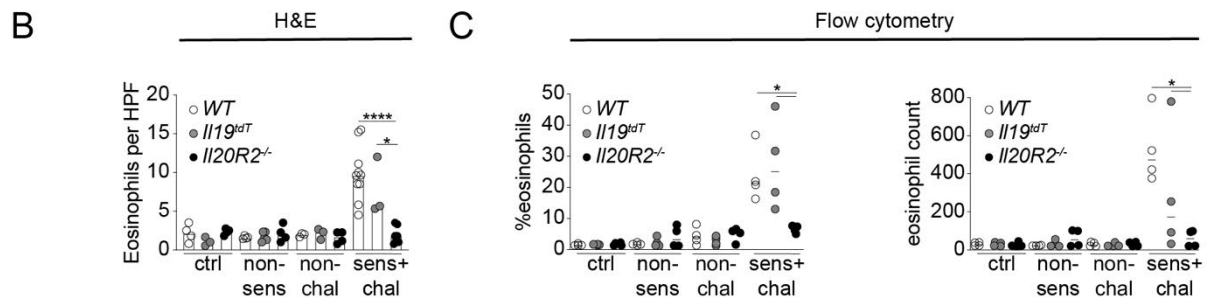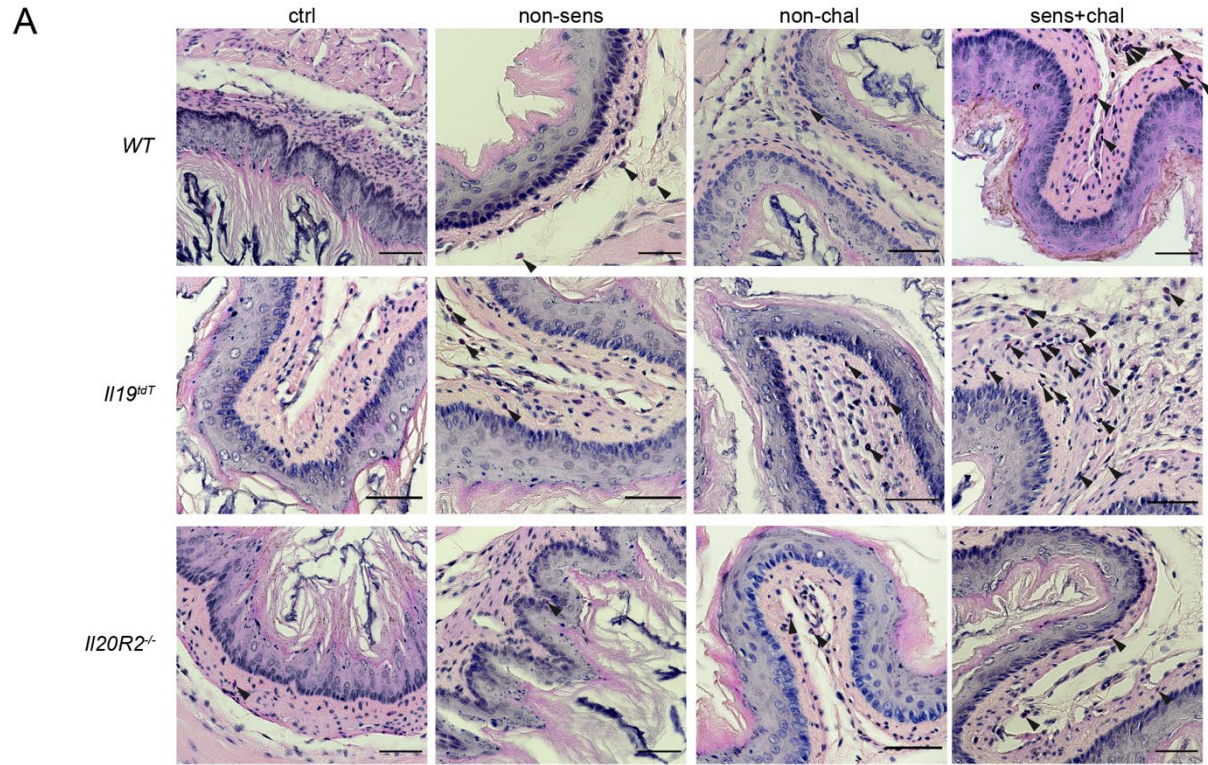esophageal eosinophil infiltration from (A). (C) The percentage and the absolute number of infiltrating eosinophils in the esophagus assessed by flow cytometry. (D) Representative flow cytometry dot plots show the percentage of eosinophils infiltrating the esophagus. Data are presented as individual values with medians, and each dot or line represents one biological replicate; *p ≤ 0.0, ****p<0.0001, by Mann-Whitney U test. ctrl: non-sensitized+non-challenged, non-sens: non-sensitized+challenged, non-chal: sensitized+non-challenged, sens+chal: sensitized+challenged. HPF: High-power field.

Therefore, we can exclude the interference of the genetic modifications with OVA-sensitization via the skin. After successful sensitization and four days of OVA-challenge chal+sens *Il20R2*^{-/-} *mice had* significantly less eosinophil infiltration into the esophagus, while *WT* animals had severe experimental EoE with overwhelming esophageal eosinophilia (Figure 3.20A-D).

Besides esophageal eosinophilia, experimental EoE was characterized by increased Th2 cytokines. While *WT* animals with severe experimental EoE had an increased *Il5* and *Il13* expression, EoE-protected chal+sens *Il20R2*^{-/-} mice did not have higher *Il5* and *Il13* expression than the control groups (Figure 3.21A+B).
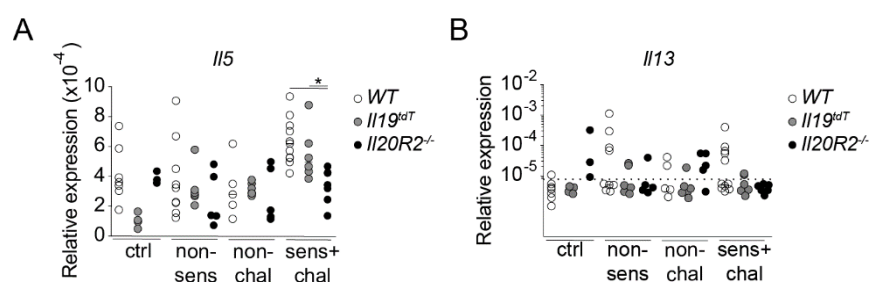
Figure 3.21   IL-20R2-deficiency interferes with Th2-signature of experimental EoE

Esophageal expression of (A) *Il5* and (B) *Il13* relative to *Actb* by RT-qPCR in *WT*, *Il19*^{tdT}, *Il20R2*^{-/-} mice. Data are presented as individual values with medians, and each dot or line represents one biological replicate; *p ≤ 0.05, by Mann-Whitney U test. ctrl: non-sensitized+non-challenged, non-sens: non-

sensitized+challenged, non-chal: sensitized+non-challenged, sens+chal: sensitized+challenged. Il: Interleukin.

3.4.2   IL-19-deficiency is not sufficient to protect from experimental EoE

While eosinophil numbers in the esophagus of $Il19^{tdT}$ mice were lower compared to WT animals, sens+chal $Il19^{tdT}$ mice still developed a significant eosinophil infiltration accompanied by increased $Il5$ expression in the esophagus (Figure 3.20A-D+ Figure 3.21A). On the other hand, novel transgenic $Il19^{\Delta CX3CR1}$ mice with a CX3CR1$^+$ macrophage-specific deletion of $Il19$ developed severe experimental EoE similar to WT mice (Figure 3.22). These results imply that alternative IL-19 sources or the remaining IL-20 subfamily members compensate for the lack of macrophage-derived IL-19 in the development of experimental EoE.
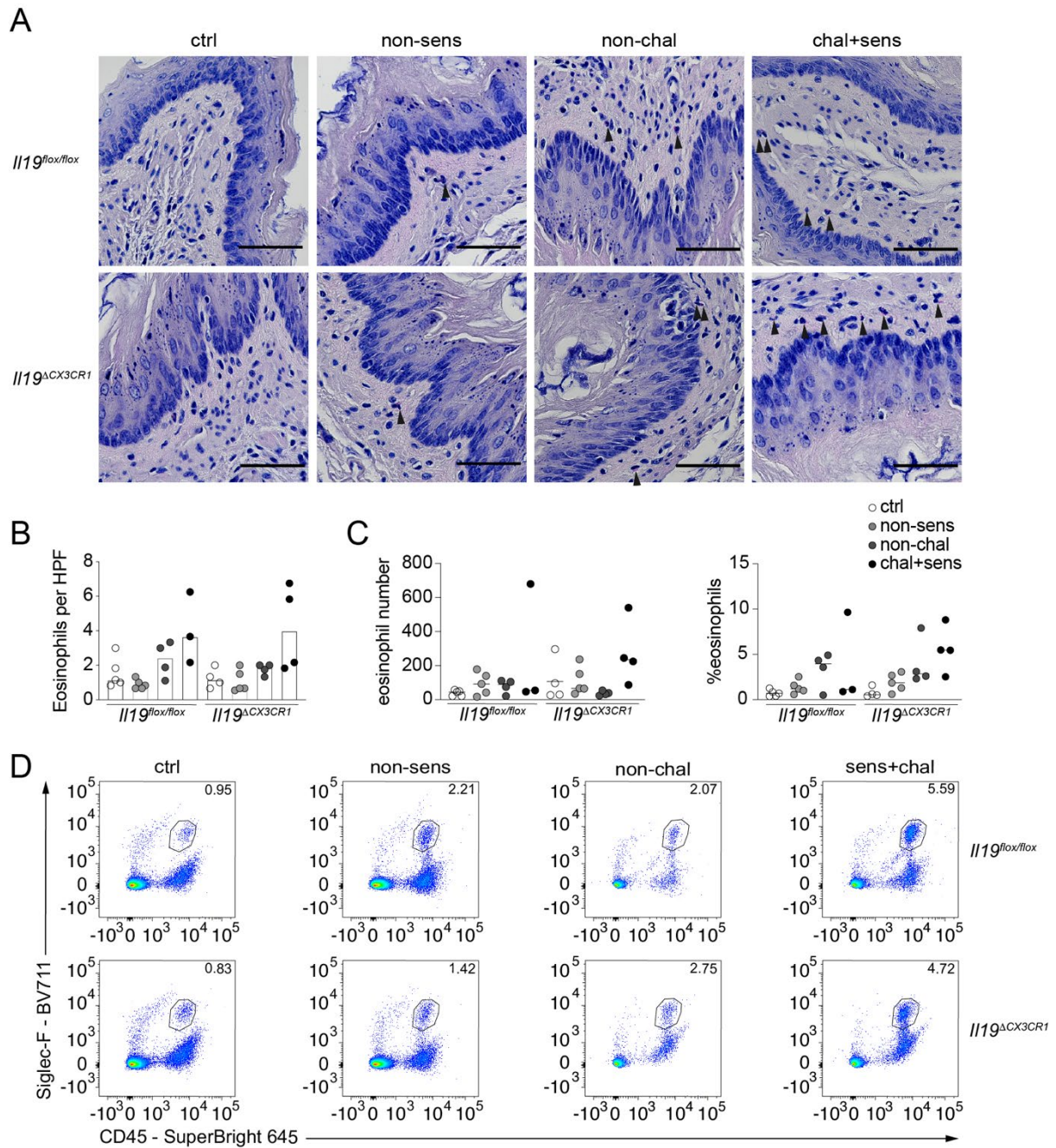
Figure 3.22 CX3CR1⁺ macrophage-specific deletion of *Il19* does not attenuate the development of experimental EoE

(A) Representative H&E staining of esophageal sections from *Il19^{flox/flox}* and *Il19^{ΔCX3CR1}* animals. Arrows mark eosinophils. Scale bars, 50 μm. (B) Quantification of esophageal eosinophil infiltration from (A). (C) The absolute number and percentage of esophageal eosinophils from *Il19^{flox/flox}* and *Il19^{ΔCX3CR1}* mice assessed by flow cytometry. (D) Representative flow cytometry dot plots showing esophageal eosinophil infiltration. Numbers indicate the percentage of infiltrating eosinophils. Data are presented as individual values with medians, and each dot represents one biological replicate. ctrl: non-

sensitized+non-challenged, non-sens: non-sensitized+challenged, non-chal: sensitized+non-challenged, sens+chal: sensitized+challenged. HPF: High-power field.

3.5 The IL-20 subfamily regulates esophageal FLG expression

3.5.1 IL-20R2-deficiency preserves FLG expression in the esophagus

To ascertain the reason for the attenuated experimental EoE phenotype in $Il20R2^{-/-}$ animals, we analyzed the expression of the filaggrin family and *Spink7* in the murine esophagus. Interestingly, *Flg* and *Flg2* expression was lower in non-chal and sens+chal *WT* mice, while *Spink7* expression retained the same level between all experimental groups (Figure 3.23A).
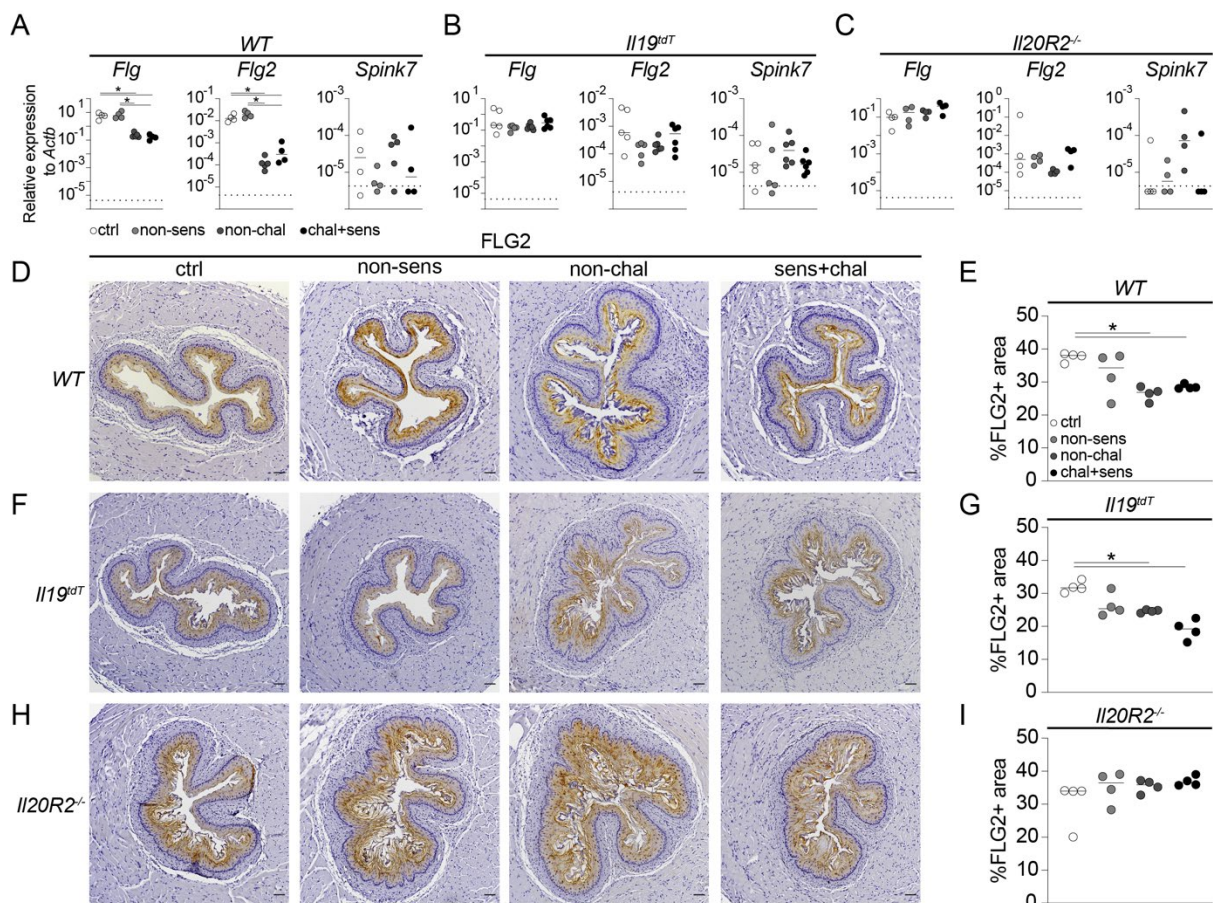

Figure 3.23   IL-20R2-deficiency preserves the esophageal expression of the filaggrin family in experimental EoE

(A-C) mRNA levels of *Flg*, *Flg2*, and *Spink7* in the esophagus of (A) *WT*, (B) $Il19^{tdT}$, and (C) $Il20R2^{-/-}$ animals assessed by RT-qPCR. (D-I) Immunohistochemistry staining and percentage of the area

stained for FLG2 (analyzed with Fiji (ImageJ, Version 2.0.0-rc-68/1.52h)) in esophageal sections from (D+E) *WT*, (F+G) *Il19^{tdT}*, and (H+I) *Il20R2^{-/-}* animals. Scale bars, 50 μm. Data are shown as individual values with medians, and each dot represents one biological replicate. *p<0.05, by Mann-Whitney U test. ctrl: non-sensitized+non-challenged, non-sens: non-sensitized+challenged, non-chal: sensitized+non-challenged, sens+chal: sensitized+challenged. FLG: Filaggrin, FLG2: Filaggrin 2, SPINK: Serine protease inhibitor kazal-type.

In *Il19^{tdT}* and *Il20R2^{-/-}* mice, on the other hand, neither MC903-treatment for sensitization nor OVA-challenge did alter *Flg* and *Flg2* expression (Figure 3.23B+C). These findings are reflected in the IHC by reduced FLG2 staining in the suprabasal epithelial layer (stratum spinosum) of the esophagus and preserved staining in the superficial stratum corneum of non-chal and sens+chal *WT* and *Il19^{tdT}* mice (Figure 3.23D-G). In non-chal and sens+chal *Il20R2^{-/-}* mice, on the contrary, FLG2 was retained in all epithelial layers (Figure 3.23H+I).

3.5.2 IL-20 subfamily-mediated regulation of FLG is independent of STAT3

Previously described phosphorylation of STAT3 by IL-20 subfamily signaling [153] lead us to hypothesize that the IL-20 subfamily-mediated decrease of epithelial barrier components is STAT3-dependent. To test our hypothesis, we took advantage of the IL-20R expressing human esophageal squamous cell carcinoma cell line KYSE-180 (Figure 3.24A), confirming the activation of STAT3 upon stimulation with IL-19, IL-20, and IL-24 (Figure 3.24B). Testing for activation of other signaling pathways, we discovered that IL-20 subfamily cytokine stimulation also resulted in phosphorylation of ERK1/2, whereas NF-κB (p65) was not activated (Figure 3.24C+D).
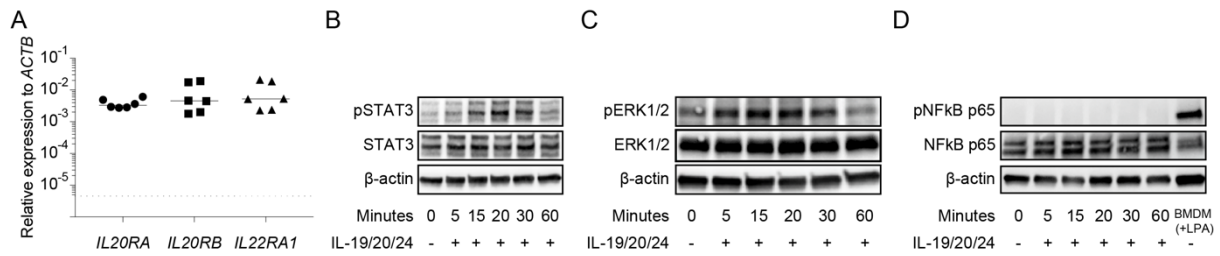
Figure 3.24 IL-20 subfamily signaling activates STAT3 and ERK1/2 pathways in IL-20R type 1 and type 2 expressing esophageal squamous cell carcinoma cell line KYSE-180

(A) Expression of *IL20RA*, *IL20RB,* and *IL22RA1* measured by RT-qPCR in KYSE-180 cell line.

(B-D) Immunoblot for IL-20 subfamily-induced activation of (B) STAT3, (C) ERK1/2, and (D) NFκB in KYSE-180 cell line. Lysophosphatidic acid (LPA)-stimulated BMDM protein lysate was used as a positive control for pNFκB p65 in (D). Data are presented as individual values with medians, and each dot represents one biological replicate. ACTB: Beta-actin, BMDM: Bone marrow-derived macrophage, ERK1/2: Extracellular-signal regulated kinases 1/2, IL: Interleukin, NF-κB: Nuclear factor kappa-light-chain-enhancer of activated B cells, STAT3: Signal transducer and activator of transcription 3.

First, following up on our hypothesis of IL-20 subfamily-mediated regulation of epithelial barrier constituents via STAT3, we treated KYSE-180 cells with the pharmacological STAT3 inhibitor cucurtabicin 1 before stimulation with the IL-20 subfamily cytokines. Contrary to our hypothesis, pharmacological STAT3 inhibition resulted in an augmented decrease of *FLG*, *FLG2,* and *SPINK7* expression (Figure 3.25A). Consistently, a consolidated reduction of *FLG*, *FLG2,* and *SPINK7* was observed in patient-derived esophageal organoids upon STAT3 inhibition (Figure 3.25B).
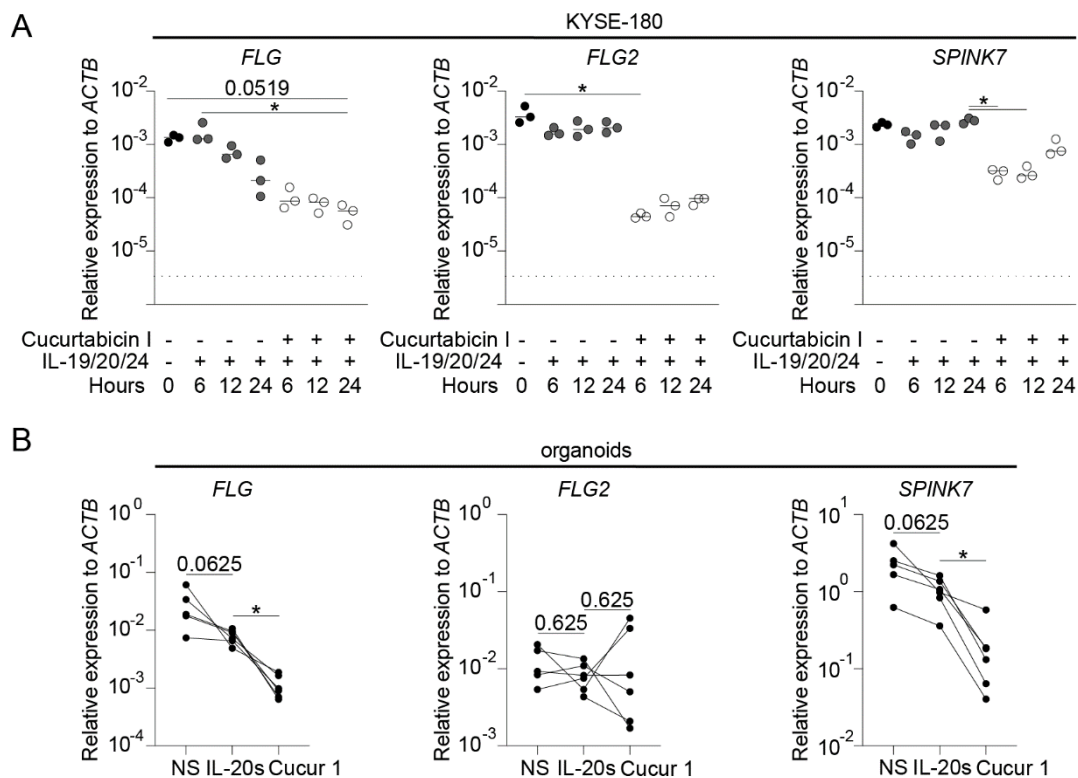
Figure 3.25   STAT3 inhibition reinforces IL-20 subfamily-mediated decrease of *FLG*, *FLG2*, and *SPINK7* expression in KYSE-180 cell line and patient-derived esophageal organoids

(A) mRNA levels of *FLG*, *FLG2,* and *SPINK7 assessed* by RT-qPCR in the KYSE-180 cell line after stimulation with IL-19, IL-20, IL-24 and when indicated with the STAT3 inhibitor cucurtabicin 1.

(B) mRNA expression of *FLG*, *FLG2,* and *SPINK7* in patient-derived esophageal organoids assessed by RT-qPCR. When indicated, organoids are stimulated with IL-20 subfamily cytokines (IL-20s) and pretreated with cucurtabicin 1 (Cucur 1). Data are presented as individual values with medians, with each dot representing one biological replicate; *$p ≤ 0.05$, by Mann-Whitney U or Wilcoxon test. ACTB: Beta-actin, FLG: Filaggrin, FLG2: Filaggrin 2, SPINK: Serine protease inhibitor kazal-type.

3.5.3   Aggravation of experimental EoE and FLG loss in *Stat3^ΔKrt5* animals

To substantiate the importance of STAT3 signaling for the esophageal epithelium, we used a transgenic mouse line with a tamoxifen (TMX)-inducible squamous epithelium-specific deletion of STAT3 (Figure 3.26).
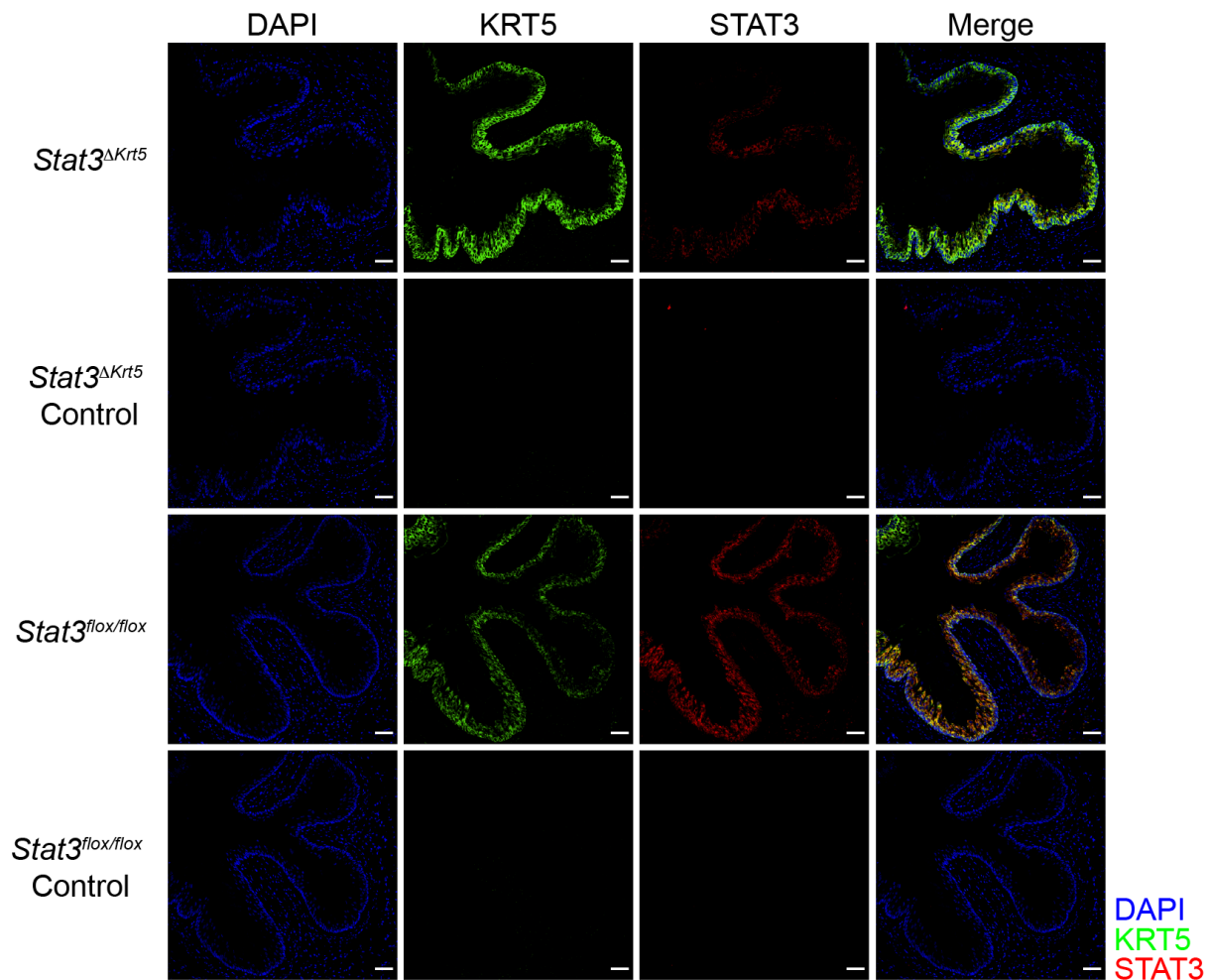
Figure 3.26 **Tamoxifen-induced epithelium-specific deletion of STAT3 in *Stat3^ΔKrt5* mice**

KRT5 and STAT3 immunofluorescence staining and control staining in esophageal sections from tamoxifen-treated *Stat3^flox/flox* and *Stat3^ΔKrt5* animals. Scale bars, 50 µm. DAPI: 4',6-diamidino-2-phenylindole, KRT5: Keratin 5, STAT3: Signal transducer and activator of transcription 3.

Squamous epithelium-specific deletion of STAT3 generally leads to increased esophageal eosinophil and SiglecF⁻CD45⁺ immune cell infiltration in TMX-injected *Stat3^ΔKrt5* mice compared to TMX-injected *Stat3^flox/flox* littermates with the maximum count in the sens+chal group (Figure 3.27A-G). In contrast, FLG2 expression is drastically reduced in the esophagus of non-chal and sens+chal *Stat3^ΔKrt5* mice (Figure 3.28A+B).
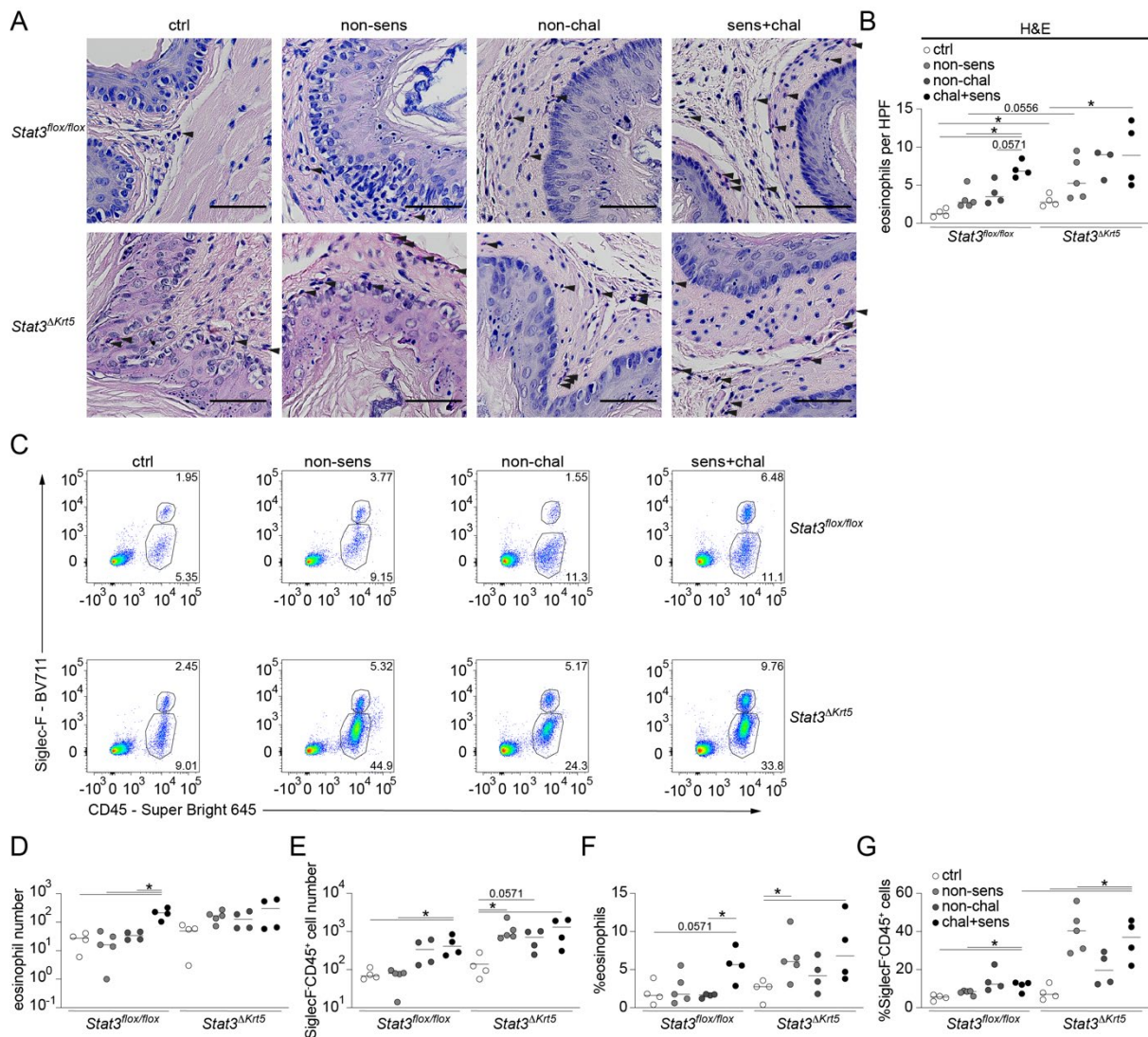
Figure 3.27 Epithelium-specific STAT3 deletion aggravates experimental EoE in Stat3$^{\Delta Krt5}$ mice

(A) Representative H&E staining of esophageal sections from Stat3$^{flox/flox}$ and Stat3$^{\Delta Krt5}$ mice. Arrows mark eosinophils. Scale bars, 50 μm. (B) Quantified esophageal eosinophilia (per HPF) from esophageal sections in (A). (C) Representative flow cytometry dot plots showing esophageal eosinophil and SiglecF$^-$CD45$^+$ immune cell infiltration. Numbers indicate percentages of infiltrating cells. (D-G) Quantification of (D+E) absolute number and (F+G) percentage of infiltrating eosinophils and SiglecF$^-$CD45$^+$ immune cells into the esophagus assessed by flow cytometry. Data are shown as individual values with medians, and each dot or line represents one biological replicate; *p ≤ 0.05 by Mann-Whitney U test. ctrl: non-sensitized+non-challenged, non-sens: non-sensitized+challenged, non-chal: sensitized+non-challenged, sens+chal: sensitized+challenged.

3.6 IL-20 subfamily signaling impairs esophageal barrier function

3.6.1 IL-20 subfamily cytokines reduce TEER and increase the permeability to FITC-dextran in patient-derived air-liquid interface cultures

The reductive effect of IL-20 subfamily cytokines on the filaggrin family and other epithelial barrier components in patient-derived esophageal organoids incited us to elaborate on whether this impairs the esophageal epithelial barrier function. We established primary keratinocyte-derived air-liquid interface (ALI) cultures to assess the barrier function. We measured the transepithelial electrical resistance (TEER), assessing epithelial barrier integrity. Subsequently, we measured epithelial permeability by quantifying the paracellular flux of the anhydroglucose-polymer dextran (3-5kDa) labeled with fluorescein isothiocyanate (FITC). The TEER was lower in IL-20 subfamily-stimulated ALI cultures than in unstimulated ALI cultures (Figure 3.29A), affirming a critical role for the IL-20 cytokine subfamily in modulating the esophageal epithelial barrier function. These findings were consolidated by elevated epithelial permeability to FITC-dextran in IL-20 subfamily-stimulated ALI cultures (Figure 3.29B).
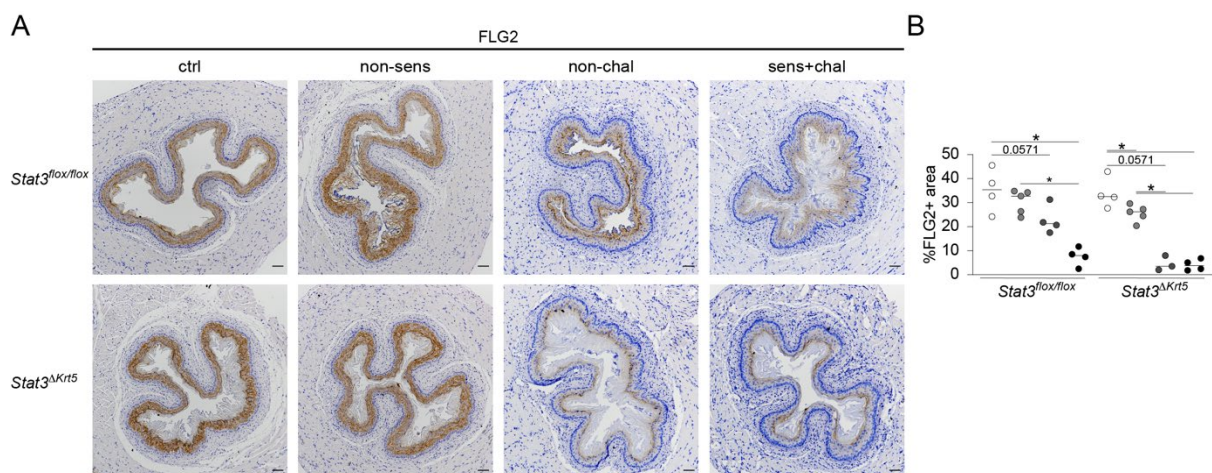
Figure 3.28   Epithelium-specific STAT3 deletion augments esophageal FLG2 loss in *Stat3$^{\Delta Krt5}$* mice

(A) Representative IHC staining for FLG2 in esophageal sections of *Stat3$^{flox/flox}$* and *Stat3$^{\Delta Krt5}$* mice. Scale bars, 50 µm. (B) Quantified percentage (analyzed with Fiji (ImageJ, Version 2.0.0-rc-68/1.52h)) of area stained for FLG2 in (A). Data are shown as individual values with medians, and each dot indicates one biological replicate. *p<0.05, by Mann-Whitney U test. ctrl: non-sensitized+non-challenged, non-sens: non-sensitized+challenged, non-chal: sensitized+non-challenged, sens+chal: sensitized+challenged. FLG2: Filaggrin 2.

Consistent with previous results, pharmacological inhibition of STAT3 signaling with cucurtabicin 1 corrupts the epithelial barrier integrity even more (Figure 3.29A). This first indication of epithelial barrier impairment was confirmed by increased permeability to FITC-dextran upon STAT3 inhibition (Figure 3.29B).

3.6.2   ERK1/2 inhibition perpetuated esophageal barrier function

We had to discard our hypothesis of a STAT3-dependent downregulation of epithelial barrier components by the IL-20 subfamily. Consequently, we moved on to test for the involvement of ERK1/2 in IL-20 subfamily signaling. Therefore, we treated ALI cultures with the pharmacological ERK1/2 inhibitor PD98059 before stimulating them with IL-20 subfamily cytokines. PD98059-pretreatment prevented the IL-20 subfamily-mediated decrease of TEER (Figure 3.29A). In line with this, ERK1/2 inhibition maintained imperviousness of the esophageal epithelial barrier in the paracellular flux assay with FITC-dextran (Figure 3.29B). H&E staining showed that IL-20 subfamily-treated ALI cultures lacked a cornified epithelial layer (Figure 3.29C). Although thinner than in non-stimulated ALI cultures, PD98059-pretreated ALI cultures retained a cornified epithelial layer (Figure 3.29C). Collectively, pharmacological ERK1/2 inhibition rescued the impairment of the esophageal epithelial barrier by the IL-20 subfamily.
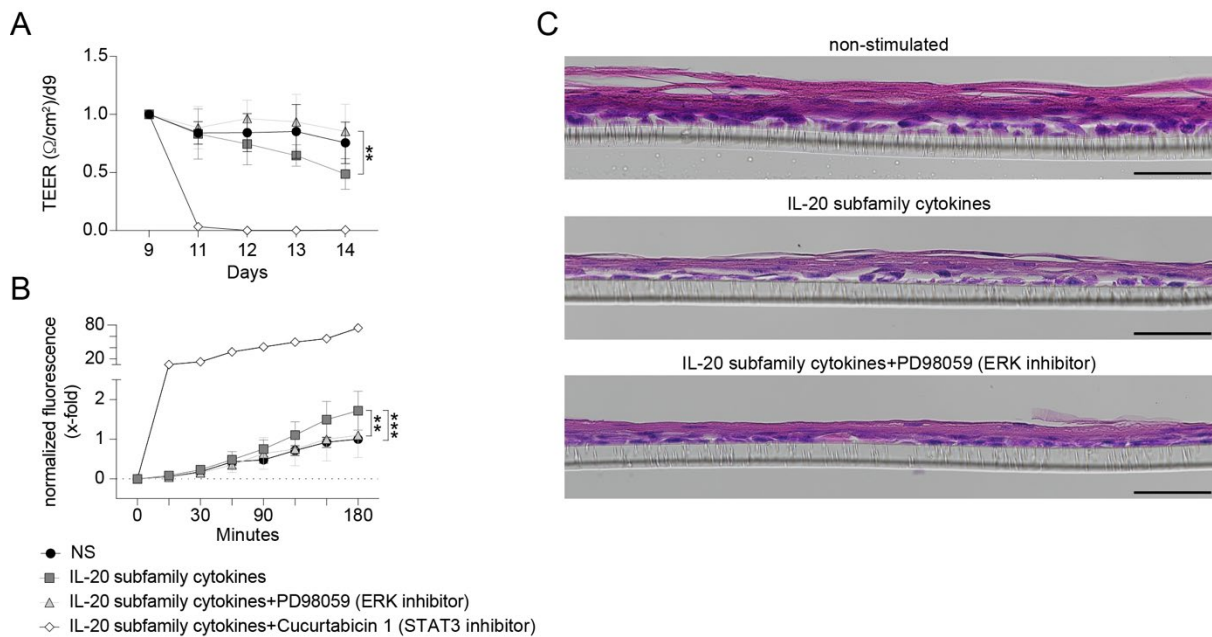
Figure 3.29 **ERK1/2 inhibition prevents IL-20 subfamily-mediated disruption of the epithelial barrier function in patient-derived ALI cultures**

(A) Transepithelial electrical resistance (TEER) and (B) paracellular flux of FITC-dextran in ALI cultures from patient-derived esophageal epithelial cells (n=4). When indicated, ALI cultures were stimulated with IL-19, IL-20, and IL-24 and pretreated with the ERK inhibitor PD98059 or the STAT3 inhibitor cucurtabicin 1. (C) Representative H&E staining of sections from non-stimulated, IL-20 subfamily-stimulated and PD98059-pretreated+IL-20 subfamily-stimulated ALI cultures. Scale bars, 50 µm. Each dot in (A+B) represents the mean of 4 biological replicates; error bars represent SD. $**p<0.01$, $***p<0.001$, by two-way ANOVA. NS: non-stimulated.

3.6.3 ERK1/2 inhibition attenuates experimental EoE

The observation that ERK1/2 inhibition has the potential to hinder epithelial impairment poses the question of whether targeting the ERK pathway could be used as a potential therapeutic strategy for EoE. To address this question, we decided to inject ctrl and sens+chal *WT* mice with PD98059. Pharmacological ERK inhibition decreased esophageal eosinophil and SiglecF⁻CD45⁺ immune cell infiltration in histological and flow cytometry analysis of PD98059-treated *WT* chal+sens animals in comparison to vehicle-treated animals (Figure 3.30A-E). Finally, suggesting that pharmacological

inhibition of ERK signaling can obstruct IL-20 subfamily-mediated impairment of the esophageal barrier function to alleviate experimental EoE in mice.
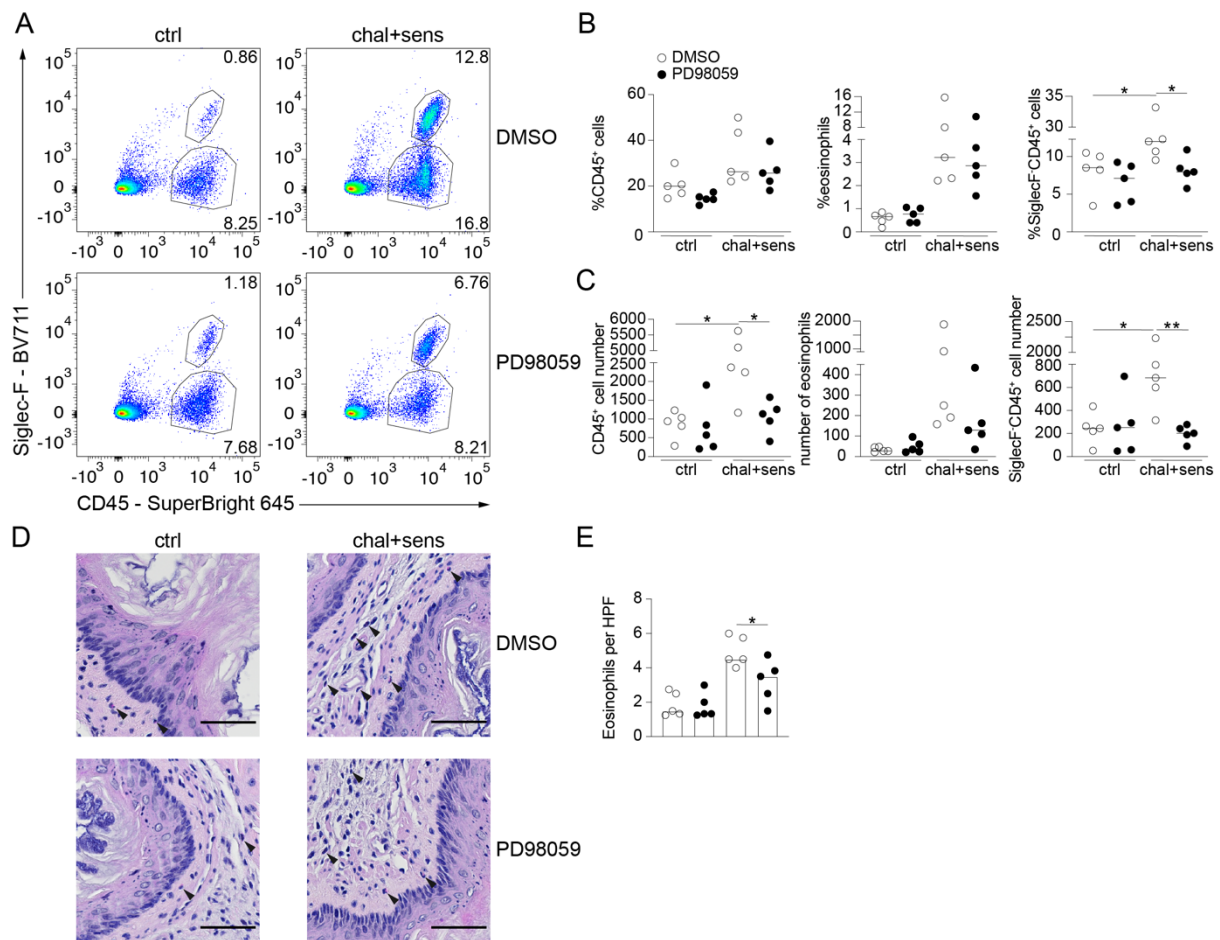
Figure 3.30   ERK-inhibitory treatment attenuates experimental EoE

(A) Representative flow cytometry dot plots showing esophageal eosinophil and SiglecF⁻CD45⁺ immune cell infiltration in DMSO (vehicle) and PD98059-treated *WT* mice with experimental EoE. Quantified (B) percentage and (C) the absolute number of total CD45⁺ cells, infiltrating eosinophils and SiglecF⁻CD45⁺ immune cells in the esophagus of DMSO (vehicle) and PD98059-treated *WT* mice with experimental EoE. (D) Representative H&E staining of esophageal sections from DMSO (vehicle) and PD98059-treated *WT* mice with experimental EoE. Scale bars, 50 μm (E) Quantified esophageal eosinophil infiltration from (D). Data are presented as individual values with medians, and each dot represents one biological replicate. *p<0.05, **p<0.01 by Mann-Whitney U test. ctrl: non-sensitized+non-challenged, sens+chal: sensitized+challenged. DMSO: Dimethyl sulfoxide.

4 DISCUSSION

4.1 Correlation between IL-20 subfamily cytokine levels and disease activity

Disease activity of EoE is assessed based on peak eosinophil count per hpf and presence of symptoms, defining active disease as >15 eos/hpf and remission as <15 eos/hpf [73]. Thus, monitoring disease activity and treatment response in EoE patients requires repetitive upper endoscopy. With the increasing prevalence of EoE, the pressing need for non-invasive biomarkers appears more relevant than ever, considering the burden of recurrent endoscopy for patients and the healthcare system [89-91, 202]. Although many promising candidates [203-205] have been identified in recent years, none found their way into the guidelines [73, 81]. Absolute eosinophil count is the only marker that consistently correlated with esophageal eosinophil count in active EoE and steroid- and PPI-induced remission [203-205]. However, insufficient diagnostic accuracy hindered inclusion in the guidelines [205]. Here, we report that patients with active EoE had an increased esophageal tissue expression and serum level of IL-20 subfamily cytokines compared to control individuals. More importantly, the high IL-20 subfamily cytokines in active EoE decreased in patients achieving remission under treatment with topical corticosteroids, indicating that the IL-20 subfamily cytokines might represent new candidates for a serum biomarker. In agreement, multiple studies recently proposed IL-20 subfamily members as new biomarkers for inflammatory skin and lung diseases [206-208]. Notably, serum levels of IL-19 reliably correlate with disease severity and therapy response in atopic dermatitis and asthma [206, 207]. Altogether, serum's non-invasive, easy accessibility, and standardized analysis with a reliable correlation to disease activity would make IL-20 subfamily serum levels ideal candidates for non-invasive biomarkers [209].

However, prospective multi-center RCTs with bigger patient cohorts and power analysis are required to verify the suitability of IL-20 subfamily serum levels to monitor EoE disease activity and therapy response.

4.2   Cellular sources of IL-20 subfamily cytokines in the esophagus

IL-20 subfamily cytokines were initially described as mainly produced by myeloid cells [150, 156]. Subsequently, skin keratinocytes were reported to express IL-20 and IL-24 constitutively [155]. In contrast, IL-19 was produced only upon inflammatory triggers like IL-1β, IL-4, and IL-17 [155, 210]. Together, with reports of increased IL-19 production by monocytes and macrophages upon stimulation with LPS [150, 156], we reason that IL-19 plays a role during epithelial inflammation. At the same time, IL-20 and IL-24 appear to be generally integrated into the regulation of epithelial homeostasis and differentiation [164]. Our results indicate that macrophages are one potential source of IL-19 in the esophagus. Although not assessed by us, keratinocytes and fibroblasts are likely to be additional producers of IL-20 subfamily cytokines [155, 210]. Because equally to the skin, the esophagus is lined by stratified squamous epithelium [211]. T cells, B cells, and DCs are other cell populations identified as producers of IL-20 subfamily cytokines [156-158]. However, our scRNA-seq data of CD45$^+$ cells from the murine esophagus indicate that these cell populations do not produce IL-20 subfamily cytokines in the esophagus. Furthermore, low to no B and T cells in the healthy esophagus [40] make it unlikely that they are a significant source of IL-20 subfamily cytokines. Fate mapping and lineage tracing [212] and the development of reporter mouse lines for IL-20 and IL-24 may prove helpful to disclose further cellular sources of IL-20 subfamily cytokines in the esophagus and the entire organism.

4.3   The IL-20 subfamily – Regulator of epithelial barrier integrity

The cytokine-mediated interplay between the epithelium and immune cells has been suggested to be crucial for the pathogenesis of EoE [116, 138, 213, 214]. The concept of epithelium-centered pathogenesis is reinforced by the substantial involvement of most EoE risk genes in regulating the epithelial barrier function [95, 135, 136] and the disruption of the esophageal epithelial barrier in EoE [32, 35, 138, 139, 142, 215]. When IL-20 was identified, it was described to cause hyperproliferation and aberrant differentiation of epidermal keratinocytes [151]. Although not initially, IL-19 and IL-24 were also associated with epithelial abnormalities [162-164]. Subsequently, IL-20 subfamily-mediated impairment of epithelial differentiation disturbed the skin's barrier function [165, 169]. Expression of the type 1 IL-20R by the esophageal epithelium insinuates the IL-20 subfamily being similarly involved in regulating epithelial differentiation and barrier function in the esophagus.

In this study, RNA-seq and mass spectrometry-based proteomics of IL-20 subfamily-stimulated esophageal organoids unveiled a decrease in epithelial cornification and differentiation-associated transcripts and proteins. We registered the most pronounced decrease in the filaggrin family. The filaggrins are a family of late differentiation proteins responsible for aggregation and alignment of intermediate keratin filaments, ensuring the prevention of water loss and barrier function by the stratum corneum [7, 19, 216]. *FLG* was recently identified as an EoE risk gene [135, 138].

Moreover, loss-of-function mutations of *FLG* are linked to disruption of the epithelial barrier epitomizing a major predisposing factor for inflammatory diseases of mucosal and dermal borders [23, 216]. A reduction of the filaggrin family in IL-20 subfamily-stimulated esophageal organoids indicated a defect in epithelial differentiation,

resulting in a dysfunctional epithelial barrier. The lack of a cornified epithelial layer in the IL-20 subfamily-stimulated ALI cultures confirms a deficient epithelial differentiation due to aberrant IL-20 subfamily signaling. In addition, the increased epithelial permeability in the IL-20 subfamily-stimulated ALI cultures verifies the IL-20 subfamily-mediated impairment of the esophageal barrier function. However, recovery of FLG expression and concurrent reduction of the IL-20 subfamily cytokines in topical corticosteroid-treated inactive EoE hint at the IL-20 subfamily-mediated barrier dysfunction as a reversible inflammatory component.

In contrast, FLG mutations cause a constant disease-inherent barrier impairment [23]. Therefore, the increase of IL-20 cytokines in EoE might result from an inherent barrier defect-induced inflammation that further corrupts the debilitated epithelial barrier. This hypothesis could be addressed by transfection of esophageal epithelial cells with the EoE-associated FLG loss-of-function mutation 2282del4 [138] and subsequent determination of IL-20 subfamily expression. Furthermore, the assessment of IL-20 subfamily cytokine levels in EoE patients with and without the FLG loss-of-function mutation 2282del4 might also provide clarification [23, 138].

4.4   Redundancy of IL-20 subfamily cytokines in epithelial biology

Our results show that stimulation of patient-derived esophageal organoids with IL-19, IL-20, and IL-24 impairs epithelial differentiation and barrier function in the esophagus. However, redundancy of the IL-20 subfamily cytokines remains to be uncovered. Analogous to human EoE, we observed transcriptional changes in the IL-20 and filaggrin family in experimental murine EoE. Albeit, experimental EoE and loss of FLG2 were not impeded in IL-19-deficient animals. Whereas IL-20R2-deficiency, disrupting signaling through the type 1 and type 2 IL-20R complex, hampered experimental EoE and retained FLG2 expression. In addition, persisting IL-20 subfamily-mediated

epidermal hyperplasia in $Il19^{-/-}$ and $Il24^{-/-}$ but not in $Il20R2^{-/-}$ *animals* [162] endorses the redundancy hypothesis for IL-20 subfamily members. Hence, targeting the IL-20 subfamily appears more efficient by blocking the IL-20R complexes or preventing dimerization of the IL-20RB subunit with IL-20RA or IL-22RA1, respectively.

4.5   Immune cells as a target of IL-20 subfamily members

Aside from their impact on epithelial cells, IL-20 subfamily members may also influence immune cells. In the early 2000s, IL-19 was shown to induce monocytes and activated T cells to produce an array of proinflammatory cytokines [166, 217, 218]. More recently, IL-19 has been reported to support neutrophil development [219]. Furthermore, IL-19 limits IL-17A$^+$ $\gamma\delta$T cell accumulation in psoriatic skin [220]. Analogous IL-24 suppresses the Th17 cytokine profile as part of an autocrine negative feedback mechanism to IL-17A [221]. Interestingly, IL-17 seems to be an inducer of IL-20 subfamily cytokines in keratinocytes and T cells [160, 210, 221, 222]. Regardless, whether IL-20 subfamily cytokines promote EoE by directly acting on immune cells in the esophagus remains to be elucidated. Since murine BMDMs and esophageal CD45$^+$ cells lack $Il20ra$ and $Il22ra1$ expression, a direct effect of IL-20 subfamily cytokines on immune cells via the known heterodimeric receptors appears highly unlikely [151, 153]. Nonetheless, a stimulatory effect on neutrophilopoiesis by IL-19 despite lack of IL-20RA [219] incites the notion of an alternative α-subunit forming a so far unknown IL-20R complex.

4.6   ERK1/2-dependent relationship between the IL-20 subfamily and the esophageal epithelium

It is well recognized that signaling through the IL-20R complexes is propagated via the STAT3 pathway and, as a result, implies IL-20 subfamily-mediated epithelial

hyperplasia and hyperproliferation to be STAT3-dependent [151, 153, 154]. However, activation of other signaling pathways by the IL-20 subfamily has been proclaimed as well [159, 160].

IL-24 has been suggested to evoke epidermal barrier dysfunction due to STAT3-mediated FLG reduction [165]. However, squamous epithelium-specific deletion of STAT3 in *Stat3ΔKrt5* mice resulted in an aggravated loss of FLG2 and exacerbation of experimental EoE. Accordingly, pharmacological inhibition of STAT3 in patient-derived esophageal organoids reduced the expression of *FLGs* and impaired the epithelial barrier function of patient-derived esophageal ALI cultures. These findings challenge a potential therapeutic benefit of JAK inhibitors [126, 127] in EoE and imply alternative pathways to mediate the barrier impairing effect of the IL-20 subfamily [154]. A potential alternative pathway facilitating IL-20 subfamily-mediated epithelial barrier impairment is the ERK1/2 pathway [159, 160]. The mitogen-activated protein kinases (MAPK) ERK1 and ERK2 (ERK1/2) are renowned for being involved in various processes, including differentiation and proliferation [223]. In contrast to STAT3 inhibition, blocking ERK1/2 signaling preserved epithelial barrier function in patient-derived esophageal ALI cultures stimulated with IL-19, IL-20, and IL-24. Hence, this suggests IL-20 subfamily-mediated disruption of the epithelial barrier to be ERK1/2-dependent. Consistent results have been reported on ERK1/2 inhibition in dermal keratinocytes overturning IL-17-mediated FLG reduction [224]. Considering our data and the evidence of IL-17 inducing keratinocytes to produce IL-20 subfamily cytokines [210, 222] allows us to anticipate that actually, IL-20 subfamily cytokines mediated the reduction of FLG overturned by ERK1/2 inhibition. Nevertheless, considering the wide range of cytokines signaling through ERK1/2, we cannot exclude the contribution of other contenders in regulating the epithelial barrier function via ERK1/2.

4.7 IL-20 subfamily modulates epithelial differentiation via regulation of esophagus-specific SPINK7

IL-20 subfamily-specific downregulation of the GO categories "TIGHT_JUNCTION", "DESMOSOME", "EPIDERMIS_MORPHOGENESIS", and "APICAL_JUNCTION_COMPLEX" in patient-derived esophageal organoids suggests that the IL-20 subfamily is a critical element for esophageal barrier function. Furthermore, comparing our RNA-seq dataset with public datasets [14, 137, 142] revealed that IL-20 subfamily cytokine stimulation recapitulates large parts of the epithelium-specific EoE transcriptome and the effects of IL-13 and SPINK7-deficiency on the esophageal epithelium. These results consolidate the concept of concurrent mechanisms modulating epithelial barrier function in EoE. IL-13 is a crucial molecular driver of EoE pathogenesis, reproducing most of the EoE transcriptome, including the impairment of the esophageal epithelial barrier [35, 139, 142]. Strikingly, the IL-20 subfamily-stimulated esophageal organoids increased the expression of the IL-13 receptor chains, *IL-4R*, *IL-13RA1,* and *IL-13RA2*. Thus, suggesting IL-20 subfamily cytokines increase the esophageal epithelium's sensitivity to IL-13 amplifying IL-13-mediated effects in EoE. SPINK7 is a member of the kazal-type family of serine protease inhibitors in the esophageal epithelium. SPINK7 emerged as a fundamental modulator of esophageal epithelial barrier homeostasis, balancing proteolytic activity of KLK5 and other proteases [12, 14]. Decreased expression of SPINK7 in the esophagus disturbs the protease-protease inhibitor equilibrium, ensuing degradation of epithelial barrier components and production of proinflammatory cytokines [12, 14]. It is noteworthy that despite regulating a broad spectrum of esophagus-specific genes, IL-13 does not influence SPINK7 expression [14, 139, 142]. Strikingly, *SPINK7* was decreased in patient-derived esophageal organoids upon stimulation with IL-20

subfamily cytokines. Thus, we allege IL-20 subfamily-specific effects on the esophageal epithelium, which might be upstream of SPINK7 and overlapping with IL-13 in the pathogenesis of EoE.

4.8 Conclusion and outlook

IL-19, IL-20, and IL-24 belong to the IL-20 cytokine subfamily, which is involved in the modulation of the epithelial proliferation and differentiation program [151, 162, 163]. In this Ph.D. project, we investigated the role of the IL-20 subfamily in the pathogenesis of EoE. We propose that aberrant IL-20 subfamily signaling is involved in the esophageal epithelium's poor differentiation and dysfunctional barrier in EoE patients. The IL-20 subfamily disturbs the esophageal barrier integrity by downregulating essential junctional components throughout all epithelial layers. These include the filaggrin family, which assures the stratum corneum's consolidation. The downregulation of junctional components leads to increased epithelial barrier permeability allowing continuous diffusion of allergens beyond the epithelial barrier and might sustain the inflammatory machinery.

The increased IL-20 subfamily-mediated epithelial barrier permeability depends on ERK1/2 rather than STAT3 signaling. Nevertheless, it remains unclear whether aberrant IL-20 subfamily signaling is a trigger of EoE pathogenesis or one of many cogwheels. However, successful treatment of other chronic inflammatory diseases in animal models and phase 2 clinical trials indicates that targeting the IL-20 subfamily pathway may be an option in the future EoE therapy regimen [170, 225, 226]. Before considering potential therapeutic targeting of the IL-20 subfamily pathway, further translational and clinical studies are required to improve the understanding of the interplay between immune cells, the esophageal epithelium, and the IL-20 subfamily. Identifying additional interactions between the immune system and the esophageal

epithelium will be central to deciphering the pathogenesis of EoE and developing novel therapies.

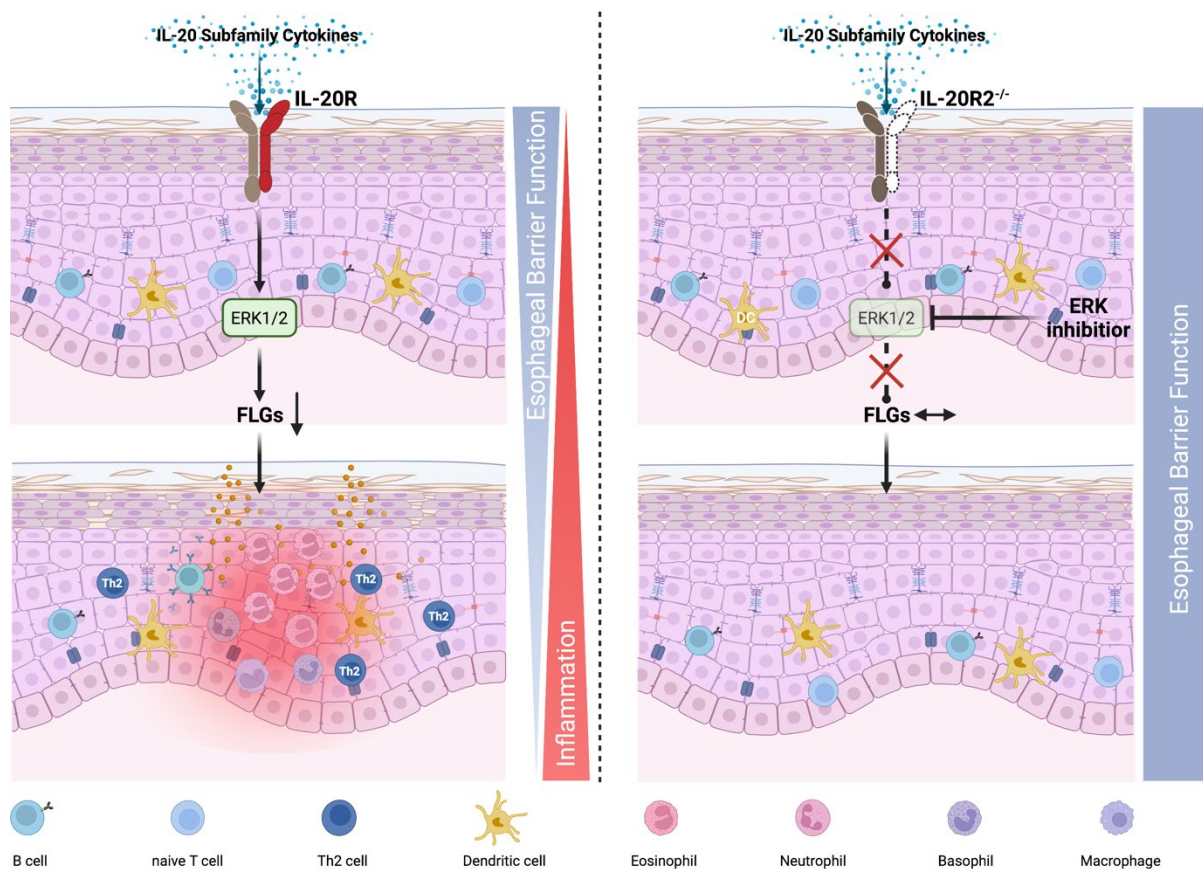**Figure 4.1**   **The role of the IL-20 subfamily in the pathogenesis of EoE**

A working model depicting IL-20 cytokine subfamily signaling reduces FLGs via the ERK1/2 pathway to impair the esophageal barrier function in EoE. In contrast, abrogating the IL-20 subfamily pathway by targeting the IL-20R or ERK1/2 can interfere with the epithelial barrier disrupting effect and reduce inflammation. Created with BioRender.com.

5 APPENDIX

5.1 Supplementary Information

Table 5.1 Genotyping primers

Il20R2^{-/-}	*Stat3-flox*
CAG TCC CAT AGA GTA CAC TGA G	CAC CAA CAC ATG CTA TTT GTA GG
GGG AGA GAA AAT GCC CCA AAC C	CCT GTC TCT GAC AGG CCA TC
	GCA GCA GAA TAC TCT ACA GCT C
Il19^{tdT}	*Cx3cr1-CreER*
TGC TGC ATG ACC AAC AAC CT	AAG ACT CAC GTG GAC CTG CT
GAA TGA CAA TGT CCT GAC TCT GCA	CGG TTA TTC AAC TTG CAC CA
CAC GAC ATT CAA CAG ACC TTG CAT	AGG ATG TTG ACT CCG AGT TG
Il19-flox	*Krt5-CreER*
CAA ACT GCA AGG GAA CTC AGT AGT G	GGA GGA AGT CAG AAC CAG GAC
CAC AGA CAA GGT TTG TTC CAC AGC	GCA AGA CCC TGG TCC TCA C
	ACC GGC CTT ATT CCA AGC

Table 5.2 RT-qPCR primers

Target gene	ENSEMBL gene code	Forward sequence	Reverese sequence
Human IL20RA	ENSG00000016402	AGA GGT GGC ACT GAC TAC AGA	ACT GGG ACC ACG TTC TGT TTG
Human IL20RB	ENSG00000174564	AAC TCA ACC ATC CTT ACC CGA C	TTC ACA CAG TAT GCA GCC CC
Human IL22RA1	ENSG00000142677	CTC TGC AGC ACA CTA CCC TCA	CGT GGG GGT AGG ATG AAC AAT C
Human IL19	ENSG00000142224	*Qiagen QT00022015*	
Human IL20	ENSG00000162891	*Qiagen QT00044905*	
Human IL24	ENSG00000162892	*Qiagen QT00059059*	
Human FLG	ENSG00000143631	TCG GCA AAT CCT GAA GAA TCC A	TGC TTT CTG TGC TTG TGT CCT
Human FLG2	ENSG00000143520	ACC CAG ATG ATC CAG ACA CAG	TTG CTG AGG ACC TTG TTG CAG
Human SPINK7	ENSG00000145879	TCC CAG GCT CTG ACT GAG TTT	TGG GTT TGT AGG GGTAGC ACA

Human CCL5	ENSG00000271503	CTG CTG CTT TGC CTA CAT TGC C	CAC ACA CTT GGC GGT TCT TTC G
Human CCL11	ENSG00000172156	AGA GGC TGA GAC CAA CCC AGA	ACT TCT TCT TGG GGT CGG CA
Human CCL24	ENSG00000106178	GGA GTG GGT CCA GAG GTA CA	TTA GCA GGT GGT TTG GTT GC
Human CCL26	ENSG00000006606	TGG AAT TGA GGC TGA GCC AAA G	CTC CCA CGT GTG GCA GTT
Human ACTB	ENSG00000075624	AGC CTC GCC TTT GCC GA	CTG GTG CCT GGG GCG
Mouse Il20ra	ENSMUSG00000020007	AAG TCG AGA AGA ACG TGG TC	GGG TGT TTT TCC TTG CCA AC
Mouse Il20rb	ENSMUSG00000044244	AAT GCT CAC CGA CCA AAA GT	AGG ACA GTT GCA TTT CGG TT
Mouse Il22Ra1	ENSMUSG00000037157	GTT CTG CAA CCT GAC TAT GGA G	GTA CAG GTG GCT TGG TGA TG
Mouse Il19	ENSMUSG00000016524	CTG GGC ATG ACG TTG ATT CT	TCT CCA GGC TTA ATG CTC CT
Mouse Il20	ENSMUSG00000026416	Qiagen; Cat No. QT00126735	
Mouse Il24	ENSMUSG00000026420	Qiagen; Cat No. QT01054634	
Mouse Il5	ENSMUSG00000036117	GAT GAG GCT TCC TGT CCC TAC T	TGA CAG GTT TTG GAA TAG CAT TTC C
Mouse Il13	ENSMUSG00000020383	AAC GGC AGC ATG GTA TGG AGT G	TGG GTC CTG TAG ATG GCA TTG C
Mouse Flg	ENSMUSG00000102439	TTC TCA GAA GGC CAG GCA GTA	CCT CGC TGT GTT CTT GCT CAT
Mouse Flg2	ENSMUSG00000049133	ACA TTC TGG ATC CGG TCA CG	GGG CAC TTC TGG TCT GAC TG
Mouse Spink7	ENSMUSG00000060201	Bio-Rad; 10025636	
Mouse Actb	ENSMUSG00000029580	TTC TTT GCA GCT CCT TCG TT	ATG AGG GGA AT ACA GCC C

Table 5.3 Key resources

Reagent or Material	Supplier	Catalog No.
Cell culture Media / Supplements		
Ascorbic Acid	Sigma-Aldrich (Merck)	A4544
Bovine pituitary extract	Gibco (Thermo Fischer Scientific)	3700015
Calcium chloride	Sigma-Aldrich (Merck)	21115
Cucurtabicin 1	Tocris (Bio-Techne)	1571/1

Dimethyl sulfoxide (DMSO), anhydrous >99,9%	Sigma-Aldrich (Merck)	276855
Epidermal growth factor	Gibco (Thermo Fischer Scientific)	3700015
Fetal Bovine Serum (FBS)	Gibco (ThermoFischer Scientific)	10500064
Keratinocyte-SFM	Gibco (Thermo Fischer Scientific)	17005042
Lipopolysaccharides from Escherichia coli O111:B4	Sigma-Aldrich (Merck)	L2630
PD98059	Cell Signaling Technology	9900
Penicillin-Streptomycin	Gibco (Thermo Fischer Scientific)	15140122
Recombinant Human IL-19 Protein	R&D Systems (Bio-Techne)	1035-IL-025
Recombinant Human IL-20 Protein	R&D Systems (Bio-Techne)	1102-IL-025
Recombinant Human IL-24 Protein	R&D Systems (Bio-Techne)	1965-IL-025
Recombinant Human KGF/FGF-7 Protein	R&D Systems (Bio-Techne)	251-KG-010/CF
Recombinant Mouse IFN-γ (carrier-free)	BioLegend	575306
Recombinant Mouse IL-13 (carrier-free)	BioLegend	575904
Recombinant Mouse IL-4 (carrier-free)	BioLegend	574304
Recombinant Mouse M-CSF (carrier-free)	BioLegend	576406

Rosell Park Memorial Institute (RPMI) 1640 Medium	Sigma-Aldrich (Merck)	R8758
Y-27632 dihydrochloride	Tocris (Bio-Techne)	1254
Reagents		
Bovine Serum Albumin (BSA)	Sigma-Aldrich (Merck)	A2153
Buffer RLT	Qiagen	79216
Calcipotriol (MC903)	Tocris (Bio-Techne)	2700
Collagenase from *Clostridium histolyticum* Type IV	Sigma-Aldrich (Merck)	C5138
Corn oil	Sigma-Aldrich (Merck)	C8267
Cultrex Basement Membrane Extract (BME), Type 2, Pathclear	R&D Systems (Bio-Techne)	3532-010-02
DAB Substrate Kit	BD Biosciences	550880
Dimethyl sulfoxide (DMSO), >99,5% BioScience Grade	Carl Roth	A994
Dispase I	Corning	354235
Dispase II	Sigma-Aldrich (Merck)	D4693
DNase I recombinant	Roche	04536282001
Dulbeccos Phosphate Buffered Saline (DPBS)	Sigma-Aldrich (Merck)	D8537
eBioscience™ Fixable Viability Dye eFluor™ 455UV	Invitrogen (Thermo Fischer Scientific)	65-0868-18
eBioscience™ Streptavidin eFluor™ 450 Conjugate	Invitrogen (Thermo Fischer Scientific)	48-4317-82
Ethylenediaminetetraacetic acid (EDTA)	Sigma-Aldrich (Merck)	EDS

Fluorescin isothiocyanate (FITC)-dextran ; average mol wt 3000-5000	Sigma-Aldrich (Merck)	FD4
Goat serum	Sigma-Aldrich (Merck)	G9023
HistoGel	Epredia	HG-4000-012
Hydrogen peroxide	Carl Roth	9681
Nuc Blue™ Live Ready Probes™ Reagent (Hoechst 33342)	Invitrogen (Thermo Fischer Scientific)	R37605
Ovalbumin Grade 5	Sigma-Aldrich (Merck)	A5503
Formaldehyde solution	Sigma-Aldrich (Merck)	F8775
PD98059	MedChemExpress	HY-12028
RIPA Lysis Buffer System	Santa Cruz	sc-24948
Sodium azide	Sigma-Aldrich (Merck)	71289
Streptavidin PE/Cyanine5	BioLegend	405205
SuperSignal™ West Femto Maximum Sensitivity Substrate	Thermo Scientific (Thermo Fischer Scientific)	34095
SuperSignal™ West Pico PLUS Chemiluminescent Substrate	Thermo Scientific (Thermo Fischer Scientific)	34580
Takyon™ Low ROX SYBR 2X MasterMix blue dTTP	Eurogentec	UF-LSMT-B0701
Tamoxifen	MedChemExpress	HY-13757A
TRI Reagent®	Sigma-Aldrich (Merck)	T9424
TrypLE Express Enzyme (1X), phenol red	Gibco (Thermo Fischer Scientific)	12605010
Trypsin inhibitor from *Glycine max* (soybean)	Sigma-Aldrich (Merck)	T9128
Trypsin-EDTA	SAFC Biosciences (Merck)	59418C
TWEEN® 20	Sigma-Aldrich (Merck)	P1379

Critical Commercial Assays		
Direct-zol RNA MiniPrep	Zymo Research	R2052
DNase Max Kit (discontinued)	Qiagen	15200
High-Capacity cDNA Reverse Transcription Kit	Applied Biosystems (Thermo Fischer Scientific)	4368813
QuantiNova SYBR Green PCR Kit	Qiagen	208056
RNeasy Plus Mini Kit	Qiagen	74136
Human IL-19 Quantikine ELISA Kit	R&D Systems (Bio-Techne)	D1900
Human IL-20 Quantikine ELISA Kit	R&D Systems (Bio-Techne)	DL200
Human IL-24 DuoSet ELISA	R&D Systems (Bio-Techne)	DY1965
ELISA MAX™ Deluxe Set Mouse IgE	BioLegend	432404
LEGEND MAX™ Mouse OVA Specific IgE ELISA Kit	BioLegend	439807

Table 5.4 Cell lines

Name	Description	Source	Reference
KYSE-180	Esophageal squamous cell carcinoma cell line established from a well differentiated esophageal squamous cell carcinoma prior to treatment	Leibniz Institute DSMZ-German Collection of Microorganisms and Cell Cultures (ACC379)	(PMID: **1728357**)

Table 5.5 Antibodies

Antibody	Clone	Probe/Fluorophore	Supplier	Cat No.
Antibodies for Immunohistochemistry staining				
Filaggrin	polyclonal		Abcam	Ab81468
Filaggrin family member 2	polyclonal		Novus Biologicals (Bio-Techne)	NBP1-91901
IL-20RA	024		Sino Biological	10397-R024
IL-20RB	polyclonal		Abcam	ab124332
Ki67	SP6		Abcam	ab16667
Peroxidase AffiniPure Goat anti-rabbit IgG (H+L)	polyclonal	Horseradish Peroxidase (HRP)	Jackson ImmunoResearch	111-035-003
Antibodies used for flow cytometry surface staining (Fortessa)				
CD11c	N418	Biotin	BioLegend	117304
CD19	6D56	Biotin	BioLegend	115504
CD3e	145-2C11	Biotin	BioLegend	100304
NK1.1	PK136	Biotin	BioLegend	108704
TER-119/Erythroid cells	TER-119	Biotin	BioLegend	116204
CD117 (c-kit)	2B8	APC/Fire 750	BioLegend	105838
CD11b	M1/70	FITC	BioLegend	101206
CD16/32	93		BioLegend	101302
CD45	30-F11	Superbright 645	Invitrogen (Thermo Fischer Scientific)	64-0451-82
CD49b (Integrin alpha2)	DX5	APC	Invitrogen (Thermo Fischer Scientific)	17-5971-82
CD64 (FcgR1)	X54-5/7.1	PE/Cy7	BioLegend	139*314*

IgE	23G3	FITC	Invitrogen (Thermo Fischer Scientific)	11-5992-81
Siglec-F	E50-2440	BV711	BD Biosciences	740764
Antibodies used for Immunofluorescence staining				
Keratin 5	Poly9059		BioLegend	905903
STAT3	D3Z2G		Cell Signaling Technology	12640S
AffiniPure Goat Anti-Chicken IgY (IgG) (H+L)	polyclonal	Alexa Fluor 488	Jackson ImmunoResearch	103-545-155
Goat Anti-Rabbit IgG (H+L)		Alexa Fluor® 647	Invitrogen (Thermo Fischer Scientific)	A21244
Antibodies used for Cell Sorting				
CD45.2	104	BV650	BioLegend	109836
Antibodies used for Cell Hashing				
TotalSeq-B0301	M1/42; 30-F11		BioLegend	155831
TotalSeq-B0302	M1/42; 30-F11		BioLegend	155833
TotalSeq-B0303	M1/42; 30-F11		BioLegend	155835
TotalSeq-B0304	M1/42; 30-F11		BioLegend	155837
TotalSeq-B0305	M1/42; 30-F11		BioLegend	155839
TotalSeq-B0306	M1/42; 30-F11		BioLegend	155841
TotalSeq-B0307	M1/42; 30-F11		BioLegend	155843
TotalSeq-B0308	M1/42; 30-F11		BioLegend	155845

TotalSeq-B0309	M1/42; 30-F11	BioLegend	155847
TotalSeq-B0310	M1/42; 30-F11	BioLegend	155849
Antibodies used for Western Blotting			
Phospho-Stat3 (Tyr705)	D3A7	Cell Signaling Technology	9145
Stat3	124H6	Cell Signaling Technology	9139
Phospho-p44/42 MAPK (ERK1/2) (Thr202/Tyr204)	D13.14.4E	Cell Signaling Technology	4370
p44/42 MAPK (ERK1/2)	137F5	Cell Signaling Technology	4695
Phospho-NF-kB p65 (Ser536)	93H1	Cell Signaling Technology	3033
NF-kB p65	D14E12	Cell Signaling Technology	8242
Actin Ab-5	C4	BD Biosciences	612656
Peroxidase AffiniPure Goat Anti-Rabbit IgG (H+L)	polyclonal	Jackson ImmunoResearch	111-035-144
Peroxidase AffiniPure Goat Anti-Mouse IgG (H+L)	polyclonal	Jackson ImmunoResearch	111-035-146

Swiss EoE Cohort Study Group (SEECS)

Patrick Aepli[2], Luc Biedermann[3], Annett Franke[4], Thomas Greuter[5], Petr Hruz[1], Pascal Juillerat[6], Peter Netzer[7], Jan Hendrik Niess[1], Jean-Benoit Rossel[8], Ekaterina Safroneeva[8], Catherine Saner[5], Alain M. Schoepfer[5], Philipp Schreiner[3], Dagmar Simon[9], Hans-Uwe Simon[10], Alex Straumann[3]

[1]University Center for Gastrointestinal and Liver Diseases, St. Clara Hospital and University Hospital of Basel, Switzerland

[2]Division of Gastroenterology and Hepatology, Kantonsspital Lucerne

[3]Division of Gastroenterology and Hepatology, University Hospital Zurich

[4]Division of Gastroenterology and Hepatology, Kantonsspital Sankt Gallen

[5]Division of Gastroenterology and Hepatology, Centre Hospitalier Universitaire Vaudois and University of Lausanne

[6]Division of Gastroenterology and Hepatology, Inselspital / University Hospital Bern

[7]GastroZentrum Netzer, Lindenhofspital, Bern

[8]Institute of Social and Preventive Medicine, University of Bern

[9]Division of Dermatology, Inselspital / University Hospital Bern

[10]Institute of Pharmacology, University of Bern

5.2 List of Tables and Figures

5.2.1 List of Tables

5.2.2 List of Figures

5.3   Acknowledgments

to being a good lab mate. My whole-hearted gratitude to Hassan Melhem, the most supportive and encouraging senior scientist with a big heart and a real friend! Special thanks to all other lab colleagues, Philipp, Korcan, Anne, Emilio, Robert, Sara, Celina, and Mao, for their help and support and for enduring my talkative temper over the years. I also want to thank everyone else I've crossed paths with; you've all had your part in this unique journey! It was an absolute pleasure working with you!

It's time to thank the most important people in my life, without whom all this would have never been possible! I want to thank all my friends, especially Quirin, Martin, Jonas Gysel, Jonas Roelli, Tobi, Manuela, and Tamara, for your support, for getting my mind off research sometimes, and for our loyal friendship over the years!

I want to thank the woman I love, Vera Katharina, for being my safe haven, for always having my back, and for unconditionally supporting me in every decision I make. Finally, I would like to thank my beloved family, my father, mother, sister, brother, stepmother, stepsister, and stepbrother. I cannot put in words how much I thank you for unconditionally loving me, believing in me, and supporting me in the good and the bad times! At last, my thoughts are with my Nine and Dede. I hope you're proud of me!

6 REFERENCES

1 Spechler SJ. Of Mice and Men and Metaplasia. *Cell Mol Gastroenterol Hepatol* 2017;4:183-84.

2 Helm JF, Dodds WJ, Pelc LR, et al. Effect of esophageal emptying and saliva on clearance of acid from the esophagus. *N Engl J Med* 1984;310:284-8.

3 Meyers RL, Orlando RC. In vivo bicarbonate secretion by human esophagus. *Gastroenterology* 1992;103:1174-8.

4 Sandilands A, Sutherland C, Irvine AD, et al. Filaggrin in the frontline: role in skin barrier function and disease. *J Cell Sci* 2009;122:1285-94.

5 Steinert PM, Cantieri JS, Teller DC, et al. Characterization of a class of cationic proteins that specifically interact with intermediate filaments. *Proc Natl Acad Sci U S A* 1981;78:4097-101.

6 Wu Z, Hansmann B, Meyer-Hoffert U, et al. Molecular identification and expression analysis of filaggrin-2, a member of the S100 fused-type protein family. *PLoS One* 2009;4:e5227.

7 McKinley-Grant LJ, Idler WW, Bernstein IA, et al. Characterization of a cDNA clone encoding human filaggrin and localization of the gene to chromosome region 1q21. *Proc Natl Acad Sci U S A* 1989;86:4848-52.

8 Marenholz I, Lovering RC, Heizmann CW. An update of the S100 nomenclature. *Biochim Biophys Acta* 2006;1763:1282-3.

9 Rothnagel JA, Mehrel T, Idler WW, et al. The gene for mouse epidermal filaggrin precursor. Its partial characterization, expression, and sequence of a repeating filaggrin unit. *J Biol Chem* 1987;262:15643-8.

10 Lonsdale-Eccles JD, Teller DC, Dale BA. Characterization of a phosphorylated form of the intermediate filament-aggregating protein filaggrin. *Biochemistry* 1982;21:5940-8.

11 Resing KA, Johnson RS, Walsh KA. Characterization of protease processing sites during conversion of rat profilaggrin to filaggrin. *Biochemistry* 1993;32:10036-45.

12 Azouz NP, Klingler AM, Pathre P, et al. Functional role of kallikrein 5 and proteinase-activated receptor 2 in eosinophilic esophagitis. *Sci Transl Med* 2020;12.

13 Deraison C, Bonnart C, Lopez F, et al. LEKTI fragments specifically inhibit KLK5, KLK7, and KLK14 and control desquamation through a pH-dependent interaction. *Mol Biol Cell* 2007;18:3607-19.

14 Azouz NP, Ynga-Durand MA, Caldwell JM, et al. The antiprotease SPINK7 serves as an inhibitory checkpoint for esophageal epithelial inflammatory responses. *Sci Transl Med* 2018;10.

References

15 Descargues P, Deraison C, Bonnart C, et al. Spink5-deficient mice mimic Netherton syndrome through degradation of desmoglein 1 by epidermal protease hyperactivity. *Nat Genet* 2005;37:56-65.

16 Hewett DR, Simons AL, Mangan NE, et al. Lethal, neonatal ichthyosis with increased proteolytic processing of filaggrin in a mouse model of Netherton syndrome. *Hum Mol Genet* 2005;14:335-46.

17 Gan SQ, McBride OW, Idler WW, et al. Organization, structure, and polymorphisms of the human profilaggrin gene. *Biochemistry* 1990;29:9432-40.

18 Candi E, Schmidt R, Melino G. The cornified envelope: a model of cell death in the skin. *Nat Rev Mol Cell Biol* 2005;6:328-40.

19 Hsu CY, Henry J, Raymond AA, et al. Deimination of human filaggrin-2 promotes its proteolysis by calpain 1. *J Biol Chem* 2011;286:23222-33.

20 Kamata Y, Taniguchi A, Yamamoto M, et al. Neutral cysteine protease bleomycin hydrolase is essential for the breakdown of deiminated filaggrin into amino acids. *J Biol Chem* 2009;284:12829-36.

21 Hoste E, Kemperman P, Devos M, et al. Caspase-14 is required for filaggrin degradation to natural moisturizing factors in the skin. *J Invest Dermatol* 2011;131:2233-41.

22 Makino T, Mizawa M, Yamakoshi T, et al. Expression of filaggrin-2 protein in the epidermis of human skin diseases: a comparative analysis with filaggrin. *Biochem Biophys Res Commun* 2014;449:100-6.

23 Palmer CN, Irvine AD, Terron-Kwiatkowski A, et al. Common loss-of-function variants of the epidermal barrier protein filaggrin are a major predisposing factor for atopic dermatitis. *Nat Genet* 2006;38:441-6.

24 Margolis DJ, Gupta J, Apter AJ, et al. Filaggrin-2 variation is associated with more persistent atopic dermatitis in African American subjects. *J Allergy Clin Immunol* 2014;133:784-9.

25 Farquhar MG, Palade GE. Junctional complexes in various epithelia. *J Cell Biol* 1963;17:375-412.

26 Anderson JM, Van Itallie CM. Physiology and function of the tight junction. *Cold Spring Harb Perspect Biol* 2009;1:a002584.

27 Al-Sadi R, Khatib K, Guo S, et al. Occludin regulates macromolecule flux across the intestinal epithelial tight junction barrier. *Am J Physiol Gastrointest Liver Physiol* 2011;300:G1054-64.

28 Claude P. Morphological factors influencing transepithelial permeability: a model for the resistance of the zonula occludens. *J Membr Biol* 1978;39:219-32.

29 Patel SD, Chen CP, Bahna F, et al. Cadherin-mediated cell-cell adhesion: sticking together as a family. *Curr Opin Struct Biol* 2003;13:690-8.

References

30 Perez-Moreno M, Fuchs E. Catenins: keeping cells from getting their signals crossed. *Dev Cell* 2006;11:601-12.

31 Getsios S, Amargo EV, Dusek RL, et al. Coordinated expression of desmoglein 1 and desmocollin 1 regulates intercellular adhesion. *Differentiation* 2004;72:419-33.

32 Simon D, Page B, Vogel M, et al. Evidence of an abnormal epithelial barrier in active, untreated and corticosteroid-treated eosinophilic esophagitis. *Allergy* 2018;73:239-47.

33 Furuse M, Hata M, Furuse K, et al. Claudin-based tight junctions are crucial for the mammalian epidermal barrier: a lesson from claudin-1-deficient mice. *J Cell Biol* 2002;156:1099-111.

34 Masterson JC, Biette KA, Hammer JA, et al. Epithelial HIF-1alpha/claudin-1 axis regulates barrier dysfunction in eosinophilic esophagitis. *J Clin Invest* 2019;129:3224-35.

35 Sherrill JD, Kc K, Wu D, et al. Desmoglein-1 regulates esophageal epithelial barrier function and immune responses in eosinophilic esophagitis. *Mucosal Immunol* 2014;7:718-29.

36 Doupe DP, Alcolea MP, Roshan A, et al. A single progenitor population switches behavior to maintain and repair esophageal epithelium. *Science* 2012;337:1091-3.

37 Marenholz I, Volz A, Ziegler A, et al. Genetic analysis of the epidermal differentiation complex (EDC) on human chromosome 1q21: chromosomal orientation, new markers, and a 6-Mb YAC contig. *Genomics* 1996;37:295-302.

38 Fuchs E. Keratins as biochemical markers of epithelial differentiation. *Trends Genet* 1988;4:277-81.

39 Moll R, Divo M, Langbein L. The human keratins: biology and pathology. *Histochem Cell Biol* 2008;129:705-33.

40 Lucendo AJ, Navarro M, Comas C, et al. Immunophenotypic characterization and quantification of the epithelial inflammatory infiltrate in eosinophilic esophagitis through stereology: an analysis of the cellular mechanisms of the disease and the immunologic capacity of the esophagus. *Am J Surg Pathol* 2007;31:598-606.

41 Olivares-Villagomez D, Van Kaer L. Intestinal Intraepithelial Lymphocytes: Sentinels of the Mucosal Barrier. *Trends Immunol* 2018;39:264-75.

42 Neutra MR, Pringault E, Kraehenbuhl JP. Antigen sampling across epithelial barriers and induction of mucosal immune responses. *Annu Rev Immunol* 1996;14:275-300.

43 Stokes CR, Soothill JF, Turner MW. Immune exclusion is a function of IgA. *Nature* 1975;255:745-6.

44 Weltzin R, Lucia-Jandris P, Michetti P, et al. Binding and transepithelial transport of immunoglobulins by intestinal M cells: demonstration using monoclonal IgA antibodies against enteric viral proteins. *J Cell Biol* 1989;108:1673-85.

45 Mantis NJ, Rol N, Corthesy B. Secretory IgA's complex roles in immunity and mucosal homeostasis in the gut. *Mucosal Immunol* 2011;4:603-11.

46 Brandtzaeg P. Mucosal and glandular distribution of immunoglobulin components: differential localization of free and bound SC in secretory epithelial cells. *J Immunol* 1974;112:1553-9.

47 Brandtzaeg P, Prydz H. Direct evidence for an integrated function of J chain and secretory component in epithelial transport of immunoglobulins. *Nature* 1984;311:71-3.

48 Phalipon A, Cardona A, Kraehenbuhl JP, et al. Secretory component: a new role in secretory IgA-mediated immune exclusion in vivo. *Immunity* 2002;17:107-15.

49 Kaymak T, Hruz P, Niess JH. Immune system and microbiome in the esophagus: implications for understanding inflammatory diseases. *FEBS J* 2021.

50 Iwasaki A. Mucosal dendritic cells. *Annu Rev Immunol* 2007;25:381-418.

51 Novak N, Haberstok J, Bieber T, et al. The immune privilege of the oral mucosa. *Trends Mol Med* 2008;14:191-8.

52 Gigon L, Yousefi S, Karaulov A, et al. Mechanisms of toxicity mediated by neutrophil and eosinophil granule proteins. *Allergol Int* 2021;70:30-38.

53 Yousefi S, Gold JA, Andina N, et al. Catapult-like release of mitochondrial DNA by eosinophils contributes to antibacterial defense. *Nat Med* 2008;14:949-53.

54 Chu VT, Beller A, Rausch S, et al. Eosinophils promote generation and maintenance of immunoglobulin-A-expressing plasma cells and contribute to gut immune homeostasis. *Immunity* 2014;40:582-93.

55 Mishra A, Hogan SP, Lee JJ, et al. Fundamental signals that regulate eosinophil homing to the gastrointestinal tract. *J Clin Invest* 1999;103:1719-27.

56 Gouon-Evans V, Rothenberg ME, Pollard JW. Postnatal mammary gland development requires macrophages and eosinophils. *Development* 2000;127:2269-82.

57 Kato M, Kephart GM, Talley NJ, et al. Eosinophil infiltration and degranulation in normal human tissue. *Anat Rec* 1998;252:418-25.

58 Jose PJ, Griffiths-Johnson DA, Collins PD, et al. Eotaxin: a potent eosinophil chemoattractant cytokine detected in a guinea pig model of allergic airways inflammation. *J Exp Med* 1994;179:881-7.

59 Forssmann U, Uguccioni M, Loetscher P, et al. Eotaxin-2, a novel CC chemokine that is selective for the chemokine receptor CCR3, and acts like eotaxin on human eosinophil and basophil leukocytes. *J Exp Med* 1997;185:2171-6.

60 Shinkai A, Yoshisue H, Koike M, et al. A novel human CC chemokine, eotaxin-3, which is expressed in IL-4-stimulated vascular endothelial cells, exhibits potent activity toward eosinophils. *J Immunol* 1999;163:1602-10.

61 Collins PD, Marleau S, Griffiths-Johnson DA, et al. Cooperation between interleukin-5 and the chemokine eotaxin to induce eosinophil accumulation in vivo. *J Exp Med* 1995;182:1169-74.

62 Sanderson CJ, Warren DJ, Strath M. Identification of a lymphokine that stimulates eosinophil differentiation in vitro. Its relationship to interleukin 3, and functional properties of eosinophils produced in cultures. *J Exp Med* 1985;162:60-74.

63 Clutterbuck EJ, Sanderson CJ. Human eosinophil hematopoiesis studied in vitro by means of murine eosinophil differentiation factor (IL5): production of functionally active eosinophils from normal human bone marrow. *Blood* 1988;71:646-51.

64 Warringa RA, Mengelers HJ, Kuijper PH, et al. In vivo priming of platelet-activating factor-induced eosinophil chemotaxis in allergic asthmatic individuals. *Blood* 1992;79:1836-41.

65 Tai PC, Sun L, Spry CJ. Effects of IL-5, granulocyte/macrophage colony-stimulating factor (GM-CSF) and IL-3 on the survival of human blood eosinophils in vitro. *Clin Exp Immunol* 1991;85:312-6.

66 Ponath PD, Qin S, Post TW, et al. Molecular cloning and characterization of a human eotaxin receptor expressed selectively on eosinophils. *J Exp Med* 1996;183:2437-48.

67 Daugherty BL, Siciliano SJ, DeMartino JA, et al. Cloning, expression, and characterization of the human eosinophil eotaxin receptor. *J Exp Med* 1996;183:2349-54.

68 Odiase E, Zhang X, Chang Y, et al. In Esophageal Squamous Cells From Eosinophilic Esophagitis Patients, Th2 Cytokines Increase Eotaxin-3 Secretion Through Effects on Intracellular Calcium and a Non-Gastric Proton Pump. *Gastroenterology* 2021;160:2072-88 e6.

69 Spencer LA, Szela CT, Perez SA, et al. Human eosinophils constitutively express multiple Th1, Th2, and immunoregulatory cytokines that are secreted rapidly and differentially. *J Leukoc Biol* 2009;85:117-23.

70 Jacobsen EA, Zellner KR, Colbert D, et al. Eosinophils regulate dendritic cells and Th2 pulmonary immune responses following allergen provocation. *J Immunol* 2011;187:6059-68.

71 Elishmereni M, Alenius HT, Bradding P, et al. Physical interactions between mast cells and eosinophils: a novel mechanism enhancing eosinophil survival in vitro. *Allergy* 2011;66:376-85.

72 Elishmereni M, Bachelet I, Nissim Ben-Efraim AH, et al. Interacting mast cells and eosinophils acquire an enhanced activation state in vitro. *Allergy* 2013;68:171-9.

73 Dellon ES, Liacouras CA, Molina-Infante J, et al. Updated International Consensus Diagnostic Criteria for Eosinophilic Esophagitis: Proceedings of the AGREE Conference. *Gastroenterology* 2018;155:1022-33 e10.

74 Straumann A, Bauer M, Fischer B, et al. Idiopathic eosinophilic esophagitis is associated with a T(H)2-type allergic inflammatory response. *J Allergy Clin Immunol* 2001;108:954-61.

75 Liacouras CA, Spergel J, Gober LM. Eosinophilic esophagitis: clinical presentation in children. *Gastroenterol Clin North Am* 2014;43:219-29.

76 Attwood SE, Smyrk TC, Demeester TR, et al. Esophageal eosinophilia with dysphagia. A distinct clinicopathologic syndrome. *Dig Dis Sci* 1993;38:109-16.

77 Straumann A, Spichtin HP, Bernoulli R, et al. [Idiopathic eosinophilic esophagitis: a frequently overlooked disease with typical clinical aspects and discrete endoscopic findings]. *Schweiz Med Wochenschr* 1994;124:1419-29.

78 Shub MD, Ulshen MH, Hargrove CB, et al. Esophagitis: a frequent consequence of gastroesophageal reflux in infancy. *J Pediatr* 1985;107:881-4.

79 Lee RG. Marked eosinophilia in esophageal mucosal biopsies. *Am J Surg Pathol* 1985;9:475-9.

80 Furuta GT, Liacouras CA, Collins MH, et al. Eosinophilic esophagitis in children and adults: a systematic review and consensus recommendations for diagnosis and treatment. *Gastroenterology* 2007;133:1342-63.

81 Lucendo AJ, Molina-Infante J, Arias A, et al. Guidelines on eosinophilic esophagitis: evidence-based statements and recommendations for diagnosis and management in children and adults. *United European Gastroenterol J* 2017;5:335-58.

82 Ngo P, Furuta GT, Antonioli DA, et al. Eosinophils in the esophagus--peptic or allergic eosinophilic esophagitis? Case series of three patients with esophageal eosinophilia. *Am J Gastroenterol* 2006;101:1666-70.

83 Molina-Infante J, Ferrando-Lamana L, Ripoll C, et al. Esophageal eosinophilic infiltration responds to proton pump inhibition in most adults. *Clin Gastroenterol Hepatol* 2011;9:110-7.

84 Dellon ES, Gonsalves N, Hirano I, et al. ACG clinical guideline: Evidenced based approach to the diagnosis and management of esophageal eosinophilia and eosinophilic esophagitis (EoE). *Am J Gastroenterol* 2013;108:679-92; quiz 93.

85 Dellon ES, Speck O, Woodward K, et al. Clinical and endoscopic characteristics do not reliably differentiate PPI-responsive esophageal eosinophilia and eosinophilic esophagitis in patients undergoing upper endoscopy: a prospective cohort study. *Am J Gastroenterol* 2013;108:1854-60.

86 Moawad FJ, Schoepfer AM, Safroneeva E, et al. Eosinophilic oesophagitis and proton pump inhibitor-responsive oesophageal eosinophilia have similar clinical, endoscopic and histological findings. *Aliment Pharmacol Ther* 2014;39:603-8.

87 Wen T, Dellon ES, Moawad FJ, et al. Transcriptome analysis of proton pump inhibitor-responsive esophageal eosinophilia reveals proton pump inhibitor-reversible allergic inflammation. *J Allergy Clin Immunol* 2015;135:187-97.

88 Shoda T, Matsuda A, Nomura I, et al. Eosinophilic esophagitis versus proton pump inhibitor-responsive esophageal eosinophilia: Transcriptome analysis. *J Allergy Clin Immunol* 2017;139:2010-13 e4.

89 Hruz P, Straumann A, Bussmann C, et al. Escalating incidence of eosinophilic esophagitis: a 20-year prospective, population-based study in Olten County, Switzerland. *J Allergy Clin Immunol* 2011;128:1349-50 e5.

90 Dellon ES, Jensen ET, Martin CF, et al. Prevalence of eosinophilic esophagitis in the United States. *Clin Gastroenterol Hepatol* 2014;12:589-96 e1.

91 Jensen ET, Kappelman MD, Martin CF, et al. Health-care utilization, costs, and the burden of disease related to eosinophilic esophagitis in the United States. *Am J Gastroenterol* 2015;110:626-32.

92 Collins MH, Blanchard C, Abonia JP, et al. Clinical, pathologic, and molecular characterization of familial eosinophilic esophagitis compared with sporadic cases. *Clin Gastroenterol Hepatol* 2008;6:621-9.

93 Jensen ET, Kuhl JT, Martin LJ, et al. Prenatal, intrapartum, and postnatal factors are associated with pediatric eosinophilic esophagitis. *J Allergy Clin Immunol* 2018;141:214-22.

94 Simon D, Marti H, Heer P, et al. Eosinophilic esophagitis is frequently associated with IgE-mediated allergic airway diseases. *J Allergy Clin Immunol* 2005;115:1090-2.

95 Kottyan LC, Trimarchi MP, Lu X, et al. Replication and meta-analyses nominate numerous eosinophilic esophagitis risk genes. *J Allergy Clin Immunol* 2021;147:255-66.

96 Dellon ES, Speck O, Woodward K, et al. Distribution and variability of esophageal eosinophilia in patients undergoing upper endoscopy. *Mod Pathol* 2015;28:383-90.

97 Collins MH, Martin LJ, Alexander ES, et al. Newly developed and validated eosinophilic esophagitis histology scoring system and evidence that it outperforms peak eosinophil count for disease diagnosis and monitoring. *Dis Esophagus* 2017;30:1-8.

98 Straumann A, Conus S, Degen L, et al. Long-term budesonide maintenance treatment is partially effective for patients with eosinophilic esophagitis. *Clin Gastroenterol Hepatol* 2011;9:400-9 e1.

References

99 Kelly KJ, Lazenby AJ, Rowe PC, et al. Eosinophilic esophagitis attributed to gastroesophageal reflux: improvement with an amino acid-based formula. *Gastroenterology* 1995;109:1503-12.

100 Kagalwalla AF, Sentongo TA, Ritz S, et al. Effect of six-food elimination diet on clinical and histologic outcomes in eosinophilic esophagitis. *Clin Gastroenterol Hepatol* 2006;4:1097-102.

101 Molina-Infante J, Arias A, Barrio J, et al. Four-food group elimination diet for adult eosinophilic esophagitis: A prospective multicenter study. *J Allergy Clin Immunol* 2014;134:1093-9 e1.

102 Arias A, Gonzalez-Cervera J, Tenias JM, et al. Efficacy of dietary interventions for inducing histologic remission in patients with eosinophilic esophagitis: a systematic review and meta-analysis. *Gastroenterology* 2014;146:1639-48.

103 Wang R, Hirano I, Doerfler B, et al. Assessing Adherence and Barriers to Long-Term Elimination Diet Therapy in Adults with Eosinophilic Esophagitis. *Dig Dis Sci* 2018;63:1756-62.

104 Klinnert MD, Silveira L, Harris R, et al. Health-related quality of life over time in children with eosinophilic esophagitis and their families. *J Pediatr Gastroenterol Nutr* 2014;59:308-16.

105 Taft TH, Kern E, Keefer L, et al. Qualitative assessment of patient-reported outcomes in adults with eosinophilic esophagitis. *J Clin Gastroenterol* 2011;45:769-74.

106 Molina-Infante J, Rivas MD, Hernandez-Alonso M, et al. Proton pump inhibitor-responsive oesophageal eosinophilia correlates with downregulation of eotaxin-3 and Th2 cytokines overexpression. *Aliment Pharmacol Ther* 2014;40:955-65.

107 Zhang X, Cheng E, Huo X, et al. Omeprazole blocks STAT6 binding to the eotaxin-3 promoter in eosinophilic esophagitis cells. *PLoS One* 2012;7:e50037.

108 Cheng E, Zhang X, Huo X, et al. Omeprazole blocks eotaxin-3 expression by oesophageal squamous cells from patients with eosinophilic oesophagitis and GORD. *Gut* 2013;62:824-32.

109 Park JY, Zhang X, Nguyen N, et al. Proton pump inhibitors decrease eotaxin-3 expression in the proximal esophagus of children with esophageal eosinophilia. *PLoS One* 2014;9:e101391.

110 van Rhijn BD, Weijenborg PW, Verheij J, et al. Proton pump inhibitors partially restore mucosal integrity in patients with proton pump inhibitor-responsive esophageal eosinophilia but not eosinophilic esophagitis. *Clin Gastroenterol Hepatol* 2014;12:1815-23 e2.

111 Lucendo AJ, Arias A, Molina-Infante J. Efficacy of Proton Pump Inhibitor Drugs for Inducing Clinical and Histologic Remission in Patients With Symptomatic Esophageal Eosinophilia: A Systematic Review and Meta-Analysis. *Clin Gastroenterol Hepatol* 2016;14:13-22 e1.

References

112 Lucendo AJ, Miehlke S, Schlag C, et al. Efficacy of Budesonide Orodispersible Tablets as Induction Therapy for Eosinophilic Esophagitis in a Randomized Placebo-Controlled Trial. *Gastroenterology* 2019;157:74-86 e15.

113 Miehlke S, Schlag C, Lucendo AJ, et al. Budesonide orodispersible tablets for induction of remission in patients with active eosinophilic oesophagitis: A 6-week open-label trial of the EOS-2 Programme. *United European Gastroenterol J* 2022;10:330-43.

114 Straumann A, Lucendo AJ, Miehlke S, et al. Budesonide Orodispersible Tablets Maintain Remission in a Randomized, Placebo-Controlled Trial of Patients With Eosinophilic Esophagitis. *Gastroenterology* 2020;159:1672-85 e5.

115 Philla KQ, Min SB, Hefner JN, et al. Swallowed glucocorticoid therapy for eosinophilic esophagitis in children does not suppress adrenal function. *J Pediatr Endocrinol Metab* 2015;28:1101-6.

116 Simon D, Simon HU. Relationship of skin barrier breakdown and eosinophilic esophagitis. *J Allergy Clin Immunol* 2020;145:90-92 e1.

117 Rochman M, Azouz NP, Rothenberg ME. Epithelial origin of eosinophilic esophagitis. *J Allergy Clin Immunol* 2018;142:10-23.

118 Mishra A, Hogan SP, Brandt EB, et al. IL-5 promotes eosinophil trafficking to the esophagus. *J Immunol* 2002;168:2464-9.

119 Masterson JC, McNamee EN, Hosford L, et al. Local hypersensitivity reaction in transgenic mice with squamous epithelial IL-5 overexpression provides a novel model of eosinophilic oesophagitis. *Gut* 2014;63:43-53.

120 Straumann A, Conus S, Grzonka P, et al. Anti-interleukin-5 antibody treatment (mepolizumab) in active eosinophilic oesophagitis: a randomised, placebo-controlled, double-blind trial. *Gut* 2010;59:21-30.

121 Assa'ad AH, Gupta SK, Collins MH, et al. An antibody against IL-5 reduces numbers of esophageal intraepithelial eosinophils in children with eosinophilic esophagitis. *Gastroenterology* 2011;141:1593-604.

122 Spergel JM, Rothenberg ME, Collins MH, et al. Reslizumab in children and adolescents with eosinophilic esophagitis: results of a double-blind, randomized, placebo-controlled trial. *J Allergy Clin Immunol* 2012;129:456-63, 63 e1-3.

123 Di Bona D, Crimi C, D'Uggento AM, et al. Effectiveness of benralizumab in severe eosinophilic asthma: Distinct sub-phenotypes of response identified by cluster analysis. *Clin Exp Allergy* 2022;52:312-23.

124 Hirano I, Dellon ES, Hamilton JD, et al. Efficacy of Dupilumab in a Phase 2 Randomized Trial of Adults With Active Eosinophilic Esophagitis. *Gastroenterology* 2020;158:111-22 e10.

125 Dellon ES. Dupilumab for EoE at ACG 2021. 2021.

126 Sandborn WJ, Su C, Sands BE, et al. Tofacitinib as Induction and Maintenance Therapy for Ulcerative Colitis. *N Engl J Med* 2017;376:1723-36.

127 Ma C, Lee JK, Mitra AR, et al. Systematic review with meta-analysis: efficacy and safety of oral Janus kinase inhibitors for inflammatory bowel disease. *Aliment Pharmacol Ther* 2019;50:5-23.

128 Mendoza Alvarez LB, Liu X, Glover S. Treatment-resistant eosinophilic oesophagitis successfully managed with tofacitinib. *BMJ Case Rep* 2019;12.

129 Straumann A, Spichtin HP, Grize L, et al. Natural history of primary eosinophilic esophagitis: a follow-up of 30 adult patients for up to 11.5 years. *Gastroenterology* 2003;125:1660-9.

130 Schoepfer AM, Safroneeva E, Bussmann C, et al. Delay in diagnosis of eosinophilic esophagitis increases risk for stricture formation in a time-dependent manner. *Gastroenterology* 2013;145:1230-6 e1-2.

131 Greuter T, Safroneeva E, Bussmann C, et al. Maintenance Treatment Of Eosinophilic Esophagitis With Swallowed Topical Steroids Alters Disease Course Over A 5-Year Follow-up Period In Adult Patients. *Clin Gastroenterol Hepatol* 2019;17:419-28 e6.

132 Schoepfer AM, Gonsalves N, Bussmann C, et al. Esophageal dilation in eosinophilic esophagitis: effectiveness, safety, and impact on the underlying inflammation. *Am J Gastroenterol* 2010;105:1062-70.

133 Straumann A, Bussmann C, Zuber M, et al. Eosinophilic esophagitis: analysis of food impaction and perforation in 251 adolescent and adult patients. *Clin Gastroenterol Hepatol* 2008;6:598-600.

134 Kuchen T, Straumann A, Safroneeva E, et al. Swallowed topical corticosteroids reduce the risk for long-lasting bolus impactions in eosinophilic esophagitis. *Allergy* 2014;69:1248-54.

135 Kottyan LC, Davis BP, Sherrill JD, et al. Genome-wide association analysis of eosinophilic esophagitis provides insight into the tissue specificity of this allergic disease. *Nat Genet* 2014;46:895-900.

136 Sleiman PM, Wang ML, Cianferoni A, et al. GWAS identifies four novel eosinophilic esophagitis loci. *Nat Commun* 2014;5:5593.

137 Sherrill JD, Kiran KC, Blanchard C, et al. Analysis and expansion of the eosinophilic esophagitis transcriptome by RNA sequencing. *Genes Immun* 2014;15:361-9.

138 Blanchard C, Stucke EM, Burwinkel K, et al. Coordinate interaction between IL-13 and epithelial differentiation cluster genes in eosinophilic esophagitis. *J Immunol* 2010;184:4033-41.

139 Rochman M, Travers J, Miracle CE, et al. Profound loss of esophageal tissue differentiation in patients with eosinophilic esophagitis. *J Allergy Clin Immunol* 2017;140:738-49 e3.

140 Katzka DA, Tadi R, Smyrk TC, et al. Effects of topical steroids on tight junction proteins and spongiosis in esophageal epithelia of patients with eosinophilic esophagitis. *Clin Gastroenterol Hepatol* 2014;12:1824-9 e1.

141 Blanchard C, Mingler MK, Vicario M, et al. IL-13 involvement in eosinophilic esophagitis: transcriptome analysis and reversibility with glucocorticoids. *J Allergy Clin Immunol* 2007;120:1292-300.

142 Kc K, Rothenberg ME, Sherrill JD. In vitro model for studying esophageal epithelial differentiation and allergic inflammatory responses identifies keratin involvement in eosinophilic esophagitis. *PLoS One* 2015;10:e0127755.

143 Kleuskens MTA, Haasnoot ML, Herpers BM, et al. Butyrate and propionate restore interleukin 13-compromised esophageal epithelial barrier function. *Allergy* 2021.

144 Wu L, Oshima T, Li M, et al. Filaggrin and tight junction proteins are crucial for IL-13-mediated esophageal barrier dysfunction. *Am J Physiol Gastrointest Liver Physiol* 2018;315:G341-G50.

145 Davis BP, Stucke EM, Khorki ME, et al. Eosinophilic esophagitis-linked calpain 14 is an IL-13-induced protease that mediates esophageal epithelial barrier impairment. *JCI Insight* 2016;1:e86355.

146 de Veer SJ, Furio L, Harris JM, et al. Proteases: common culprits in human skin disorders. *Trends Mol Med* 2014;20:166-78.

147 Afonina IS, Muller C, Martin SJ, et al. Proteolytic Processing of Interleukin-1 Family Cytokines: Variations on a Common Theme. *Immunity* 2015;42:991-1004.

148 Ono Y, Sorimachi H. Calpains: an elaborate proteolytic system. *Biochim Biophys Acta* 2012;1824:224-36.

149 Shoda T, Kaufman KM, Wen T, et al. Desmoplakin and periplakin genetically and functionally contribute to eosinophilic esophagitis. *Nat Commun* 2021;12:6795.

150 Gallagher G, Dickensheets H, Eskdale J, et al. Cloning, expression and initial characterization of interleukin-19 (IL-19), a novel homologue of human interleukin-10 (IL-10). *Genes Immun* 2000;1:442-50.

151 Blumberg H, Conklin D, Xu WF, et al. Interleukin 20: discovery, receptor identification, and role in epidermal function. *Cell* 2001;104:9-19.

152 Jiang H, Su ZZ, Lin JJ, et al. The melanoma differentiation associated gene mda-7 suppresses cancer cell growth. *Proc Natl Acad Sci U S A* 1996;93:9160-5.

153 Dumoutier L, Leemans C, Lejeune D, et al. Cutting edge: STAT activation by IL-19, IL-20 and mda-7 through IL-20 receptor complexes of two types. *J Immunol* 2001;167:3545-9.

154 Parrish-Novak J, Xu W, Brender T, et al. Interleukins 19, 20, and 24 signal through two distinct receptor complexes. Differences in receptor-ligand interactions mediate unique biological functions. *J Biol Chem* 2002;277:47517-23.

155 Kunz S, Wolk K, Witte E, et al. Interleukin (IL)-19, IL-20 and IL-24 are produced by and act on keratinocytes and are distinct from classical ILs. *Exp Dermatol* 2006;15:991-1004.

156 Wolk K, Kunz S, Asadullah K, et al. Cutting edge: immune cells as sources and targets of the IL-10 family members? *J Immunol* 2002;168:5397-402.

157 Wang F, Lee E, Lowes MA, et al. Prominent production of IL-20 by CD68+/CD11c+ myeloid-derived cells in psoriasis: Gene regulation and cellular effects. *J Invest Dermatol* 2006;126:1590-9.

158 Schaefer G, Venkataraman C, Schindler U. Cutting edge: FISP (IL-4-induced secreted protein), a novel cytokine-like molecule secreted by Th2 cells. *J Immunol* 2001;166:5859-63.

159 Tritsaris K, Myren M, Ditlev SB, et al. IL-20 is an arteriogenic cytokine that remodels collateral networks and improves functions of ischemic hind limbs. *Proc Natl Acad Sci U S A* 2007;104:15364-9.

160 Li X, Huang J, Chen X, et al. IL-19 induced by IL-13/IL-17A in the nasal epithelium of patients with chronic rhinosinusitis upregulates MMP-9 expression via ERK/NF-kappaB signaling pathway. *Clin Transl Allergy* 2021;11:e12003.

161 Su ZZ, Madireddi MT, Lin JJ, et al. The cancer growth suppressor gene mda-7 selectively induces apoptosis in human breast cancer cells and inhibits tumor growth in nude mice. *Proc Natl Acad Sci U S A* 1998;95:14400-5.

162 Chan JR, Blumenschein W, Murphy E, et al. IL-23 stimulates epidermal hyperplasia via TNF and IL-20R2-dependent mechanisms with implications for psoriasis pathogenesis. *J Exp Med* 2006;203:2577-87.

163 He M, Liang P. IL-24 transgenic mice: in vivo evidence of overlapping functions for IL-20, IL-22, and IL-24 in the epidermis. *J Immunol* 2010;184:1793-8.

164 Sa SM, Valdez PA, Wu J, et al. The effects of IL-20 subfamily cytokines on reconstituted human epidermis suggest potential roles in cutaneous innate defense and pathogenic adaptive immunity in psoriasis. *J Immunol* 2007;178:2229-40.

165 Mitamura Y, Nunomura S, Nanri Y, et al. The IL-13/periostin/IL-24 pathway causes epidermal barrier dysfunction in allergic skin inflammation. *Allergy* 2018;73:1881-91.

166 Liao SC, Cheng YC, Wang YC, et al. IL-19 induced Th2 cytokines and was up-regulated in asthma patients. *J Immunol* 2004;173:6712-8.

167 Gong W, Wang X, Zhang Y, et al. Interleukin-20 promotes airway remodeling in asthma. *Inflammation* 2014;37:2099-105.

References

168 Wu J, Wang G, Hao J, et al. The correlation between IL-20 and the Th2 immune response in human asthma. *Asian Pac J Allergy Immunol* 2014;32:316-20.

169 Cornelissen C, Marquardt Y, Czaja K, et al. IL-31 regulates differentiation and filaggrin expression in human organotypic skin models. *J Allergy Clin Immunol* 2012;129:426-33, 33 e1-8.

170 Weng YH, Chen WY, Lin YL, et al. Blocking IL-19 Signaling Ameliorates Allergen-Induced Airway Inflammation. *Front Immunol* 2019;10:968.

171 Pace E, Scafidi V, Di Bona D, et al. Increased expression of IL-19 in the epithelium of patients with chronic rhinosinusitis and nasal polyps. *Allergy* 2012;67:878-86.

172 Steinert A, Linas I, Kaya B, et al. The Stimulation of Macrophages with TLR Ligands Supports Increased IL-19 Expression in Inflammatory Bowel Disease Patients and in Colitis Models. *J Immunol* 2017;199:2570-84.

173 Wahl C, Muller W, Leithauser F, et al. IL-20 receptor 2 signaling down-regulates antigen-specific T cell responses. *J Immunol* 2009;182:802-10.

174 Alonzi T, Maritano D, Gorgoni B, et al. Essential role of STAT3 in the control of the acute-phase response as revealed by inducible gene inactivation [correction of activation] in the liver. *Mol Cell Biol* 2001;21:1621-32.

175 Kasagi Y, Chandramouleeswaran PM, Whelan KA, et al. The Esophageal Organoid System Reveals Functional Interplay Between Notch and Cytokines in Reactive Epithelial Changes. *Cell Mol Gastroenterol Hepatol* 2018;5:333-52.

176 Noti M, Wojno ED, Kim BS, et al. Thymic stromal lymphopoietin-elicited basophil responses promote eosinophilic esophagitis. *Nat Med* 2013;19:1005-13.

177 Schindelin J, Arganda-Carreras I, Frise E, et al. Fiji: an open-source platform for biological-image analysis. *Nat Methods* 2012;9:676-82.

178 Bankhead P, Loughrey MB, Fernandez JA, et al. QuPath: Open source software for digital pathology image analysis. *Sci Rep* 2017;7:16878.

179 Dobin A, Davis CA, Schlesinger F, et al. STAR: ultrafast universal RNA-seq aligner. *Bioinformatics* 2013;29:15-21.

180 Liao Y, Smyth GK, Shi W. featureCounts: an efficient general purpose program for assigning sequence reads to genomic features. *Bioinformatics* 2014;30:923-30.

181 Amezquita RA, Lun ATL, Becht E, et al. Orchestrating single-cell analysis with Bioconductor. *Nat Methods* 2020;17:137-45.

182 Huber W, Carey VJ, Gentleman R, et al. Orchestrating high-throughput genomic analysis with Bioconductor. *Nat Methods* 2015;12:115-21.

183 Robinson MD, McCarthy DJ, Smyth GK. edgeR: a Bioconductor package for differential expression analysis of digital gene expression data. *Bioinformatics* 2010;26:139-40.

References

184 Robinson MD, Oshlack A. A scaling normalization method for differential expression analysis of RNA-seq data. *Genome Biol* 2010;11:R25.

185 Lun AT, Chen Y, Smyth GK. It's DE-licious: A Recipe for Differential Expression Analyses of RNA-seq Experiments Using Quasi-Likelihood Methods in edgeR. *Methods Mol Biol* 2016;1418:391-416.

186 Wu D, Smyth GK. Camera: a competitive gene set test accounting for inter-gene correlation. *Nucleic Acids Res* 2012;40:e133.

187 Liberzon A, Birger C, Thorvaldsdottir H, et al. The Molecular Signatures Database (MSigDB) hallmark gene set collection. *Cell Syst* 2015;1:417-25.

188 Yates AD, Achuthan P, Akanni W, et al. Ensembl 2020. *Nucleic Acids Res* 2020;48:D682-D88.

189 Griffiths JA, Richard AC, Bach K, et al. Detection and removal of barcode swapping in single-cell RNA-seq data. *Nat Commun* 2018;9:2667.

190 Lun ATL, Riesenfeld S, Andrews T, et al. EmptyDrops: distinguishing cells from empty droplets in droplet-based single-cell RNA sequencing data. *Genome Biol* 2019;20:63.

191 Lun AT, McCarthy DJ, Marioni JC. A step-by-step workflow for low-level analysis of single-cell RNA-seq data with Bioconductor. *F1000Res* 2016;5:2122.

192 McCarthy DJ, Campbell KR, Lun AT, et al. Scater: pre-processing, quality control, normalization and visualization of single-cell RNA-seq data in R. *Bioinformatics* 2017;33:1179-86.

193 Ilicic T, Kim JK, Kolodziejczyk AA, et al. Classification of low quality cells from single-cell RNA-seq data. *Genome Biol* 2016;17:29.

194 Vallejos CA, Risso D, Scialdone A, et al. Normalizing single-cell RNA sequencing data: challenges and opportunities. *Nat Methods* 2017;14:565-71.

195 Ahrne E, Glatter T, Vigano C, et al. Evaluation and Improvement of Quantification Accuracy in Isobaric Mass Tag-Based Protein Quantification Experiments. *J Proteome Res* 2016;15:2537-47.

196 Wang Y, Yang F, Gritsenko MA, et al. Reversed-phase chromatography with multiple fraction concatenation strategy for proteome profiling of human MCF10A cells. *Proteomics* 2011;11:2019-26.

197 Ritchie ME, Phipson B, Wu D, et al. limma powers differential expression analyses for RNA-sequencing and microarray studies. *Nucleic Acids Res* 2015;43:e47.

198 Perez-Riverol Y, Bai J, Bandla C, et al. The PRIDE database resources in 2022: a hub for mass spectrometry-based proteomics evidences. *Nucleic Acids Res* 2022;50:D543-D52.

199 Hsieh KY, Tsai CC, Wu CH, et al. Epicutaneous exposure to protein antigen and food allergy. *Clin Exp Allergy* 2003;33:1067-75.

200 Lack G, Fox D, Northstone K, et al. Factors associated with the development of peanut allergy in childhood. *N Engl J Med* 2003;348:977-85.

201 Rothenberg ME. Molecular, genetic, and cellular bases for treating eosinophilic esophagitis. *Gastroenterology* 2015;148:1143-57.

202 Votto M, Castagnoli R, De Filippo M, et al. Behavioral issues and quality of life in children with eosinophilic esophagitis. *Minerva Pediatr* 2020;72:424-32.

203 Wechsler JB, Ackerman SJ, Chehade M, et al. Noninvasive biomarkers identify eosinophilic esophagitis: A prospective longitudinal study in children. *Allergy* 2021;76:3755-65.

204 Min SB, Nylund CM, Baker TP, et al. Longitudinal Evaluation of Noninvasive Biomarkers for Eosinophilic Esophagitis. *J Clin Gastroenterol* 2017;51:127-35.

205 Schlag C, Miehlke S, Heiseke A, et al. Peripheral blood eosinophils and other non-invasive biomarkers can monitor treatment response in eosinophilic oesophagitis. *Aliment Pharmacol Ther* 2015;42:1122-30.

206 Konrad RJ, Higgs RE, Rodgers GH, et al. Assessment and Clinical Relevance of Serum IL-19 Levels in Psoriasis and Atopic Dermatitis Using a Sensitive and Specific Novel Immunoassay. *Sci Rep* 2019;9:5211.

207 Saheb Sharif-Askari F, Saheb Sharif-Askari N, Goel S, et al. Upregulation of interleukin-19 in severe asthma: a potential saliva biomarker for asthma severity. *ERJ Open Res* 2021;7.

208 Gedebjerg A, Johansen C, Kragballe K, et al. IL-20, IL-21 and p40: potential biomarkers of treatment response for ustekinumab. *Acta Derm Venereol* 2013;93:150-5.

209 Votto M, De Filippo M, Castagnoli R, et al. Non-invasive biomarkers of eosinophilic esophagitis. *Acta Biomed* 2021;92:e2021530.

210 Xu X, Prens E, Florencia E, et al. Interleukin-17A Drives IL-19 and IL-24 Expression in Skin Stromal Cells Regulating Keratinocyte Proliferation. *Front Immunol* 2021;12:719562.

211 Yu WY, Slack JM, Tosh D. Conversion of columnar to stratified squamous epithelium in the developing mouse oesophagus. *Dev Biol* 2005;284:157-70.

212 VanHorn S, Morris SA. Next-Generation Lineage Tracing and Fate Mapping to Interrogate Development. *Dev Cell* 2021;56:7-21.

213 Dunn JLM, Caldwell JM, Ballaban A, et al. Bidirectional crosstalk between eosinophils and esophageal epithelial cells regulates inflammatory and remodeling processes. *Mucosal Immunol* 2021;14:1133-43.

214 Wen T, Aronow BJ, Rochman Y, et al. Single-cell RNA sequencing identifies inflammatory tissue T cells in eosinophilic esophagitis. *J Clin Invest* 2019;129:2014-28.

215 Simon D, Radonjic-Hosli S, Straumann A, et al. Active eosinophilic esophagitis is characterized by epithelial barrier defects and eosinophil extracellular trap formation. *Allergy* 2015;70:443-52.

216 Kezic S, Kemperman PM, Koster ES, et al. Loss-of-function mutations in the filaggrin gene lead to reduced level of natural moisturizing factor in the stratum corneum. *J Invest Dermatol* 2008;128:2117-9.

217 Jordan WJ, Eskdale J, Boniotto M, et al. Human IL-19 regulates immunity through auto-induction of IL-19 and production of IL-10. *Eur J Immunol* 2005;35:1576-82.

218 Liao YC, Liang WG, Chen FW, et al. IL-19 induces production of IL-6 and TNF-alpha and results in cell apoptosis through TNF-alpha. *J Immunol* 2002;169:4288-97.

219 Xiao M, Zhang W, Liu W, et al. Osteocytes regulate neutrophil development through IL-19: a potent cytokine for neutropenia treatment. *Blood* 2021;137:3533-47.

220 Ha HL, Wang H, Claudio E, et al. IL-20-Receptor Signaling Delimits IL-17 Production in Psoriatic Inflammation. *J Invest Dermatol* 2020;140:143-51 e3.

221 Chong WP, Mattapallil MJ, Raychaudhuri K, et al. The Cytokine IL-17A Limits Th17 Pathogenicity via a Negative Feedback Loop Driven by Autocrine Induction of IL-24. *Immunity* 2020;53:384-97 e5.

222 Tohyama M, Hanakawa Y, Shirakata Y, et al. IL-17 and IL-22 mediate IL-20 subfamily cytokine production in cultured keratinocytes via increased IL-22 receptor expression. *Eur J Immunol* 2009;39:2779-88.

223 Roskoski R, Jr. ERK1/2 MAP kinases: structure, function, and regulation. *Pharmacol Res* 2012;66:105-43.

224 Tan Q, Yang H, Liu E, et al. P38/ERK MAPK signaling pathways are involved in the regulation of filaggrin and involucrin by IL17. *Mol Med Rep* 2017;16:8863-67.

225 Liu X, Zhou H, Huang X, et al. A Broad Blockade of Signaling from the IL-20 Family of Cytokines Potently Attenuates Collagen-Induced Arthritis. *J Immunol* 2016;197:3029-37.

226 Senolt L, Leszczynski P, Dokoupilova E, et al. Efficacy and Safety of Anti-Interleukin-20 Monoclonal Antibody in Patients With Rheumatoid Arthritis: A Randomized Phase IIa Trial. *Arthritis Rheumatol* 2015;67:1438-48.

7 CURRICULUM VITAE

PERSONAL INFORMATION

Tanay Kaymak

M.D.-Ph.D. Student

Department of Biomedicine

University of Basel

Hebelstrasse 20, 4031 Basel, Switzerland

Tel: +41612652328

E-mail: tanay.kaymak@unibas.ch

EDUCATION

09/2018-10/2022 (expected)	**M.D.-Ph.D. in Immunology, University of Basel, Switzerland** Gastroenterology
09/2017-09/2018	**Doctor of Medicine, University of Basel, Switzerland** Gastroenterology
09/2017	**Swiss State Examination Human Medicine**
09/2011-08/2017	**Medical Studies, University of Basel, Switzerland**
2004-2010	**Gymnasium Bäumlihof, Basel, Switzerland** Major in Biology and Chemistry

WORK EXPERIENCE

Since 09/2018	**Doctoral Dissertation, Gastroenterology, Department of Biomedicine Basel, University of Basel, Switzerland** "Aberrant IL-20 Subfamily Signaling Disturbs Epithelial Barrier Function in Eosinophilic Esophagitis" Advisor: Prof. Jan Hendrik Niess
09/2017-08/2018	**Medical Dissertation, Gastroenterology, University Hospital Basel, University of Basel, Switzerland** "Low discontinuation rate of Infliximab treatment in steroid-dependent/refractory Crohn's disease patients" Advisor: Prof. Petr Hruz

04/2016-03/2017	**Elective Period in Final Year of Medical Studies:**	
	01/2017-03/2017	Department of Biomedicine Basel, Gastroenterology
	10/2016-12/2016	Cantonal Hospital Lucerne, Internal medicine
	08/2016-09/2016	University Children's Hospital Basel, Paediatrics
	05/2016-07/2016	Cantonal Hospital Chur, Surgery
	04/2016	University Hospital Basel, Radiology

2016-2017	**Master Thesis, Gastroenterology, University Hospital Basel, University of Basel, Switzerland**
	"Effectiveness of Vedolizumab induction therapy in IBD patients"
	Advisor: Prof. Petr Hruz

Since 2013	**Organization and Person Responsible for Medical Care in Swiss Muscle Society Summer Camps**

2012-2016	**Nursing and Medical Attendance in Mathilde Escher Heim (MEH), Zürich**

EXTRA-CURRICULAR ACTIVITIES

06/2022	Annual Congress and General Assembly SMPA 2022, Rigi Kaltbad, Organizing Committee
04/2022	International Day of Immunology 2022, UBICO, Organizing Committee
06/2021	Annual Congress and General Assembly SMPA 2021, Organizing Committee
04/2021	International Day of Immunology 2021, UBICO, Organizing Committee
06/2020	Annual Congress and General Assembly SMPA 2020, Organizing Committee
Since 2020	Swiss MD-Ph.D. Association (SMPA), Vice President
2019-2020	Swiss MD-Ph.D. Association (SMPA), Board Member
11/2019	MD-Ph.D. Retreat Zürich-Basel 2019, Kandersteg, Organizing Committee
10/2019	8th European & Swiss MD-Ph.D. Conference, Genf, Organizing Committee
Since 09/2019	University of Basel Immunology Community (UBICO), Ph.D. Representative in Steering Committee

Since 09/2018   Immunology Ph.D. Club, Department of Biomedicine Basel,
                     Organizing Committee

FELLOWSHIPS/GRANTS

09/2018-09/2021   National MD-Ph.D. Fellowship awarded by SNSF and SAMS

AWARDS

3rd Prize for Best Presentation, Zürich-Basel MD-Ph.D. Retreat 2021, Flüeli-Ranft, Switzerland, 13-15 October 2021

National Scholar Award for best abstract from Switzerland, United European Gastroenterology Week Virtual 2021, 3-5 October 2021

PUBLICATIONS

Research articles

Kaymak T, Kaya B, Wuggenig P, Nuciforo S, Göldi A, Swiss EoE Cohort Study Group, Oswald F, Roux J, Noti M, Melhem H, Hruz P, Niess JH. IL-20 subfamily cytokines impair the esophageal epithelial barrier by diminishing filaggrin in eosinophilic esophagitis. *Gut* (Accepted)

Melhem H, Kaya B, **Kaymak T**, Wuggenig P, Flint E, Roux J, Oost KC, Cavelti-Weder C, Balmer ML, Walser JC, Morales RA, Riedel CU, Liberali P, Villablanca EJ, Niess JH. Epithelial GPR35 protects from Citrobacter rodentium infection by preserving goblet cells and mucosal barrier integrity. *Mucosal Immunol*, 03/2022

Kaya B, Doñas C, Wuggenig P, Diaz OE, Morales RA, Melhem H; Swiss IBD. Cohort Investigators, Hernández PP, **Kaymak T**, Das S, Hruz P, Franc Y, Geier F, Ayata CK, Villablanca EJ, Niess JH. Lysophosphatidic Acid-Mediated GPR35 Signaling in CX3CR1 $^+$ Macrophages Regulates Intestinal Homeostasis. *Cell Rep*, 08/2020

Kaymak T, Moriconi F, Niess JH, Beglinger C, Hruz P. Low discontinuation rate of Infliximab treatment in steroid-dependent/refractory Crohn's disease patients. *Inflamm Intest Dis,* 03/2018

Review articles

Kaymak T, Hruz P, Niess JH. Immune system and microbiome in the esophagus: implications for understanding inflammatory diseases. *FEBS J*, 07/2021

Niess JH, **Kaymak T**, Hruz P. The Role of the Exposome in the Emergence of Chronic Inflammatory Bowel Diseases. *Ther Umsch*, 01/2019

Niess JH, Hruz P, **Kaymak T**. The Interleukin-20 Cytokines in Intestinal Diseases. *Front Immunol,* 06/2018

PRESENTATIONS

Oral presentations

Kaymak T, Kaya B, Göldi A, Hruz P, Melhem H, Niess JH. (2021) The IL-20 cytokines decrease the expression of epithelial barrier filaggrins in eosinophilic esophagitis. United European Gastroenterology Week Virtual 2021

Kaymak T, Kaya B, Göldi A, Hruz P, Melhem H, Niess JH. (2021) IL-20 Cytokine Signaling Reduces Epithelial Barrier Filaggrins in Eosinophilic Esophagitis. Annual Meeting of the Swiss Society of Gastroenterology (SGG-SSG) 2021, Interlaken, Switzerland

Kaymak T, Kaya B, Wuggenig P, Göldi A, Melhem H, Noti M, Hruz P, Niess JH. (2021) IL-20 cytokines regulate epithelial integrity in the esophagus. 33rd DACED Annual Conference 2021 (Virtual)

Kaymak T, Kaya B, Melhem H, Göldi A, Hruz P, Niess JH. (2021) IL-20 Subfamily Cytokines reduce Expression of Epithelial Barrier Filaggrins in Eosinophilic Esophagitis. Zürich-Basel MD-Ph.D. Retreat 2021, Flüeli-Ranft, Switzerland

Kaymak T, Kaya B, Wuggenig P, Melhem H, Ayata K, Noti M, Hruz P, Niess JH. (2019) IL-20 cytokine signaling modulates eosinophilic esophagitis. Annual Meeting of the Swiss Society of Gastroenterology (SGG-SSG) 2019, Interlaken, Switzerland

Kaymak T, Kaya B, Wuggenig P, Melhem H, Ayata K, Noti M, Hruz P, Niess JH. (2019) Significance of IL-20 cytokines in the development of Eosinophilic Esophagitis. DACED Annual Conference 2019, Mainz, Germany

Kaymak T. (2018) Eosinophilic Esophagitis. Swiss MD-Ph.D. Association (SMPA) General Assembly 2018, Bern, Switzerland

Kaymak T, Kaya B, Wuggenig P, Ayata K, Noti M, Hruz P, Niess JH. (2018) The role of the Interleukin-20 Cytokine Family in Eosinophilic Esophagitis. Alumni Medicine Basel Research Day 2018, Basel, Switzerland

Poster presentations

Kaymak T, Kaya B, Göldi A, Hruz P, Melhem H, Niess JH. (2021) IL-20 Cytokine Signaling Reduces Expression of Epithelial Barrier Filaggrins in Eosinophilic Esophagitis. DBM Ph.D. Retreat 2021, Studen, Switzerland

Kaymak T, Kaya B, Wuggenig P, Ayata K, Melhem H, Noti M, Hruz P, Niess JH. (2019) The role of the IL-20 cytokine family in eosinophilic esophagitis. 31st Meeting of the Swiss Immunology Ph.D. students, Thun, Switzerland

Kaymak T, Kaya B, Wuggenig P, Ayata K, Melhem H, Noti M, Hruz P, Niess JH. (2018) The role of IL-20 cytokine family in eosinophilic esophagitis. Zürich-Basel MD-Ph.D. Retreat 2018, Engelberg, Switzerland

Kaymak T, Niess JH, Hruz P. (2017) Effectiveness of Vedolizumab Induction Therapy in IBD Patients. Annual Meeting of the Swiss Society of Gastroenterology (SGG-SSG) 2017, Lausanne, Switzerland

Kaymak T, Moriconi F, Mecklenburg I, Beglinger C, Hruz P. (2015) Infliximab treatment outcome in steroid-dependent or steroid-refractory Crohn's disease patients. Annual Meeting of the Swiss Society of Gastroenterology (SGG-SSG) 2015, Interlaken, Switzerland